Mathematical Modelling of Rod Photoreceptor Metabolism

Wannapa Kunpasuruang, MSc.

Thesis submitted to the University of Nottingham
for the degree of Master of Philosophy

September 2008

Abstract

Rod photoreceptors are cells that sense and receive light. They consist of two major parts, an outer and an inner segment, which are linked by a connecting cilium. Continual growth of the rod outer segment is balanced by shedding of the tip of the outer segment. We start this thesis by developing nonlinear ordinary differential equations to describe the metabolic activity of the rod photoreceptor cells in order to investigate whether changes in metabolic demand during periods of light and dark are responsible for the observed (daily) variation in the length of the outer segment of the rod photoreceptors. Analysis of the rod system is carried out by investigating the steady-state solutions.

Secondly, because the eyes form part of the nervous system, we have also developed an ordinary differential model involving the glutamate-glutamine cycle in the nervous system in order to study how the rates at which glutamate and glutamine are released influence the metabolic demand of the system. We use a combination of numerical simulation and asymptotic techniques to understand the system dynamics. The asymptotic analysis provides insight into processes that control different stages of the glutamate-glutamine cycle.

Although glutamate is the main excitatory neurotransmitter in the mammalian central nervous system, it can be toxic to neuronal cells. Excitotoxicity occurs when there is overactivation of neuronal-glutamate receptors caused by excessive extracellular glutamate levels. This can lead to intracellular calcium overload and neurodegeneration. In the later stages of this thesis we extend our model of the glutamate-glutamine cycle by including an additional equation for intracellular calcium levels in order to study how calcium interacts with the glutamate-glutamine cycle and how it triggers excitotoxicity. Moreover, we find that as the extracellular volume fraction decreases, the concentration of components in the extracellular space increases, resulting in a neuron's responsiveness to a fixed amount of neurotransmitter consistent with clinical evidence.

Acknowledgements

Firstly, I am particularly indebted to the Ministry of Science and Technology, Royal Thai Government, whose financial support has made my study at The University of Nottingham possible.

I would like to thank my principal supervisor, Professor Helen Byrne, for her expert guidance, invaluable advice, supervision and patient encouragement throughout this research which enabled me to complete this thesis successfully. She has never been lacking in kindness and support.

Moreover, I appreciate the excellent support, helpful comments, guidance and advice given by my co-supervisor, Professor John King.

I wish to thank Dr. Sara Jabbari and Dr. Alexander Foss for their assistance with my problems and for their friendly explanations.

I am grateful to the support of my landlady, Mrs. Catherine Hammond, and her careful proof reading of my drafts.

I wish to thank my friends in Nottingham, Ms. Jongkol Iammi, Mr. Phinit Srithorn and Mr. Kongpan Areerak who have made my life here as a home and always had my terrible cakes.

Finally, I like to thank to my family and my boyfriend in Thailand for their continual support, encouragement and understanding.

List of Figures

List of Tables

Contents

CHAPTER 1

Introduction

1.1 Background Biology

The eye is the first part of the visual system which allows people to communicate with each other. It is a highly specialised organ of photoreception, using a process by which light energy from the surrounding environment produces changes in nerve [1] cells in the retina. These changes result in nerve action potentials, which are subsequently relayed to the optic nerve and then to the brain, where the information is processed and consciously appreciated as vision.

In this background biology section we firstly give a brief introduction to the retina which is where the rod photoreceptors are located. We then describe cellular energy metabolism and explain how this information can be used to develop our model of light-dark regulation of outer segment length. Next we introduce the nervous system of the brain focusing on neurotransmitter metabolism which forms the basis for our second model, which describes the glutamate-glutamine cycle. This is interesting because the human eyes are known as a part of the nervous system. Pathophysiology involving medical disorders and ageing that affect the photoreceptor cells and the metabolism of the nervous system are also briefly reviewed at the end of this section.

1.1.1 The Retina

Human eyes consist of three main layers: the sclera, the choroid and the retina. The retina is located in the innermost part of the eye and consists of five layers, namely ganglion cells (inner layer of the retina), bipolar cells, horizontal cells, amacrine cells, and

[1] See the Glossary in Appendix.

photoreceptor cells (outermost layer of the retina). The horizontal and amacrine cells modulate communication between the cells in the retina (see Figure 1.1). The retina lies against a darkly coloured layer of cells called the retinal pigment epithelium (RPE). Between the RPE and the sclera, which forms the visible white part of the eye, is the choroid. The choroid is rich in blood vessels which provide nutrition and oxygen for the RPE and deep layers of the retina.

The initial step in vision is the absorption of light by visual pigments in the outer segments of the retinal photoreceptor cells. Any light rays that escape the photoreceptor cells are absorbed by the RPE. The light absorption of the RPE prevents distracting light from reflecting inside the eye and distorting the visual image. The photoreceptors convert light energy into nerve impulses that can ultimately be transmitted to the brain via the optic nerve [1, 4, 5].

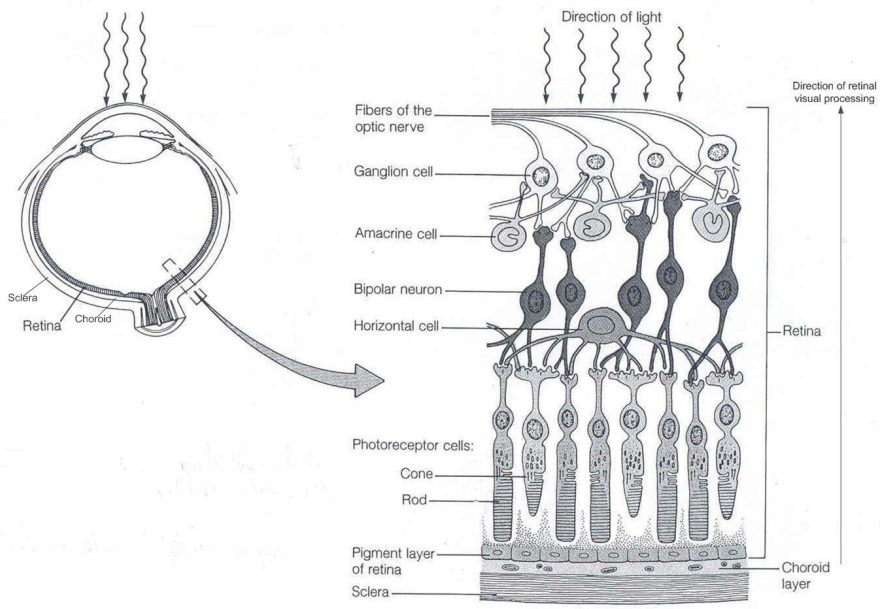

Figure 1.1: Retinal Layers: The retinal visual pathway is from the photoreceptor cells (rods and cones) to the bipolar cells to the ganglion cells. The amacrine and horizontal cells act locally for the retinal processing of visual input. (Figure is adapted from [1].)

There are two types of photoreceptors, rods and cones, situated on the outer side of the retina. Each photoreceptor is a long narrow cell with an outer and inner segment, connected by the cilium, and a synaptic terminal at the end of the photoreceptor, lying closest to the bipolar cells. The inner segment contains a large number of mitochondria and a nucleus. By contrast, the outer segment (see Figure 1.2) is composed of membra-

nous discs with an abundance of photopigment molecules. Photopigment molecules undergo chemical alterations when activated by light. The photopigment consists of the enzymatic protein, opsin. The photoreceptors' opsins vary slightly, enabling them to absorb differentially various wavelengths of light. There are four different photopigments. The photopigment rhodopsin is found in the rods, while red, green and blue colour pigments are found in the cones. Therefore rods and cones have different functions. Humans typically have three million cones and 100 million rods per eye. Rods have high sensitivity to light but low sharpness, so they are important in vision at night. Cones, on the other hand, have low sensitivity but high sharpness. Thus cones provide sharp colour vision during the day. As a result, the photoreceptors are cells that sense and receive light.

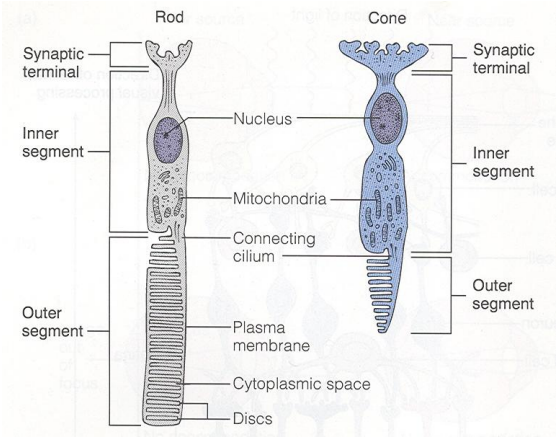

Figure 1.2: Photoreceptor cells (adapted from [1]).

New discs grow in the region of the cilium. As each new disc is formed at the junction between the outer and inner segment, the older discs are pushed outward towards the RPE. The photoreceptors shed the oldest discs from the outer segments, and these are taken up and digested by the RPE. The process of shedding in rods occurs mainly in the morning or, following prolonged periods of darkness, when light reappears. In humans, the rod outer segment is entirely replaced every 8 to 14 days. By contrast, in cone cells this process occurs at night and it takes approximately one month for complete renewal [5–8]. It is known that the length of the rod outer segment increases during the dark period [9]. By contrast the length of the cone outer segment (in the lizard) increases during the light period [10].

Photopigment has to be synthesised to maintain a photoreceptor's ability to respond to light. Synthesis of photopigment requires energy which is typically derived from the

high-energy phosphate compound ATP (adenosine triphosphate).

1.1.2 Cellular Energy Metabolism

There are two main types of cellular energy metabolism [4]: anaerobic metabolism which does not involve oxygen consumption, and aerobic metabolism which does involve oxygen consumption.

Anaerobic Metabolism

Anaerobic metabolism occurs in the cytoplasm and can happen in two different ways. The first source for supplying additional ATP (adenosine triphosphate) is creatine phosphate (CP) which is used to convert ADP (adenosine diphosphate) rapidly to ATP and creatine (Cr) (see reaction (1.1.1)).

$$\mathrm{CP} + \mathrm{ADP} \underset{\mathrm{CPK}}{\overset{\mathrm{CK}}{\rightleftharpoons}} \mathrm{Cr} + \mathrm{ATP}\,. \tag{1.1.1}$$

The reaction (1.1.1) is reversible. The forward reaction occurs when the cells need energy and is catalysed by the enzyme creatine kinase (CK); the reverse reaction occurs when the cells have excess energy and is catalysed by the enzyme creatine phosphokinase (CPK).

When the cell needs energy the forward reaction in (1.1.1) is believed to act as the main energy source [11]. However, the amount of ATP that can be formed by this process is limited by the amount of CP in the cell. If energy is needed for more than a few seconds, the cell must be able to form ATP from other sources. The main secondary source of energy is anaerobic glycolysis. Here glucose in the bloodstream diffuses into the cytoplasm and produces two moles of ATP and two moles of pyruvate (see the irreversible reaction (1.1.2) and Figure 1.3):

$$\mathrm{Glucose} + 2\mathrm{NAD}^+ + 2\mathrm{ADP} + 2\mathrm{P_i} \rightarrow 2\mathrm{Pyruvate} + 2\mathrm{ATP} + 2\mathrm{NADH} + 2\mathrm{H}^+, \tag{1.1.2}$$

where NAD^+ is nicotinamide adenine dinucleotide, $\mathrm{P_i}$ is inorganic phosphate, NADH is the reduced form of NAD^+ and H^+ is a hydrogen ion.

Aerobic Metabolism

Aerobic metabolism takes place within the mitochondria, which are the sites of energy production and contain enzymes of the Krebs cycle. The Krebs cycle, which is also known as the tricarboxylic acid cycle (TCA), refers specifically to a complex series of chemical reactions all of which utilise oxygen as part of their respiration process [4].

Pyruvate which is produced from the glycolysis pathway is converted to acetyl coenzyme A (or acetyl CoA) which enters the Krebs cycle in the mitochondria (see Figure 1.3). This process produces 36 moles of ATP from one mole of glucose and six moles of oxygen. Although providing a rich yield of ATP for each molecule of glucose, this process is relatively slow because of the number of steps involved. In addition, it requires a constant supply of oxygen. If the oxygen supply is inadequate to permit operation of the Krebs cycle, any excess pyruvate may be temporarily disposed of by reducing it to lactate (see the forward reaction (1.1.3)). At the expense of accumulating lactate, glycolysis continues to operate and produce two moles of ATP. When oxygen is restored to normal levels, lactate is converted back to pyruvate and the Krebs cycle continues (see the reverse reaction (1.1.3)). Pyruvate then is converted to acetyl CoA which enters the Krebs cycle.

$$2\text{Pyruvate} + 2\text{NADH} \rightleftharpoons 2\text{Lactate} + 2\text{NAD}^{+}. \tag{1.1.3}$$

Within the photoreceptor, the outer segment relies upon anaerobic metabolism because it does not contain any mitochondria. By contrast, the inner segment utilises both aerobic and anaerobic metabolism (the latter if oxygen is insufficient). Since the formation of ATP from CP occurs in the first few second and is limited [11], we neglect the amount of ATP that is generated from CP.

As mentioned above, the rods are present in much greater numbers than the photoreceptors. Therefore in our first model (see Chapter 2) we will focus on modelling the metabolic activity of the rod photoreceptor cells and investigate whether changes in metabolic demand during periods of light and dark are able to explain the observed (daily) variation in the length of the photoreceptor cells. In particular, as stated before, it is believed that the length of the rod outer segment is greater under dark than light conditions [9].

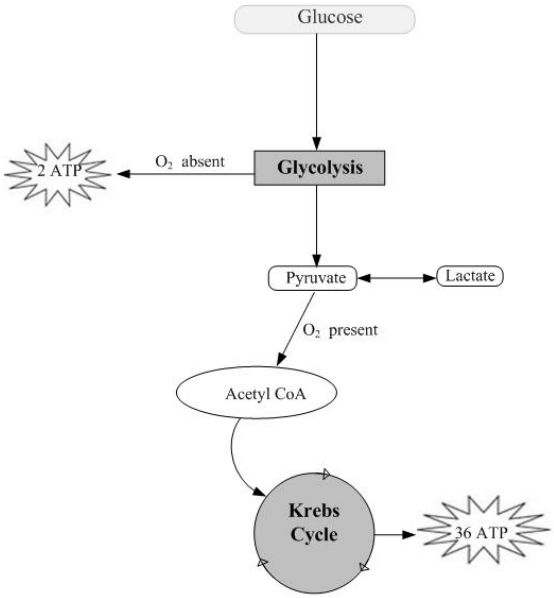

Figure 1.3: A schematic diagram of anaerobic glycolysis and aerobic metabolism.

Now, the eyes form part of the nervous system. The neural pathways associated with vision begin with the rods and cones [11]. These photoreceptor cells communicate via electrical synapses with each other and with second-order neuronal cells such as bipolar cells and ganglion cells. In the next section, we introduce the nervous system of the brain in order to clearly how the visual nervous system operates.

1.1.3 The Nervous System

All animals, including humans, obtain information about their environment through a variety of sensory receptors. The information from these receptors is transformed by the brain into perceptions or into commands for movement. The brain is the control centre of the nervous system. The outstanding tasks of the brain are accomplished using only neurons and the connections between them [12].

The nervous system is a very complicated system. It controls and maintains diverse biological processes that are essential for maintaining an acceptable quality of life [2, 12]. For a thorough understanding of the basic functions of the nervous system and how this system is affected by pathological conditions such as disease, toxin and injury, it is essential to understand the anatomy, physiology and biochemistry of the nervous system. In Chapter 3 of this thesis we develop a mathematical model that focuses

on the metabolic fundamentals of the nervous system of the brain, in particular neurotransmitter metabolism and metabolic trafficking (glutamate-glutamine cycle) between neurons and glial cells. These are related to the human eyes which are the part of the nervous system.

The nervous system is divided into two main parts, the central nervous system (CNS) and the peripheral nervous system (PNS). The CNS contains the brain and the spinal cord and represents the major pathway for the flow of information between the brain and other parts of the body. The PNS comprises all the nerves and wiring. The nervous system is dominated by two cell types: neurons (or neuronal cells) which are the basic signalling units of the nervous system, and the support cells which are known as glial cells (or glia or neuroglia) [2, 12–14]. While both cells play important roles in the vitality of the system, only the neuronal cells can transmit messages from one part of the CNS to another or out of the system altogether (e.g. to the muscles and glands), and vice versa (e.g. from the sensory organs into the CNS). We describe briefly neuronal and glial cells below.

Neuronal Cells

Neurons are excitable cells that generate and carry electrical signals. The neuron is the smallest structure that can carry out the functions of the nervous system. Neuronal cells have long appendages that extend outward from the cell body. The cell body contains the nucleus, storing the cell's genes, and the organelles, which synthesise its proteins. Moreover, the cell body consists of a large number of dendrites (which receive incoming signals) and axons (which transmit information). Their main role is to allow neurons to communicate with each other and with other cells. Several neurons are similar to the diagrammatic neuron depicted in Figure 1.4 [2, 12, 13].

In Figure 1.4, mitochondria and membrane-bound vesicles that are filled with neurocrine molecules are contained in the axon terminal. The anatomically-specialised junction between two neurons, where one neuron alters the activity of another, is called a synapse (see Figure 1.4). At most synapses, the signal is packaged within synaptic vesicles and is transmitted from one neuron to another by neurotransmitters, a term which also includes the chemicals by which neurons communicate with target cells. The neurotransmitters released from one neuron alter the receiving neuron by binding with specific membrane receptors on the receiving neuron [2]. The neuronal cell that

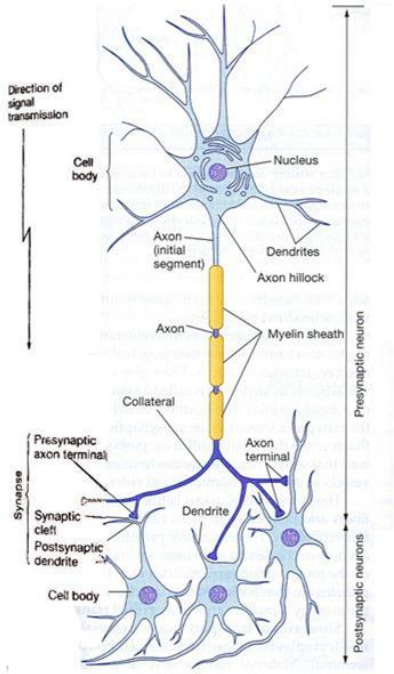

Figure 1.4: Diagrammatic representation of a neuron: the neuron shown is a typical neuron, consisting of a cell body and numerous extensions. The region where axon terminals communicate with their target cells is known as a synapse (taken from [2]).

receives the signal is known as the postsynaptic cell, and the cell that sends the signal is called the presynaptic cell. These two cells are separated at the synapse by a gap, the synaptic cleft [2, 12]. In a neural reflex, information moves from the presynaptic to the postsynaptic cell.

Glial Cells

In addition to neuronal cells, the nervous system also contains glial cells. There are approximately 10 times more glial cells than neurons. However, since glial cells are approximately one-tenth the size of the neuronal cells, both neuronal and glial cells take up equal space [2]. They are known as the supporting cells of the nervous system because they hold the neurons together in proper spatial relationships. The four principal roles of glial cells are: to surround neuronal cells and hold them in place, to supply oxygen and nutrients to neurons, to insulate one neuron from another and to destroy and remove the dead neurons. Without glial cells, the neurons would not work properly. Even though these neuronal support cells do not participate directly in the transmission of electrical signals over long distances, they communicate with neurons

and with each other using electrical and chemical signals. The glial cells serve as the connective tissue of the CNS and, as such, help support the neuronal cells both physically and metabolically [2, 12].

Glial cells in the vertebrate nervous system are divided into two main classes: microglia and macroglia [12]. Microglia are phagocytes (cells that ingest and destroy dead cells) that are mobilised after injury, infection or disease. However, three types of macroglia predominate in the vertebrate nervous system: oligodendrocytes, Schwann cells and astrocytes. However, Schwann cells are known as the glial cells of the PNS. Oligodendrocytes (which is in the CNS) and Schwann cells (which is in the PNS) form the myelin sheaths that insulate axons. Astrocytes are the most abundant glial cells. They appear in the CNS and help to maintain the correct potassium ion concentration in the synaptic cleft that separated two neurons. Moreover, astrocytes take up neurotransmitters from the synaptic cleft after release by neurons and help regulate synaptic activities by removing transmitters. For our purposes the astrocytes are the glial cells of interest.

Neurons and glial cells are separated from each other by extracellular space (synaptic cleft) [15, 16]. The extracellular space (ECS) comprises approximately 20% of brain tissue volume and is responsible for the exchange from neurons to glial cells of ions, neurotransmitters and metabolites [17]. Recent studies indicate that some glial cells provide metabolic support to neurons, help maintain the composition of the extracellular fluid, and even participate in information transfer [2, 15, 16]. In addition, glial cells are particularly characterised by high concentrations of glutamine synthetase (GS), a glial-specific enzyme that converts the amino acid glutamate (Glu) to the amino acid glutamine (Gln) [1, 5, 15, 16].

1.1.4 Glutamate-Glutamine Metabolism

Glutamate (Glu) is the principal excitatory neurotransmitter in the mammalian brain and retina [18, 19], and is removed to, or from, the ECS by an energy-dependent process (active transport) involving neuronal and glial cell transporters [18]. Glu uptake is an active process, its mediated transport across membranes requiring the expenditure of cellular energy. During an ischaemic (less blood supply) episode, however, extracellular Glu concentrations may rise to excitotoxic (nerve injury produced by Glu) levels [15, 20, 21]. Therefore, the regulation of Glu release and absorption is critical. Glu secreted from the neuron (called the presynaptic neuron) must be removed rapidly. There

are three possibilities after Glu is released into the ECS (see Figure 1.5): ① uptake into the postsynaptic compartment; ② reuptake into the presynaptic compartment; and ③ uptake into a non-neuronal compartment (glial cell) [22, 23]. Since most Glu secreted into the ECS is transported into the glial cells [16, 22, 24], we will consider only the third mechanism when we develop our model (see Chapter 3). Once released into the ECS, Glu is absorbed by glial cells via neuronal or glial Glu transporters [20, 21].

A major role of the Glu transporter is to maintain the concentration of free Glu in the ECS at low levels [18, 23]. In the absence of normally functioning Glu transporters, Glu levels would build up and kill cells in a process called excitotoxicity (here excessive amounts of Glu are toxic to neurons by triggering a number of biochemical cascades). There are many types of Glu transporter which are dependent on the target cells. For instance, the Glu-Asp transporter (GLAST) is associated with glial cells (Müller cells in the retina) and the EAAT5 transporter (excitatory amino acid transporter 5) is associated with neuronal cells (photoreceptor and bipolar cells in the retina) [20]. The glial and neuronal Glu-uptake system thus terminates the excitatory signal and reduces the possibility of excitotoxic neuronal damage. Glu neurotoxicity has been implicated the neuronal degeneration that follows injury or focal ischemia and in the pathophysiology of a wide variety of neurological disorders such as Alzheimer's disease (AD), Parkinson's disease (PD) and glaucoma [15, 25–27].

Glu which is released from neuronal cells is transported, via the ECS, into glial cells and converted by the enzyme GS in the cytosol to the non-toxic amino acid Gln. This process requires energy and can be schematised as follows:

$$\text{Glutamate} + \text{NH}_4^+ + \text{ATP} \xrightarrow{\text{GS}} \text{Glutamine} + \text{ADP} + \text{P}_\text{i}, \tag{1.1.4}$$

where NH_4^+ is ammonia. It is known that reaction (1.1.4) protects neurons from excitotoxicity by converting Glu to Gln.

Additionally, there is evidence [28] that Glu can be released from glial cells in order to reduce the rate of ATP production in glial cells. Furthermore, several authors [16, 23, 29–31] state that, rather than Glu being mainly converted to Gln in the glial cell, there

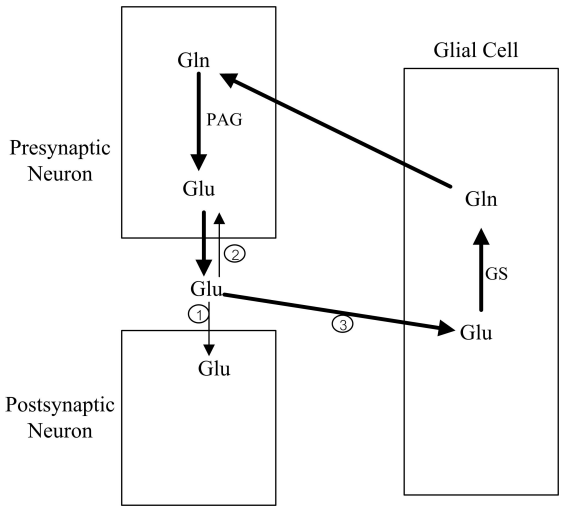

Figure 1.5: A schematic diagram of Glu uptake and the Glu-Gln cycle. Glu released from the presynaptic terminals is ① taken up by postsynaptic neurons, ② reabsorbed by presynaptic neurons, or ③ transported into glial cells. Glu released from presynaptic neurons is mostly transported to glial cells, where it is converted to Gln via the enzyme GS. This Gln is taken up by the neurons where Glu is regenerated via the enzyme PAG (glutaminase), a mitochondrial enzyme.

are three other biochemical reactions involving Glu:

$$\text{Glutamate + Pyruvate} \longrightarrow \text{Alanine} + \text{a} - \text{Ketoglutarate}, \tag{1.1.5}$$

$$\text{Glutamate + Oxaloacetate} \rightleftharpoons \text{a} - \text{Ketoglutarate} + \text{Aspartate}, \tag{1.1.6}$$

$$\text{Glutamate + NAD}^+ \longrightarrow \text{a} - \text{Ketoglutarate + NADH +NH}_3, \tag{1.1.7}$$

where NAD^+ is nicotinamide adenine dinucleotide, NADH is the reduced form of NAD^+, and NH_3 is ammonia (reduced form of NH_4^+).

Reactions (1.1.4), (1.1.5) and (1.1.6) occur in the cytoplasm whereas (1.1.6) and (1.1.7) occur in the mitochondria. Reactions (1.1.5)-(1.1.7) describe the transamination process which is the transfer of the amino group to an a-keto acid. In [31] reaction (1.1.4) which is catalysed by the enzyme GS was shown to be the main route. Moreover, it can be said that ammonia is trapped by the enzyme GS whereas Gln production is controlled by Glu. When the flux through the enzyme GS reaction is limited due to insufficient ammonia (below 10 mM), more Glu is available for reactions (1.1.6) and (1.1.7). In additional to ammonia, ATP is important for reaction (1.1.4). It is suggested that a major part of the ATP used by GS is produced through the glycolytic pathway. Furthermore, pyruvate which is used in reaction (1.1.5) is also produced from the glycolysis pathway. These details could be included in future work. In the model that we develop below it

is assumed that in the glial cell Glu conversion to Gln is the dominant reaction.

After its conversion from Glu in the glial cell, Gln is released into the ECS before being absorbed by the neuronal cell [30, 32]. As for Glu, Gln must use a transporter in order to travel from the glial cell to the ECS and from the ECS to the neuronal cell. The System N transporter, SN1, mediates efflux and influx of Gln by glial cells, and System A transporters, SA1 and SA2, mediate its uptake by neurons [33, 34]. Gln transport is probably mediated by passive diffusion (i.e. movement from a region of high concentration to one of lower concentration [35]). In neurons, Gln and water are converted back to Glu via the enzyme phosphate-activated glutaminase (PAG) or glutaminase which is localised on the inner mitochondrial membrane of the glutamatergic nerve terminals which is called hydrolysis process [22] (see reaction (1.1.8)):

$$\text{Glutamine} + H_2O \xrightarrow{\text{PAG}} \text{Glutamate} + NH_4^+. \tag{1.1.8}$$

As with glial cells, Glu can be transaminated to Asp (reaction (1.1.6)) via the Kerbs cycle in the neuronal cells. However, Asp levels are assumed to be very low. We therefore assume that reaction (1.1.6) does not occur in our interesting model. Newly synthesised Glu is then packaged and stored in high concentrations (in excess of 20 mM [36]) within synaptic vesicles. Subsequently, when the neurons are excited, Glu is released into the ECS [18, 23] via EAAT5. This interaction between neuronal and glial cells is called the Glu-Gln cycle (see Figure 1.6). It acts to replenish the neurotransmitter pool to prevent neurotoxicity.

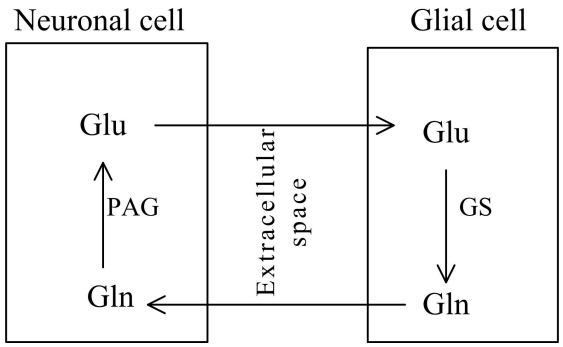

Figure 1.6: A schematic diagram of the Glu-Gln cycle. Glu released from the neuronal cell to the glial cell is converted to Gln via the enzyme GS. Gln is released back to the neurons where Glu is regenerated via the enzyme PAG.

The Glu-Gln cycle plays a special role not only in glutamatergic neurotransmission but also in the removal of excess ammonia (ammonia detoxification process). Hence any

disorder in the Glu-Gln cycle caused by pathological conditions may result in a different pattern of brain damage. In order to understand such situations more information is needed about the metabolism of the substrates involved in the Glu-Gln cycle.

There is further evidence [24] which shows that Glu metabolism in the human brain is compartmentalised, involving two main metabolic pools of Glu; a neuronal compartment and a glial compartment. In our second model (see Chapter 3), we will study the metabolic activity in the Glu-Gln cycle of three different compartments in the nervous system: the neuron, the ECS and the glial cell.

In fact, the release of Glu from the synaptic vesicle in the neuronal cell into the ECS needs an intra-calcium [36–40]. We extend the model of the Glu-Gln cycle in Chapter 3 by adding the intracellular calcium levels. In this model (see Chapter 4) we study how calcium interacts with the Glu-Gln cycle and how it triggers excitotoxicity.

Furthermore, there is some evidence [41] supporting that Glu can be a toxin in the nervous system. In 1957 Lucas and Newhouse [41] found that feeding glutamate to infant mice destroys neurons in the retina. This is called as excitotoxicity. Excitotoxicity refers to the ability of glutamate or similar substances to destroy neuronal cells by excessive activation of glutamate receptors. Normally, the glutamate concentration released into the ECS rises to high levels (1 mM), but it remains at this level for only a few milliseconds. If abnormally high levels of glutamate accumulate in the ECS, the excessive activation of neuronal glutamate receptors can excite neurons to death [36–38].

When Glu receptors are activated, ion channels on the cell membrane open. This allows flow of sodium and small amounts of calcium into the cells and potassium out of the cells. The secretion of neurotransmitter (Glu) is triggered by calcium influx through voltage-gated channels, which gives rise to a transient increase in calcium concentration with in the presynaptic terminal. The rise in calcium concentration causes synaptic vesicles to fuse with the presynaptic plasma membrane and release their contents into the extracellular space. However, high levels of extracellular Glu allow high levels of calcium into the cells. This can cause excitotoxicity. Calcium influx to cells activates a number of enzymes. These enzymes go on to damage cell structures and the cells die. We also investigate excitotoxicity of the Glu-Gln cycle at the end of Chapter 4.

1.1.5 Pathophysiology

There is evidence that certain medical disorders and ageing affect photoreceptor cells [42–44]. For example, age-related retinal degeneration involves the progressive loss of photoreceptor cells from the peripheral retina. By contrast, diabetes reduces the rate at which rhodopsin is regenerated and hence leads to a decrease in the length of the outer segments. These features lead to vision changes and may eventually cause blindness.

In additional, neuronal damage is one of the problems which involves the eye. Neurotoxicity has been defined as an adverse change in the structure or function of the nervous system following exposure to a chemical (natural or synthetic) or physical agent. This can eventually disrupt or even kill neurons. A chemical is considered to be a neurotoxicant if it induces a consistent pattern of neural dysfunction or lesion in the nervous system. Neurotoxicity can result from exposure to substances used in chemotherapy, radiation treatment, drug therapies and organ transplants, as well as exposure to heavy metals such as lead and mercury, certain foods, pesticides, or cleaning solvents. Symptoms may appear immediately after exposure or be delayed. Individuals with certain disorders may be especially vulnerable to neurotoxins.

Neurotoxicity can also be called excitotoxicity if excitatory neurotransmitters such as Glu, aspartate (Asp) and glycine act as a toxin to neurons [2, 15]. Excess Glu, for example, chronically over stimulates NMDA (N-methyl-D-aspartate) receptors cause the release of excess intracellular calcium and leading to neuronal cell death [27, 36–38]. Glu excitotoxicity also contributes to ganglion cell (which is located in the inner layer of the retina) death which causes to glaucoma [27]. It can cause to retinitis pigmentosa (RP) that primarily affects the photoreceptors [45].

As mentioned above excitotoxicity occurs when Glu levels in the ECS exceed a threshold value. In [29, 46] it is proposed that the extracellular Glu is maintained below 0.06 mM in order to avoid excitotoxicity to neurons. In more details there is a Glu transporter to limit free Glu levels in the ECS and after being transported into the glial cell, Glu is converted to Gln by the enzyme GS. However, there are some factors to destroy this natural protection such as aging, some diseases and anti-epileptic drugs [25–27, 47, 48].

Parkinson's disease (PD) and Alzheimer's disease (AD) are strongly associated with

aging and can cause glial dysfunction [26, 49], increasing neuronal degeneration due to regional loss of the enzyme GS. Recall that GS is a key enzyme in the Glu-Gln cycle: decreased uptake of Glu, due to decrease GS activity, could have neurotoxic effects. By contrast, the activity of other enzymes involved in the Glu-Gln cycle such as the enzyme PAG (involving in our second model) seems to be unchanged during aging [50].

There is some clinical evidence [51], which supports the hypothesis that high levels of Glu in the ECS may contribute to progressive dysfunction of the glutamatergic system. Cauquil-Caubère *et al.* [51] propose that after being injected into the striatum of rats, Glu levels increase in the synaptic cleft. This can contribute to progressive dysfunctions of neurotransmitters, and, thereby, contribute to neurotoxicity. Moreover, in vitro study Choi [52] suggests that a 5 minute exposure to 1-100 $\mathtt{m}$M Glu destroys many cultured cortical neurons and by one hour neuronal damage is almost complete. However, the glial cells remain intact.

1.2 Previous Mathematical Models

In this section we focus on the previous mathematical models relating to our models such as the model of rod photoreceptors, neurotransmitter, and intracellular calcium. The modelling approach in this thesis involves the formulation of a system of ordinary differential equations.

Firstly we address some previous mathematical models for rod photoreceptors. Andreucci *et al.* [53] have developed a model describing the correlation between the transversal and longitudinal diffusion of cGMP which is a cyclic guanosine monophosphate derived from guanosine triphosphate (GTP) and calcium in the rod outer segment of vertebrates. It is noted that cGMP acts as a second messenger. This model presents the excitation phase of the signalling cascade of rod outer segment in response to illumination. Upon activation of a single rhodopsin (a pigment of the retina), cGMP changes are local and exhibit both a longitudinal and a transversal component and changes in the membrane are also highly localised. The spatial spread of the single photon response along the longitudinal axis of the outer segment is predicted to be $3-5$ $\mathtt{m}$m.

In addition, the models of Caruso *et al.* [54] and Khanal *et al.* [55] incorporate the mechanisms presented by Andreucci *et al.* [53] to operate in rod phototransduction.

These models are reduced to simpler models. A spatio-temporal model for diffusion of second messengers in rod phototransduction to predict single-photon response is presented in [54]. This model shows strong localisation of the response about the activation site and allows quantification of the longitudinal spread at any particular time. They notice that maximum separation of activated sites produces maximum responses, which by itself can build variability of dim light responses apart from any other factors. Khanal *et al.* [55] in turn study this model by comparing the electrical response from rod geometry of mouse and human with that of salamander. They demonstrate that the thinner the rod outer segment the higher the response, and the higher the number of disc of outer segment the lower the response.

Next, there are many mathematical models studied in the Glu-Gln cycle, since this cycle is important to the neurotransmitter metabolism and involves cell death. Kleinle *et al.* [56] develop a three-dimensional model for release and diffusion of Glu in the synaptic cleft. This model composes of a source function describing transmitter release from the vesicle and a diffusion function describing the spread of transmitter in the cleft. They suggest that for each release site a corresponding receptor aggregate exists, subdividing an individual synapse into independent functional subunits without the need for specific lateral diffusion barriers.

In addition, Gruetter *et al.* [24] propose an ODE model for cerebral compartmentation of three different amino acids (Glu, Gln and Asp) after administration of glucose, the major source of energy in the brain. This study assesses the rate of exchange between the cytosolic amino acids and their mitochondrial Krebs cycle counterparts. This exchange is disputed by the malate-aspartate shuttle, providing a mechanism by which Asp and Glu can be labelled from the Krebs cycle through transport of Asp and Glu by the Asp/Glu antiporter. The metabolic relationship between Glu and Gln implies that the relative distribution of the label in the different positions of Gln must be the same as that of Glu, with the assumption that the large neuronal pool is the dominant source of the label for the glial pool of Gln.

Recently, Uffmann and Gruetter [57] have presented a new approach for the mathematical modelling of carbon-13 (^{13}C) label incorporation into amino acids (Glu and Asp) via the TCA cycle (Krebs cycle) that eliminates the explicit calculation of the labelling of the TCA cycle intermediate. This model is based on the model of [24] that includes the following steady-state assumption: metabolic concentrations and fluxes are constant,

and the TCA cycle concentration is compared with Glu and Asp concentrations. They conclude that the explicit solution of the labelling of the TCA cycle intermediates can be eliminated from the model. This model offers a formal method to study the principles of label kinetics in such ^{13}C turnover experiments leading to analytical expressions.

We now turn our attention to models for intracellular calcium. Calcium plays a similar role as a messenger, not only within single cells but also between multiple cells. The study of the calcium dynamics shows many mathematical similarities with models based on electrical excitability. The early model of Goldbeter *et al.* [58] for calcium release assumes the existence of two distinct internal calcium stores. One is sensitive to inositol (1,4,5)-triphosphate (IP_3) receptor, and another is sensitive to calcium. Stimulation leads to the production of IP_3 which releases calcium from the IP_3-sensitive store through IP_3 receptors. A key assumption of the model is that the concentration of calcium in the IP_3-sensitive store remains constant, as the store is rapidly refilled from the extracellular matrix.

Subsequently, in 1993 Sneyd *et al.* [59] include diffusion in the model of [58] and consider a piecewise linear simplification of the model and also construct travelling pulse and periodic plane wave solutions to the simplified model. They show the existence of a travelling pulse in the simplified model and it appears to be unique. The travelling pulse is the limit of a family of periodic plane wave solutions as the period tends to infinity. There are two travelling pulse solutions, one stable and one unstable.

This model is then extended in [60] for calcium oscillations so that it includes spatial diffusion of calcium in a cell with discrete active loci of wave amplification. The new model predicts that different locations in the cell can have different frequencies of oscillations. The amplification loci are thought to be specialised areas of the endoplasmic reticulum (ER) membrane containing a higher density or higher sensitivity of IP_3 receptors. It is showed that in astrocytes (one of the glial cell types) receptor mediated calcium signals appear as waves supported by calcium release at multiple cellular loci acting as weakly coupled oscillators each with its intrinsic latency and frequency of oscillation. Thus the appearance of propagated calcium wave may be a reflection of these differences rather than an actual diffusional wave propagation.

Recently, many mathematical models have been proposed to describe intracellular calcium oscillations that are oscillatory changes in free cytosol calcium concentration,

playing an important role in cell signalling. Marhl *et al.* [61] present a mechanism for complex calcium oscillations focussing on calcium exchange between the cytosol and the three calcium stores in the cell: the ER, mitochondria and cytosolic proteins. They have found that the most calcium (approximately 80%) released from the ER is cleared first into the mitochondria. By contrast, a very slow calcium release from the mitochondria back to the cytosol is crucial for understanding this mechanism of complex calcium oscillations. This causes bursting calcium oscillations.

Furthermore, [62] proposes a mathematical model for a role of mitochondria in the regulation of the amplitude during calcium oscillations. In this model mitochondria act as buffers effectively limiting the amplitude of calcium oscillations and keeping the amplitude constant. The simple plausible rate laws for mitochondrial calcium influx and efflux have been used with a positive effect on the constancy of the amplitude. However, as the effect is only observed in one specific model and there is a need for finding universal effects in order to make theoretical results far-reaching, it is important to verify the observations with other models.

Grubelnik *et. al* [63] use the same kinetic equations for calcium exchange across the inner mitochondrial membrane as in [62], and they can be inserted in a modular way in other mathematical models for spiking and bursting calcium oscillations including a store-operated model of [61]. They find that the amplitude of calcium oscillations is regulated by the sequestration of calcium in the mitochondria. Once entering the mitochondrial matrix, calcium is buffered very rapidly in a reversible manner with a very high effective calcium binding ratio (approximately 5000).

Finally, we will move to the excitotoxicity models, in particular the occurrence of glutamate and calcium by referring to the previous models. For example, Dronne *et al.* [40] present a mathematical model in order to simulate neuron and glial behaviours during stroke, and in order to study the influence of glial cell on the surrounding cell survival. This model is based on electrophysiological mechanisms and reproduces the movements of several ionic species such as glutamate, calcium, sodium, potassium and chloride ionised form, across the neuronal and glial membranes during the excitotoxicity process. This model is shown to be robust both in severe and moderate ischaemia. Furthermore, this model is improved by the same authors in [40]. The new model is studied the influence of diffusion phenomena on brain cell behaviours during ischaemia by including diffusion terms in the ECS and from the glial cell to another

through gap junctions [64].

Tiveci *et al.* [65] propose a model of calcium dynamics in brain energy metabolism in order to study Alzheimer's disease (AD). Calcium is not only an important molecule for signalling in neurons but it is also essential for memory storage. They find that in the case of AD, the effect of halved cerebral blood flow increase results in a negative blood oxygenation level dependent signal implying suppressed neural activity.

1.3 Outline of Thesis

In this work, we shall focus on two different models, rod photoreceptor metabolism and the glutamate-glutamine cycle. Firstly we present a nonlinear mathematical model for rod photoreceptor metabolism consisting of the length of the outer segment of the rod, and the concentrations of glucose and oxygen both in the outer and inner segments. Secondly, we describe nonlinear ordinary differential equations of the glutamate-glutamine cycle in the nervous system as the eye uses one of these systems. Next calcium signalling in the glutamate-glutamine cycle is presented as the basis of excitotoxicity. The work is organised as follows:

In Chapter 2 we present the model development for rod photoreceptor metabolism composed of five time-dependent ordinary differential equations. Analysis of the rod system will be carried out by investigating the steady-state solutions for the full model together with results for submodels in which either oxygen or glucose is assumed to be the rate-limiting metabolite. Numerical simulations of the system for each submodel are shown to agree with our analysis.

In Chapter 3 a mathematical model is developed to describe the glutamate-glutamine cycle in the nervous system. The model is studied using a combination of numerical and analytical techniques. Numerical solutions imply that qualitative dynamics of the system do not change when e is varied from a physically realistic value ($e = 0.5$) to an asymptotically small value ($e = 0.05 \ll 1$). The qualitative agreement motivates performing an asymptotic analysis of the governing equations in the asymptotic limit ($e \ll 1$). The analysis provides insight into the processes that regulate different timescales of the glutamate-glutamine cycle.

In Chapter 4 we extend the model of the glutamate-glutamine cycle from Chapter 3 in order to investigate how calcium, an important intracellular messenger, regulates the glutamate-glutamine cycle. Model analysis and simulations are presented. In addition, we consider when our system affects excitotoxicity by including a constant toxic source into the ODE for extracellular glutamate. This model forms the basis of our study of excitotoxicity.

In Chapter 5 the main conclusions from Chapters 2-4 are presented in addition to suggestions for future work.

CHAPTER 2

Model of Light/Dark Regulation of Length of the Outer Segment

In this chapter we examine rod photoreceptor metabolism. Our model will be presented in term of oxygen and glucose levels in two segments: the inner and outer segments. We investigate whether changes in metabolic demand during periods of light and dark are able to explain the observed (daily) variation in the length of the photoreceptor cells.

In §2.1, we recap the biology background, describing rod photoreceptors and cellular energy metabolism in order to develop a mathematical model in the subsequent section. In §2.2 we begin by developing a mathematical model for rod photoreceptor metabolism in which oxygen and glucose are assumed to be the rate-limiting nutrients and all other species are assumed to be present in abundance. In order to account for observed changes in the length of the outer segment during periods of light and dark, we couple our metabolic model to an ordinary differential equation (ODE) for the length of the rod outer segment. Model analysis and numerical simulations are presented in the following section. In the last section we summarise our findings and discuss model shortcomings and possible extensions.

2.1 Introduction

The photoreceptor cell is one of five layers in the retina which is important in sending and receiving light (see Figure 2.1 for a re-cap of the retinal layers). There are two different cell types of photoreceptors, rods and cones, situated on the outer side of the retina.

Each photoreceptor is a long narrow cell with an outer and inner segment, connected by the cilium, and a synaptic terminal at the end of the photoreceptor, lying closest to the bipolar cells. The inner segment contains a large number of mitochondria and a nucleus. We note that we consider the synaptic terminal as a part of the inner segment in our developed model. On the other hand, the outer segment (see Figure 2.2 for a re-cap of the photoreceptor cells) is composed of membranous discs with an abundance of photopigment molecules. Photopigments are able to distinguish between rod and cone. The rod cells consist of one photopigment, rhodopsin, which is important in vision at night, while colour pigments are in the cone cells only. The latter are important for vision in day time [1, 4, 5]. It can be said that rod cells dominate the human retina since there are approximately 30 times more rods than cones.

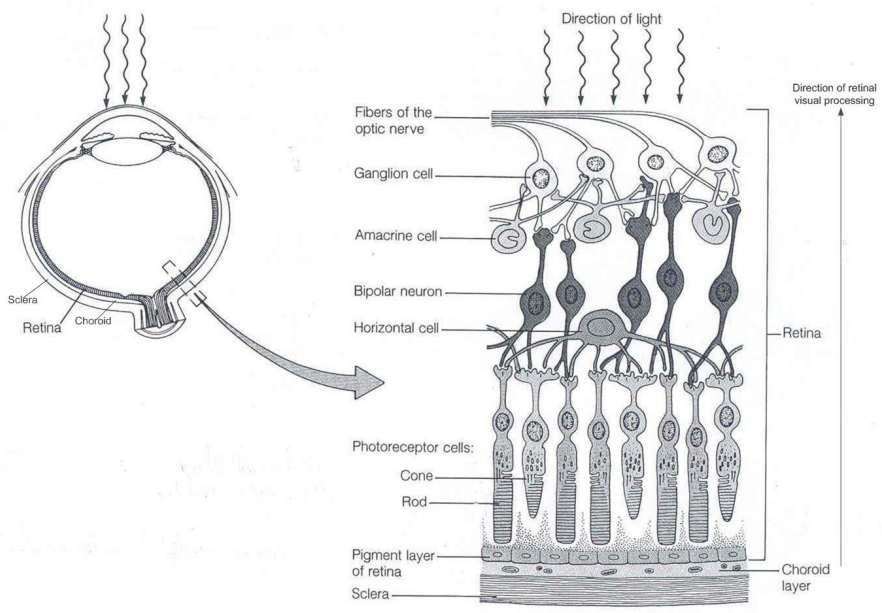

Figure 2.1: A re-cap of the retinal layers. (Figure is adapted from [1].)

The photoreceptors shed the oldest discs from the outer segments, and these are taken up and digested by the retinal pigment epithelium (RPE). New discs grow in the region of the cilium. As each new disc is formed at the junction between the outer and inner segment, the older discs are pushed outward towards the RPE. The process of shedding in rods occurs mainly in the morning or, following prolonged periods of darkness, when light reappears. In humans, the rod outer segment is entirely replaced every 8 to 14 days. By contrast, in cone cells this process occurs at night and it takes approximately one month for complete renewal [5–8]. It is known that the length of the rod outer segment increases during the dark period [9]. In our work we focus on only the

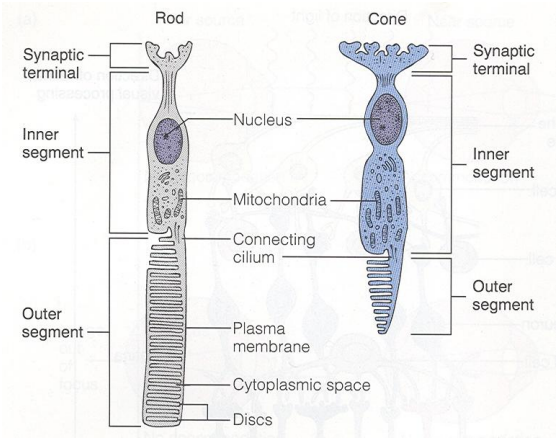

Figure 2.2: A re-cap of the photoreceptor cells (adapted from [1]).

rod photoreceptor metabolism since it is believed that it dominates the photoreceptor cells.

Photopigment has to be synthesised to maintain a photoreceptor's ability to respond to light. Synthesis of photopigment requires energy and the energy for physiological function is derived from the high-energy phosphate compound ATP. There are two main types of cellular energy metabolism [4]: anaerobic and aerobic metabolism.

- Anaerobic metabolism does not consume oxygen and is able to occur in two different ways. The first source for supplying additional ATP is CP which is used to convert ADP rapidly to ATP and Cr (see reaction (2.1.1) for a re-cap reaction (1.1.1)). This reaction is reversible. The forward reaction occurs when the cells need energy by using the enzyme CK and the reverse reaction occurs when the cells have excess energy by using the enzyme CPK.

$$\mathrm{CP} + \mathrm{ADP} \underset{\mathrm{CPK}}{\overset{\mathrm{CK}}{\rightleftharpoons}} \mathrm{Cr} + \mathrm{ATP}\,, \tag{2.1.1}$$

  When the cell needs energy, the forward reaction of reaction (2.1.1) is the first source. However, the amount of ATP is limited by the initial concentration of CP in the cell by this process. If the cell needs energy for more than a few seconds, the other sources to form ATP must be used.

  The other approach is anaerobic glycolysis, in which glucose produces two moles

of ATP and two moles of pyruvate (see reaction (2.1.2) for a re-cap reaction (1.1.2)).

$$\text{Glucose} + 2\text{NAD}^+ + 2\text{ADP} + 2\text{P}_\text{i} \rightarrow 2\text{Pyruvate} + 2\text{ATP} + 2\text{NADH} + 2\text{H}^+ \quad (2.1.2)$$

- The latter metabolism, aerobic metabolism, does consume oxygen. This takes place within the mitochondria, which are the sites of energy production and contain enzymes of the Krebs cycle. The Krebs cycle, also named as the tricarboxylic acid cycle (TCA) refers specially to a complex series of chemical reactions in all utilise oxygen as part of their respiration process [4].

  Pyruvate, which is produced from glycolysis pathway, is converted to acetyl CoA on entering the Krebs cycle in the mitochondria (see Figure 2.3 for a re-cap of anaerobic glycolysis and aerobic metabolism). This process produces 36 moles of ATP from one mole of glucose and six moles of oxygen. Although providing a rich yield of ATP for each molecule of glucose, this process is relatively slow because of the number of steps involved. In addition, it requires a constant supply of oxygen.

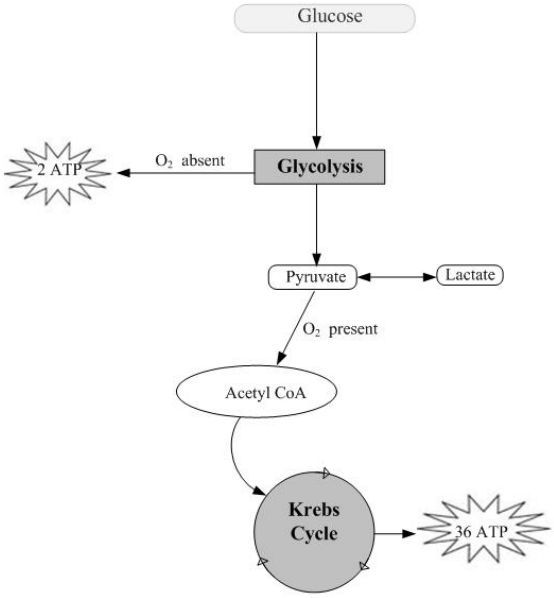

Figure 2.3: A re-cap of the anaerobic glycolysis and aerobic metabolism.

Since the amount of ATP that can be formed by CP process is limited, we only consider the amount of ATP that can be formed by glycolysis for anaerobic metabolism. The outer segment relies upon anaerobic metabolism because it does not contain any mito-

chondria. By contrast, the inner segment uses both aerobic metabolism and anaerobic metabolism (the latter if oxygen is insufficient).

2.2 Model Development and Nondimensionalisation

In this section, we develop an ordinary differential equation (ODE) model of rod photoreceptor metabolism in which oxygen and glucose are assumed to be the rate-limiting nutrients and all other species are assumed to be present in abundance. In order to account for observed changes in the length of the outer segment during periods of light and dark, we couple our metabolic model to an ODE for the length of the outer segment, $L_{os}(t)$.

We treat the outer segment (OS) and inner segment (IS) as cylinders of equal radii. We denote by L_{is} and L_{os} the lengths (in metres, m) of the IS and OS, respectively, and by A the (assumed constant) cross-sectional area (m^2) of each rod. Our model is an ODE model in which the rod photoreceptor cell is decomposed into two compartments: the OS and the IS, i.e. we assume that each metabolite is uniformly distributed in each of the OS and the IS, but allow the concentrations in the two compartments to differ. We introduce x_{os}, x_{is}, y_{os} and y_{is} to denote the concentrations (in millimolars, mM) of oxygen (x) and glucose (y) in the OS and IS. We use the principle of mass balance to derive ODEs for the concentrations of oxygen and glucose in both compartments. Figure 2.4 illustrates how oxygen and glucose enter the rod and how oxygen exchanges between the OS and the IS.

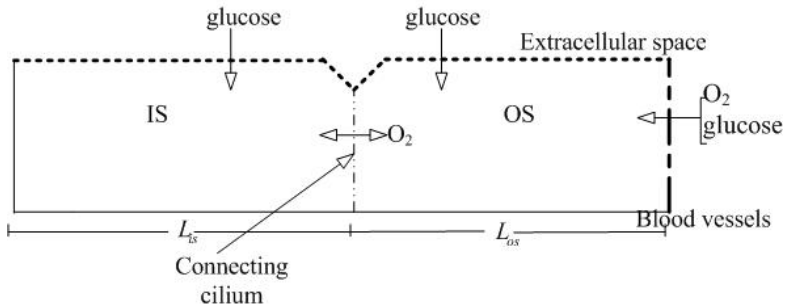

Figure 2.4: A schematic diagram of rod photoreceptor showing how oxygen and glucose enter the OS and the IS and how oxygen exchange between the OS and the IS (see description of this diagram in §2.2.1).

2.2.1 Mass Balance Equations

Here we apply the principle of mass balance to oxygen and glucose in each compartment to derive ODEs for their time evolution. Oxygen and glucose enter the cell through the OS from the blood vessels of the choroid. Since glucose is water soluble and transported across cell membranes, it can also diffuse through the extracellular space and, from there, enter both the OS and IS [66, 67]. Not all chemicals can pass, via the cilium, between the OS and IS. For example, while oxygen is freely exchanged, glucose is not (see Figure 2.4) [68]. Here we introduce x^{bl} and y^{bl} to represent the assumed constant concentrations of oxygen and glucose, respectively, in the vasculature. We assume that the concentration of glucose in the ECS is equal to y^{bl}.

When considering the evolution of x_{os}, the oxygen concentration in the OS, we suppose that the dominant factors are:

- the rate at which oxygen enters from the vasculature,
- the rate at which it exchanges with the IS (via the connecting cilium),
- the rate at which it undergoes natural decay.

We assume that the rate at which oxygen enters the OS from the vasculature is proportional to $(x^{bl} - x_{os})$. Similarly the rate at which oxygen passes from the OS to the IS is proportional to $(x_{os} - x_{is})$. Combining the above and noting that the total amount of oxygen in the OS is given by $(AL_{os}x_{os})$, we deduce that the evolution of x_{os} satisfies:

$$\frac{d(AL_{os}x_{os})}{dt} = k_{os}A(x^{bl} - x_{os}) - k_oA(x_{os} - x_{is}) - k_rAL_{os}x_{os}. \tag{2.2.1}$$

In equation (2.2.1), the positive constants k_{os}, k_o and k_r represent respectively the rates at which oxygen enters the OS from the blood, the rate at which it exchanges with the IS and its natural decay rate.

Next we consider the evolution of the oxygen concentration in the IS, x_{is}. We presume that there are three factors:

- the rate at which oxygen passes from the OS to the IS,
- the rate at which oxygen is consumed in the IS,
- the rate at which it undergoes natural decay.

We assume that because glucose, which is used in glycolysis, serves as a common pathway for aerobic respiration, the rate at which oxygen is consumed in the IS is proportional to the concentration of glucose in the IS, y_{is}, multiplied by the total amount of oxygen in the IS ($AL_{is}x_{is}$). Combining the above factors, we deduce that the evolution of x_{is} satisfies:

$$\frac{d(AL_{is}x_{is})}{dt} = k_o A(x_{os} - x_{is}) - KAL_{is}x_{is}y_{is} - k_{rr}AL_{is}x_{is}. \tag{2.2.2}$$

The positive constants K and k_{rr} in equation (2.2.2) are the rates at which oxygen is consumed in the IS and its natural decay rate, respectively.

In a similar manner, we may derive an ODE for the glucose concentration in the OS, y_{os}. We assume that the dominant factors are:

- the rate at which glucose enters from the blood and the ECS,
- the rate at which it is consumed in the OS,
- the rate at which it undergoes natural decay.

We denote by A_1 the assumed constant area for exchange of glucose from the blood and the ECS into the OS and we assume that A_1 is equal to the area for exchange of glucose from the extracellular space into the IS ($A_1 = 2\mathrm{p}rL_{is} \approx 60\mathrm{p}r^2$ (m^2) where r is a radius of the rod (1×10^{-6} m [69])). Here we assume that the rate at which glucose enters the OS from the vasculature and the ECS is proportional to $(y^{bl} - y^{os})$. As for x_{is} (see equation (2.2.2)), we assume that the rate at which glucose is consumed in the OS is $y_{os}x_{os}$. By combining the above we deduce that the evolution of y_{os} is:

$$\frac{d(AL_{os}y_{os})}{dt} = k_{in}A_1(y^{bl} - y_{os}) - RAL_{os}y_{os}x_{os} - k_g AL_{os}y_{os}. \tag{2.2.3}$$

In equation (2.2.3), the positive constants k_{in}, R and k_g represent respectively the rates at which glucose enters the OS, the rate at which it is consumed in the OS and its natural decay.

Finally, we consider the evolution of the glucose concentration in the IS, y_{is}. We presume that the main factors are:

- the rate at which glucose enters from the extracellular space,

- the rate at which glucose is consumed due to glycolysis (when the oxygen supply is not high enough) and due to aerobic respiration,
- the rate at which it undergoes natural decay.

We assume that the rate at which glucose enters the IS is proportional to $(y^{bl} - y_{is})$. We also assume that the rate at which glucose is consumed due to glycolysis is proportional to x_{is}, multiplied by the total amount of glucose in the IS ($AL_{is}y_{is}$). Thus we obtain:

$$\frac{d(AL_{is}y_{is})}{dt} = k_{in}A_1(y^{bl} - y_{is}) - QAL_{is}y_{is}x_{is} - PAL_{is}y_{is} - k_aAL_{is}y_{is}. \quad (2.2.4)$$

The positive constants Q, P and k_a in equation (2.2.4) represent respectively the rates at which glucose is consumed due to glycolysis and aerobic respiration, and its natural decay rate.

2.2.2 The length of the OS

Since the OS sheds and renews discs, its length varies over time and we must therefore incorporate the growth rate of the OS into our model. We assume that the OS obtains energy from the IS to maintain and increase its length, so that any excess energy that is produced in the IS is transported into the OS, where it is used to maintain the length of the OS. If there is sufficient surplus energy, then growth of the OS occurs [5]. If there is a deficit of energy, then the OS sheds discs into the RPE.

We assume that there is a surplus of oxygen and glucose only in the IS. These surpluses are given by the net difference between energy production and energy consumption. Energy can be produced from oxygen only in the IS but is consumed in both the IS and the OS. We assume that energy is produced and consumed due to glucose in the same way. However, there is a maximum rate at which discs in the OS can be produced, [1, 5]. We suppose that the energy production in the IS from the oxygen and glucose is proportional to respectively $x_{is}L_{is}$ and $y_{is}L_{is}$, the energy consumption due to oxygen and glucose in the OS and IS are X_1L_{is}, x_2L_{os}, and Y_1L_{is} and y_2L_{os}, respectively, and the maximum rate at which discs are produced is proportional to $(k_4x_{is}L_{is} + 1)^{-1}$ (for oxygen), and $(g_4y_{is}L_{is} + 1)^{-1}$ (for glucose). By combining these ideas we deduce that:

$$\frac{d(L_{os})}{dt} = \frac{k_1x_{is}L_{is} - k_2X_1L_{is} - k_3x_2L_{os}}{(k_4x_{is}L_{is} + 1)} + \frac{g_1y_{is}L_{is} - g_2Y_1L_{is} - g_3y_2L_{os}}{(g_4y_{is}L_{is} + 1)}, \quad (2.2.5)$$

where k_1, k_2, k_3, k_4, g_1, g_2, g_3, g_4, X_1, x_2, Y_1 and y_2 are positive constants.

In summary, our model system comprises equations (2.2.1)-(2.2.5). The physical meaning and units of all model parameters are given in Table 2.1.

2.2.3 Nondimensionalisation

Since the rates of oxygen and glucose consumption are different under light and dark conditions (see Table 2.2), we separate our model (2.2.1)-(2.2.5) into two submodels, for dark and light conditions. The parameters that are affected are K, R, P, Q, X_1 and Y_1.

We now nondimensionalise the model equations (2.2.1)-(2.2.5) by introducing the following dimensionless variables:

$$\hat{x}_{os} = \frac{x_{os}}{X}, \;\; \hat{x}_{is} = \frac{x_{is}}{X}, \;\; \hat{L}_{os} = \frac{L_{os}}{L}, \;\; \hat{y}_{os} = \frac{y_{os}}{Y}, \;\; \hat{y}_{is} = \frac{y_{is}}{Y}, \;\; \hat{t} = \frac{t}{T}, \tag{2.2.6}$$

where the constants X, Y, L and T are characteristic values of oxygen and glucose concentration, length and time, respectively, and are chosen as follows

$$X = x^{bl}, \;\; Y = y^{bl} \;\text{ and }\; L = L_{is}.$$

We use the length of the IS divided by the oxygen flow from the OS to IS to fix the timescale, so that $T = \dfrac{L_{is}}{k_o}$. Therefore, under dark conditions our model equations become:

$$\frac{d\hat{x}_{os}}{d\hat{t}} = \frac{\hat{k}_{os}}{\hat{L}_{os}}(1-\hat{x}_{os}) - \frac{1}{\hat{L}_{os}}(\hat{x}_{os}-\hat{x}_{is}) - \hat{k}_r\hat{x}_{os} - \frac{\hat{x}_{os}}{\hat{L}_{os}}\frac{d\hat{L}_{os}}{d\hat{t}}, \tag{2.2.7}$$

$$\frac{d\hat{x}_{is}}{d\hat{t}} = (\hat{x}_{os}-\hat{x}_{is}) - (\hat{k}_d\hat{y}_{is} + \hat{k}_{rr})\hat{x}_{is}, \tag{2.2.8}$$

$$\frac{d\hat{y}_{os}}{d\hat{t}} = \frac{\hat{k}_{in}}{\hat{L}_{os}}(1-\hat{y}_{os}) - (\hat{k}_d\hat{x}_{os} + \hat{k}_g)\hat{y}_{os} - \frac{\hat{y}_{os}}{\hat{L}_{os}}\frac{d\hat{L}_{os}}{d\hat{t}}, \tag{2.2.9}$$

$$\frac{d\hat{y}_{is}}{d\hat{t}} = \hat{k}_{in}(1-\hat{y}_{is}) - (\hat{q}_d\hat{x}_{is} + \hat{p}_d + \hat{k}_a)\hat{y}_{is}, \tag{2.2.10}$$

$$\frac{d\hat{L}_{os}}{d\hat{t}} = \frac{(\hat{k}_1\hat{x}_{is} - \hat{k}_2\hat{x}_d - \hat{k}_3\hat{x}_2\hat{L}_{os})}{(\hat{k}_4\hat{x}_{is}+1)} + \frac{(\hat{g}_1\hat{y}_{is} - \hat{g}_2\hat{y}_d - \hat{g}_3\hat{y}_2\hat{L}_{os})}{(\hat{g}_4\hat{y}_{is}+1)}, \tag{2.2.11}$$

Parameter	Physical Meaning	Units	Notes
L_{is}	the rod inner segment length	m	$L_{is} = 32 \times 10^{-6}$ m [69]
x^{bl}	the concentration of oxygen in blood vessels	mM	$x^{bl} = 0.0672$ mM [70]
y^{bl}	the concentration of glucose in blood vessels	mM	$y^{bl} = 4.5$ mM [70]
k_{os}	the flux per unit area of oxygen from blood vessels to the OS	ms^{-1}	$k_{os} = \frac{\text{oxygen diffusion}}{L_{is}}$ [70]
k_o	the flux per unit area of oxygen from the OS to IS	ms^{-1}	$k_o = \frac{\text{oxygen diffusion}}{L_{is}}$ [70]
k_{in}	the flux per unit area of glucose from blood vessels to the OS and IS	ms^{-1}	$k_{in} = \frac{\text{glucose diffusion}}{L_{is}}$ [70]
K	the rate of oxygen utilisation in the IS	$(\mathrm{mMs})^{-1}$	separated into dark (k_d) and light (k_l) [a1]
R	the rate of glucose consumption due to anaerobic respiration	$(\mathrm{mMs})^{-1}$	separated into dark (r_d) and light (r_l) [a1]
P	the rate of glucose consumption due to aerobic respiration	s^{-1}	separated into dark (p_d) and light (p_l) [a1]
Q	the rate of glucose consumption due to glycolysis respiration	$(\mathrm{mMs})^{-1}$	separated into dark (q_d) and light (q_l) [a1]
k_r and k_{rr}	the rate of oxygen removal through the outer surface of the OS and IS, respectively	s^{-1}	[a2]
k_g and k_a	the rate of glucose removal through the outer surface of the OS and IS, respectively	s^{-1}	[a2]
k_1 and g_1	that rate at which energy is produced by oxygen and glucose, respectively, supplied to IS	$(\mathrm{mMs})^{-1}$	[a2]
k_2 and k_3	the rate at which energy is consumed by oxygen in the IS and OS, respectively	$(\mathrm{mMs})^{-1}$	[a2]
X_1 and x_2	the concentration of oxygen constants in the IS and OS, respectively	mM	X_1 varying under dark (x_d) and light (x_l) conditions [a3]
g_2 and g_3	the rate at which energy is consumed by glucose in the IS and OS, respectively	$(\mathrm{mMs})^{-1}$	[a2]
k_4 and g_4	saturating energy by oxygen and glucose, respectively	$(\mathrm{mMm})^{-1}$	[a2]
Y_1 and y_2	the concentration of glucose constants in the IS and OS, respectively	mM	Y_1 varying under dark (y_d) and light (y_l) conditions [a3]

Table 2.1: Parameter values for the equations (2.2.1)-(2.2.5), ([a1] taken from Table 2.2, [a2] estimated in section 2.2.4 and [a3] fixed as shown in section 2.3.1).

where

$$\hat{k}_{os} = \frac{k_{os}}{k_o}, \quad \hat{k}_r = \frac{k_r L_{is}}{k_o}, \quad \hat{k}_{rr} = \frac{k_{rr} L_{is}}{k_o}, \quad \hat{k}_d = \frac{k_d L_{is} y^{bl}}{k_o}, \quad \hat{k}_1 = \frac{k_1 x^{bl} L_{is}}{k_o},$$
$$\hat{k}_2 = \frac{k_2 x^{bl} L_{is}}{k_o}, \quad \hat{k}_3 = \frac{k_3 x^{bl} L_{is}}{k_o}, \quad \hat{k}_4 = k_4 x^{bl} L_{is}, \quad \hat{x}_d = \frac{x_d}{x^{bl}}, \quad \hat{x}_2 = \frac{x_2}{x^{bl}},$$
$$\hat{k}_{in} = \frac{60 k_{in}}{k_o}, \quad \hat{r}_d = \frac{r_d L_{is} x^{bl}}{k_o}, \quad \hat{k}_g = \frac{k_g L_{is}}{k_o}, \quad \hat{k}_a = \frac{k_a L_{is}}{k_o}, \quad \hat{p}_d = \frac{p_d L_{is}}{k_o},$$
$$\hat{g}_1 = \frac{g_1 y^{bl} L_{is}}{k_o}, \quad \hat{g}_2 = \frac{g_2 y^{bl} L_{is}}{k_o}, \quad \hat{g}_3 = \frac{g_3 y^{bl} L_{is}}{k_o}, \quad \hat{g}_4 = g_4 y^{bl} L_{is}, \quad \hat{y}_d = \frac{y_d}{y^{bl}},$$
$$\hat{y}_2 = \frac{y_2}{y^{bl}}, \quad \hat{q}_d = \frac{q_d L_{is} x^{bl}}{k_o}.$$

We also obtain the analogous dimensionless model under light conditions by replacing $\hat{k}_d$, $\hat{r}_d$, $\hat{p}_d$, $\hat{q}_d$, $\hat{x}_d$ and $\hat{y}_d$ in equations (2.2.7)-(2.2.11) by $\hat{k}_l$, $\hat{r}_l$, $\hat{p}_l$, $\hat{q}_l$, $\hat{x}_l$ and $\hat{y}_l$, respectively, where $k_l = \frac{k_l L_{is} y^{bl}}{k_o}$, $\hat{r}_l = \frac{r_l L_{is} x^{bl}}{k_o}$, $\hat{p}_l = \frac{p_l L_{is}}{k_o}$, $\hat{q}_l = \frac{q_l L_{is} x^{bl}}{k_o}$, $\hat{x}_l = \frac{x_l}{x^{bl}}$ and $\hat{y}_l = \frac{y_l}{y^{bl}}$.

After dropping the hats for notational simplicity in the dimensionless equations, under dark conditions the full model becomes:

$$\frac{dx_{os}}{dt} = \frac{k_{os}}{L_{os}}(1 - x_{os}) - \frac{1}{L_{os}}(x_{os} - x_{is}) - k_r x_{os} - \frac{x_{os}}{L_{os}}\frac{dL_{os}}{dt}, \tag{2.2.12}$$
$$\frac{dx_{is}}{dt} = (x_{os} - x_{is}) - (k_d y_{is} + k_{rr}) x_{is}, \tag{2.2.13}$$
$$\frac{dy_{os}}{dt} = \frac{k_{in}}{L_{os}}(1 - y_{os}) - (r_d x_{os} + k_g) y_{os} - \frac{y_{os}}{L_{os}}\frac{dL_{os}}{dt}, \tag{2.2.14}$$
$$\frac{dy_{is}}{dt} = k_{in}(1 - y_{is}) - (q_d x_{is} + p_d + k_a) y_{is}, \tag{2.2.15}$$
$$\frac{dL_{os}}{dt} = \frac{(k_1 x_{is} - k_2 x_d - k_3 x_2 L_{os})}{(k_4 x_{is} + 1)} + \frac{(g_1 y_{is} - g_2 y_d - g_3 y_2 L_{os})}{(g_4 y_{is} + 1)}. \tag{2.2.16}$$

We obtain the analogous dimensionless model under light conditions by replacing k_d, r_d, p_d, q_d, x_d and y_d in equations (2.2.12)-(2.2.16) by k_l, r_l, p_l, q_l, x_l and y_l, respectively, where these new dimensionless parameters are also defined above.

2.2.4 Parameter Estimation

Where possible we obtain estimates from the literature (see references [3, 69–71]) as follows. The concentrations of oxygen and glucose in the blood vessels are 0.0672 (x^{bl}) and 4.5 (y^{bl}) mM, respectively and the length of the IS is 32×10^{-6} m [69, 70]. Diffusion co-

efficients of oxygen and glucose in water at 37^0C are 2.11×10^{-9} and 2×10^{-11} (m^2/s), respectively [70]. Values for ATP consumption rates (mM/s) [3] in each compartment under dark and light conditions are shown in Table 2.2 and we convert ATP consumption rates into oxygen and glucose consumption rates in each compartment (see Note under Table 2.2 for conversion of ATP consumption rates into oxygen and glucose consumption rates). In this way, the parameters k_{os}, k_d, k_l, k_{in}, r_d, r_l, p_d, p_l, q_d and q_l can be estimated (see Table 2.3).

We assume that the oxygen natural decay rate in the OS (k_r) equals the oxygen natural decay rate in the IS (k_{rr}) and that this rate of decay is less than the oxygen consumption (k_d and k_l). We also assume the glucose natural decay rate in the OS (k_g) equals the glucose natural decay rate in the IS (k_a) but the rate of decay is similarly less than the consumption of glucose (r_d, p_d, q_d, r_l, p_l and q_l). We fix $k_r = k_{rr} = 0.1$ and $k_g = k_a = 0.01$. Additionally we set $k_1 = 12$, $k_2 = 2$, $k_3 = 12$, $k_4 = 1$, $g_1 = 0.2$, $g_2 = 0.2$, $g_3 = 0.4$ and $g_4 = 1$. We also assume that the concentrations of oxygen and glucose constants in the IS and OS under dark and light conditions (x_d, x_l, x_2 and y_d, y_l, y_2, respectively) are less than x^{bl} and y^{bl}, respectively. However, it is noted that the available information about these six parameters (x_d, x_l, x_2, y_d, y_l and y_2) is insufficient to enable an estimation of their values.

	ATP (mM/s)[b]		oxygen (mM/s)		glucose (mM/s)	
	dark	light	dark	light	dark	light
OS	0.03	0.135	-	-	0.015	6.75×10^{-2}
IS	2.52	1.14	0.42	0.19	1.26 (anaerobic) 0.07 (aerobic)	0.57(anaerobic) 3.2×10^{-2} (aerobic)

Table 2.2: ATP, oxygen and glucose consumptions in each compartment under dark and light conditions ([b] taken from [3]).

Notes:

- As mentioned in section 2.1, in cell metabolism a mole of glucose yields two moles of ATP for anaerobic glycolysis. In addition, for aerobic metabolism (in the Krebs cycle) one mole of glucose and six moles of oxygen convert to 36 moles of ATP, [5, 67].
- Values for ATP consumption in the IS are divided by six to give the oxygen consumption in the IS and those in the OS are divided by two to give the glucose consumption in the OS. For glucose consumption in the IS, there are two pathways, anaerobic and aerobic metabolism. Thus ATP consumption values are divided by two to give the glucose consumption due to anaerobic metabolism and by 36 to give that due to aerobic metabolism. Oxygen and glucose consumption in each compartment under dark and light conditions is shown as Table 2.2.

We set $x_2 = 0.03$ and $y_2 = 1.8$ and then we consider how values, x_d, x_l, y_d and y_l affect the length of the OS. We plot a contour (see Figure 2.5) of the length of the OS under light conditions (L^l_{os}) against its value under dark conditions (L^d_{os}) (see expressions of L^d_{os} and L^l_{os} in §2.3.1) by varying only the concentrations of the oxygen constant under light conditions (x_l) from 0 to 0.07 mM and those of the glucose constant under light conditions (y_l) from 0 to 4 mM, with other parameter values stated above. The contour plot shows that when $x_l > x_d$ and $y_l > y_d$, the ratio of L^l_{os}: L^d_{os} is less than one. By contrast, when $x_l < x_d$ or $y_l < y_d$, the ratio is greater than one. Therefore, we predict that we need $y_l > y_d$ and $x_l > x_d$ in order to ensure that the length of the OS is greater under dark than light conditions, replicating the biological results [9]. Hence we fix $x_d = 0.01$, $x_l = 0.06$, $x_2 = 0.03$, $y_d = 1.5$, $y_l = 2.5$ and $y_2 = 1.8$.

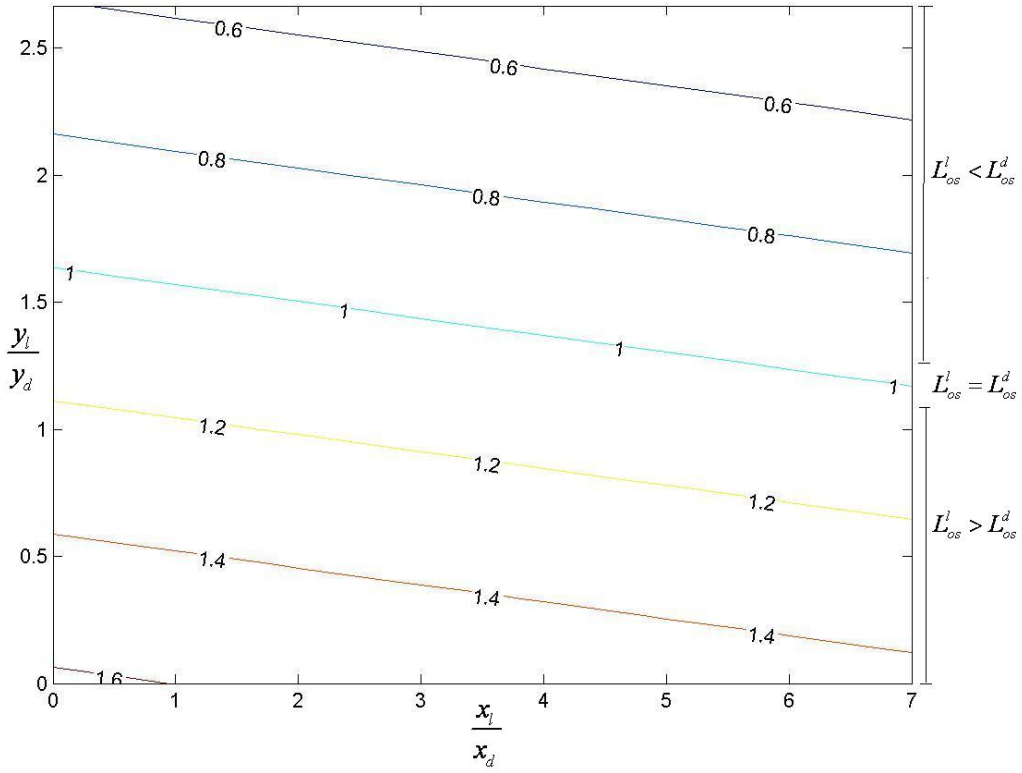

Figure 2.5: A contour plot of $\frac{L^l_{os}}{L^d_{os}}$ in the full model with the parameter values in 2.3 and varying only the values of x_l from 0 to 0.07 and y_l from 0 to 4, shows that $L^d_{os} > L^l_{os}$ only where $\frac{x_l}{x_d}$ and $\frac{y_l}{y_d}$ are sufficiently large. By contrast, $L^l_{os} > L^d_{os}$, when $\frac{x_l}{x_d}$ or $\frac{y_l}{y_d}$ are sufficiently small.

The dimensional parameter values as mentioned above are shown in Table 2.3 where we also show dimensionless parameter values of the full model under dark and light

Parameters	Dimensional	Dimensionless
k_{os}	6.59×10^{-5} (ms^{-1}) [70]	1
k_d	0.42 $(mMs)^{-1}$ [c1]	0.917
k_l	0.19 $(mMs)^{-1}$ [c1]	0.415
k_r	0.1 (s^{-1}) [c2]	0.0485
k_{rr}	0.1 (s^{-1}) [c2]	0.0485
x_d	0.01 (mM) [c3]	0.15
x_l	0.06 (mM) [c3]	0.89
x_2	0.03 (mM) [c3]	0.45
k_1	12 $(mMs)^{-1}$ [c4]	3.9×10^{-1}
k_2	2 $(mMs)^{-1}$ [c4]	6.5×10^{-2}
k_3	12 $(mMs)^{-1}$ [c4]	3.9×10^{-1}
k_4	1 $(mMm)^{-1}$ [c4]	2.2×10^{-6}
k_{in}	6.25×10^{-7} (ms^{-1}) [70]	0.569
r_d	0.015 $(mMs)^{-1}$ [c1]	4.89×10^{-4}
r_l	6.75×10^{-2} $(mMs)^{-1}$ [c1]	2.2×10^{-3}
p_d	0.07 (s^{-1}) [c1]	3.4×10^{-2}
p_l	32×10^{-2} (s^{-1}) [c1]	1.54×10^{-2}
q_d	1.26 (mMs^{-1}) [c1]	4.11×10^{-2}
q_l	0.57 (mMs^{-1}) [c1]	1.86×10^{-2}
k_g	0.01 (s^{-1}) [c2]	4.85×10^{-3}
k_a	0.01 (s^{-1}) [c2]	4.85×10^{-3}
y_d	1.5 (mM) [c3]	0.33
y_l	2.5 (mM) [c3]	0.56
y_2	1.8 (mM) [c3]	0.40
g_1	0.2 $(mMs)^{-1}$ [c4]	0.44
g_2	0.2 $(mMs)^{-1}$ [c4]	0.44
g_3	0.4 $(mMs)^{-1}$ [c4]	0.87
g_4	1 $(mMm)^{-1}$ [c4]	1.44×10^{-4}

Table 2.3: All dimensional and dimensionless parameter values of the full model.

Notes:
- [c1] taken from Table 2.2,
- [c2] we estimate $k_r = k_{rr} <$ oxygen consumption, and $k_g = k_a <$ glucose consumption,
- [c3] we estimate $x_d,\ x_2,\ x_l < x^{bl}$ and $y_d,\ y_2,\ y_l < y^{bl}$,
- [c4] we have fixed these values.

conditions.

2.3 Model Analysis and Simulations

In the previous section we developed a simple model to describe how the length of the OS changes over time and how its evolution is related to the oxygen and glucose levels in the IS and OS. In this section we analyse our model by first finding steady-state solutions and then presenting numerical simulations.

2.3.1 The Full Model

We start by constructing steady-state solutions of equations (2.2.12)-(2.2.16) under dark conditions. We denote by x_{os}^d, x_{is}^d, y_{os}^d, y_{is}^d and L_{os}^d the steady-state solutions under dark conditions of, respectively, the concentrations of oxygen in the OS and IS, glucose in the OS and IS and the OS length.

Steady-State Analysis

From equations (2.2.13) and (2.2.15), we deduce

$$y_{is}^d = \frac{k_{in}}{k_{in} + p_d + k_a + q_d x_{is}^d} \equiv \frac{k_{in}}{(\mathrm{n}_1 + q_d x_{is}^d)}, \tag{2.3.1}$$

where $\mathrm{n}_1 = k_{in} + p_d + k_a$,

$$x_{os}^d \;=\; (1 + k_{rr} + k_d y_{is}^d) x_{is}^d = \left(1 + k_{rr} + k_d \frac{k_{in}}{\mathrm{n}_1 + q_d x_{is}^d}\right) x_{is}^d. \tag{2.3.2}$$

From equation (2.2.12), (2.3.1) and (2.3.2), we have

$$L_{os}^d = -\frac{q_d(k_{os}(1+k_{rr}) + k_{rr}){x_{is}^d}^2 + ((1+k_{os})(k_{rr}\mathrm{n}_1 + k_d k_{in}) + k_{os}(\mathrm{n}_1 - q_d))x_{is}^d - k_{os}\mathrm{n}_1}{k_r q_d (1+k_{rr}){x_{is}^d}^2 + k_r(\mathrm{n}_1(1+k_{rr}) + k_d k_{in})x_{is}^d}, \tag{2.3.3}$$

while equations (2.2.16) and (2.3.1) give us

$$\begin{aligned} L_{os}^d \;=\; & [q_d(k_1 - g_2 y_d k_4){x_{is}^d}^2 + (k_{in}(g_1 k_4 + k_1 g_4) + \mathrm{n}_1(k_1 - g_2 y_d k_4) - q_d(k_2 x_d - g_2 y_d))x_{is}^d \\ & - k_2 x_d(\mathrm{n}_1 + g_4 k_{in}) - g_2 y_d \mathrm{n}_1 + g_1 k_{in}] / [g_3 y_2 k_4 q_d {x_{is}^d}^2 + (k_3 x_2 q_d + g_3 y_2(k_4 \mathrm{n}_1 + q_d))x_{is}^d \\ & + k_3 x_2 g_4 k_{in} + k_3 x_2 \mathrm{n}_1 + g_3 y_2 \mathrm{n}_1]. \end{aligned} \tag{2.3.4}$$

By equating equations (2.3.3) and (2.3.4), we derive a quartic equation for x_{is}^d, namely:

$$D_1(x_{is}^d)^4 + D_2(x_{is}^d)^3 + D_3(x_{is}^d)^2 + D_4(x_{is}^d) + D_5 = 0, \tag{2.3.5}$$

where

$$
\begin{aligned}
D_1 &= {q_d}^2[k_r(1+k_{rr})(k_1-g_2y_dk_4)+g_3y_2k_4(k_{os}(1+k_{rr})+k_{rr})],\\
D_2 &= k_rq_d(1+k_{rr})[k_1(g_4k_{in}+\mathrm{n}_1)+k_4(g_1k_{in}-g_2y_d\mathrm{n}_1)-q_d(k_2x_d-g_2y_d)]\\
&\quad +g_3y_2k_4q_d[k_{rr}\mathrm{n}_1+k_dk_{in}-k_{os}(q_d+\mathrm{n}_1(1+k_{rr})+k_dk_{in})]\\
&\quad [k_3x_2q_d+g_3y_2(k_4\mathrm{n}_1+q_d)][k_{os}q_d(1+k_{rr})+k_{rr}q_d]\\
&\quad +k_rq_d(k_1-g_2y_dk_4)[\mathrm{n}_1(1+k_{rr})+k_dk_{in}],\\
D_3 &= q_d(k_{os}(1+k_{rr})+k_{rr})[k_3x_2(g_4k_{in}+\mathrm{n}_1)+g_3y_2\mathrm{n}_1][k_{os}q_d(1+k_{rr})+k_{rr}q_d]\\
&\quad +[k_3x_2q_d+g_3y_2(k_4\mathrm{n}_1+q_d)][k_{rr}\mathrm{n}_1+k_dk_{in}-k_{os}(q_d+\mathrm{n}_1(1+k_{rr})+k_dk_{in})]\\
&\quad -k_{os}\mathrm{n}_1g_3y_2k_4q_d-k_rq_d(1+k_{rr})[\mathrm{n}_1(k_2x_d+g_2y_d)+k_{in}(k_2x_dg_4-g_1)]\\
&\quad +k_r(\mathrm{n}_1(1+k_{rr})+k_dk_{in})[k_1(g_4k_{in}+\mathrm{n}_1)+k_4(g_1k_{in}-g_2y_d\mathrm{n}_1)-q_d(k_2x_d+g_2y_d)],\\
D_4 &= [[k_3x_2(g_4k_{in}+\mathrm{n}_1)+g_3y_2\mathrm{n}_1][k_{os}(q_d+\mathrm{n}_1(1+k_{rr})+k_dk_{in})-k_{rr}\mathrm{n}_1-k_dk_{in}]\\
&\quad +k_r(\mathrm{n}_1(1+k_{rr})+k_dk_{in})[\mathrm{n}_1(k_2x_d+g_2y_d)+k_{in}(k_2x_dg_4-g_1)]]\\
&\quad +k_{os}\mathrm{n}_1[k_3x_2q_d+g_3y_2(k_4\mathrm{n}_1+q_d)],\\
D_5 &= -(k_3x_2(g_4k_{in}+\mathrm{n}_1)+g_3y_2\mathrm{n}_1)k_{os}\mathrm{n}_1.
\end{aligned}
$$

When x_{is}^d is known, we can then determine y_{is}^d, x_{os}^d and L_{os}^d from equations (2.3.1), (2.3.2), and (2.3.3), respectively. Using equations (2.2.14), (2.3.2) and (2.3.3) we deduce

$$
\begin{aligned}
y_{os}^d &= k_{in}(\mathrm{n}_1+q_dx_{is}^d)/[L_{os}^dr_dq_d(1+k_{rr}){x_{is}^d}^2\\
&\quad +(L_{os}^dr_d\mathrm{n}_1(1+k_{rr})+L_{os}^d(r_dk_dk_{in}+k_gq_d)+k_{in}q_d)x_{is}^d+\mathrm{n}_1(k_{in}+k_gL_{os}^d)].
\end{aligned}
\tag{2.3.6}
$$

We remark that if x_{is}^d and L_{os}^d are greater than zero, then the steady-state values of the other dependent variables are also greater than zero (see equations (2.3.1), (2.3.2) and (2.3.6)), this of course being required for the steady state to be physically meaningful. Assuming $x_{is}^d = a_0$ to be a positive real root of equation (2.3.5), we may rewrite (2.3.5) as

$$
\begin{aligned}
&(x_{is}^d-a_0)[D_1(x_{is}^d)^3+(D_2+a_0D_1)(x_{is}^d)^2+(D_3+a_0(D_2+a_1D_1))(x_{is}^d)\\
&+(D_4+a_0(D_3+a_0(D_2+a_0D_1)))(x_{is}^d)]=0,
\end{aligned}
\tag{2.3.7}
$$

using (from (2.3.5)) $D_5+a_0[D_4+a_0D_3+a_0^2D_2+a_0^3D_1]=0$.

We can in principle use Descartes' rule of signs to find the number of real positive roots,

real negative roots or complex roots from the signs of the coefficients in (2.3.7) to ensure that the quartic equation (2.3.5) has only one positive real root (for further information about the Descartes' rule of signs see, for example, [72]). Equation (2.3.5) will have only one positive real root (a_0) if and only if

$$D_1 > 0, \tag{2.3.8}$$

$$(D_2 + a_0 D_1) > 0, \tag{2.3.9}$$

$$(D_3 + a_0(D_2 + a_0 D_1)) > 0, \tag{2.3.10}$$

$$(D_4 + a_0(D_3 + a_0(D_2 + a_0 D_1)) > 0. \tag{2.3.11}$$

We remark that if one of the four inequalities above does not hold, equation (2.3.5) will have more than one positive real root for x_{is}^d. The model would then not have a unique positive steady-state solution. However, in practice there only ever seems to be one physical steady-state solution. Nevertheless, to date, we have not been able to confirm that the inequalities (2.3.8)-(2.3.11) are necessarily all satisfied.

The steady-state solutions of the full model under light conditions $(x_{is}^l, x_{os}^l, y_{is}^l, y_{os}^l, L_{os}^l)$ may be determined in a similar manner. Therefore, x_{is}^l will be obtained by equating the following two equations of L_{os}^l:

$$L_{os}^l = -\frac{q_l(k_{os}(1+k_{rr})+k_{rr}){x_{is}^l}^2 + ((1+k_{os})(k_{rr}\mathrm{n}_2 + k_l k_{in}) + k_{os}(\mathrm{n}_2 - q_l))x_{is}^l - k_{os}\mathrm{n}_2}{k_r q_l(1+k_{rr}){x_{is}^l}^2 + k_r(\mathrm{n}_2(1+k_{rr}) + k_l k_{in})x_{is}^l}, \tag{2.3.12}$$

$$\begin{aligned} L_{os}^l = {} & [q_l(k_1 - g_2 y_l k_4){x_{is}^l}^2 + (k_{in}(g_1 k_4 + k_1 g_4) + \mathrm{n}_2(k_1 - g_2 y_l k_4) - q_l(k_2 x_l - g_2 y_l))x_{is}^l \\ & -k_2 x_l(\mathrm{n}_2 + g_4 k_{in}) - g_2 y_l \mathrm{n}_2 + g_1 k_{in}]/[g_3 y_2 k_4 q_l {x_{is}^l}^2 + (k_3 x_2 q_l + g_3 y_2(k_4 \mathrm{n}_2 + q_l))x_{is}^l \\ & +k_3 x_2 g_4 k_{in} + k_3 x_2 \mathrm{n}_2 + g_3 y_2 \mathrm{n}_2], \end{aligned} \tag{2.3.13}$$

where $\mathrm{n}_2 = k_{in} + p_l + k_a$.

When x_{is}^l is known, we can determine L_{os}^l in equation (2.3.12) and the steady-state values of other dependent variables which are stated below:

$$y_{is}^{l} = \frac{k_{in}}{(\mathrm{n}_2 + q_l x_{is}^{l})}, \tag{2.3.14}$$

$$x_{os}^{l} = \left(1 + k_{rr} + k_l \frac{k_{in}}{\mathrm{n}_2 + q_l x_{is}^{l}}\right) x_{is}^{l}, \tag{2.3.15}$$

$$\begin{aligned} y_{os}^{l} = {} & k_{in}(\mathrm{n}_2 + q_l x_{is}^{l}) / [L_{os}^{l} r_l q_l (1 + k_{rr}) {x_{is}^{l}}^2 \\ & + (L_{os}^{l} r_l \mathrm{n}_2 (1 + k_{rr}) + L_{os}^{l}(r_l k_l k_{in} + k_g q_l) + k_{in} q_l) x_{is}^{l} + \mathrm{n}_2 (k_{in} + k_g L_{os}^{l})] \end{aligned} \tag{2.3.16}$$

Numerical Results

We now present numerical results for the full model system. All parameter values are taken from the §2.2.4 (Parameter Estimation).

The dimensionless parameter values (see Table 2.3) are applied to the steady-state solutions of the dimensionless full model both under dark and under light conditions, as stated above. We then obtain the dimensionless steady-state values of the dependent variables for the full model under dark and light conditions, shown in Table 2.4. The dimensional steady-state values of each variable are also shown in Table 2.4, these being obtained by substituting the dimensionless steady-state values of each dependent variable into equation (2.2.6).

	Dimensionless		Dimensional	
	Dark	Light	Dark	Light
x_{os}	0.6642	0.7484	0.0446 mM	0.0503 mM
x_{is}	0.3520	0.5187	0.0237 mM	0.0349 mM
y_{os}	0.9933	0.9931	4.4699 mM	4.4689 mM
y_{is}	0.9143	0.9501	4.1144 mM	4.2755 mM
L_{os}	0.7375	0.6063	23.60×10^{-6}m	19.40×10^{-6}m

Table 2.4: Steady-state values of the dependent variables for the full model under dark and light conditions. Dimensionless and dimensional values are stated.

From Table 2.4, we can see that the oxygen concentration is greater under light than dark conditions and higher in the OS than in the IS. These trends are because the rate of oxygen consumption decreases under light conditions (see Table 2.2). We note that since glucose and oxygen are consumed to produce energy, their rates of consumption are inversely proportional to their concentrations. As previously mentioned, oxygen enters the cell through the OS (see Figure 2.4) from the blood vessels and is transported through the IS, so the oxygen concentration is greater in the OS than in the IS. By contrast, glucose consumption is greater under light than dark conditions in the OS but

less under light than dark conditions in the IS (see Table 2.2). As a result, the glucose concentration is less under light than dark conditions in the OS but greater under light than dark conditions in the IS. Moreover, glucose is used for energy production in both aerobic and anaerobic glycolysis in the IS but in the OS it is used only in anaerobic glycolysis. Therefore, the glucose concentration is higher in the OS than in the IS. In addition, the length of the OS is greater under dark than light conditions, which is consistent with what happens in vivo and results here because the rod OS disc shedding occurs after the onset of light, as stated above. Moreover, the dimensional values of oxygen and glucose both in the OS and in the IS are reasonable under both dark and light conditions because these values are less than the concentrations of oxygen and glucose in blood vessels, respectively. By contrast, the lengths of the OS under dark and light conditions are not in close agreement with the lengths from the literature (28 μm) [69]. A reason for this disagreement may be that in our model only glucose and oxygen control the length of the OS: in practice, Cr, CP, ATP and ADP also play important roles.

We carry out the numerical simulations of the full model system (throughout this chapter and indeed throughout this work) by using the ode15s solver in MATLAB v. 7.1 (The MathWorks, Inc.). We assume that under dark and light conditions at the initial glucose and oxygen both in the OS and in the IS are equal to glucose and oxygen in the blood vessels, respectively, and also assume that the length of the OS equals the length of the IS at the beginning. By applying these values in equation (2.2.6) in §2.2.3, we use 1 to be the initial conditions for each variable. Figure 2.6 shows time courses of the full model under dark and light conditions, as they tend towards steady-state values.

Next we consider continuous exposure to alternating dark and light periods under two different lifestyles, a normal person and an insomniac (eight hours in dark and 16 hours in light for the normal person and four hours in dark and 20 hours in light for the insomniac). Figures 2.7 and 2.8 show the numerical simulations of the full model under these different lifestyles by solving the full model under dark and light conditions and assuming continuity of each of the variables at the transitions from the dark periods to the light periods, with parameter values from Table 2.3. We observe oscillations in each variable between the dark period and the light period. During the dark period the glucose level in the IS and the oxygen levels both in the OS and in the IS decrease rapidly and tend towards their (dark) steady-state values. When the light period begins, they rapidly increase and tend to their (light) steady-state values prior to

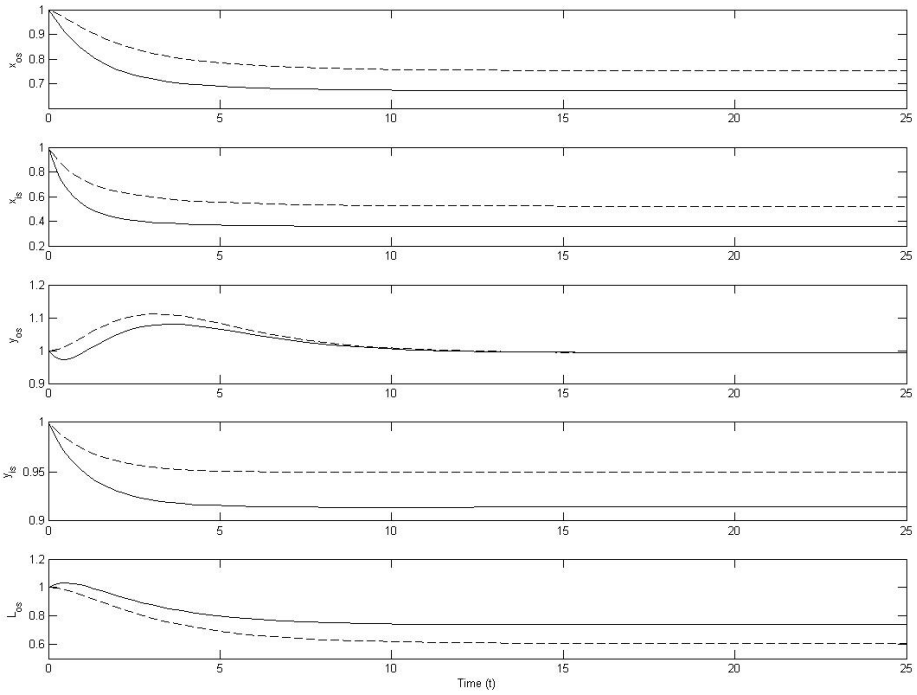

Figure 2.6: Time courses of the dimensionless model variables under dark and light conditions of the full model with parameter values, as shown in Table 2.3.Key: solid line (dark periods); dashed line (light periods).

the transition from light to dark. By contrast, the length of the OS increases rapidly and tends to its steady-state value during the dark period but rapidly decreases and tends towards its steady-state value during the light period. We note that the dynamics of the glucose concentration in the OS differ from those of the other variables. During the light period, glucose levels decrease rapidly before increasing to their steady-state value. By contrast during the dark period they rapidly increase before decreasing to their steady-state value at the transition from dark to light. The glucose trend in the OS is because glucose is the main source of energy. During the light period a lot of glucose is used to produce energy at the beginning until the OS has enough energy or the OS obtains excess energy from the IS, and then the need for glucose is reduced. However, during the dark period no energy generation is required since there is initially spare energy from the light period, so the glucose level increases. When the spare energy has been consumed, glucose becomes the source of energy production until there is adequate energy in the OS. These two lifestyles affect photoreceptor dynamics, having different maximum and minimum values for the length of the OS and different concentrations of oxygen and glucose. For the parameter values chosen, the timescales to reach steady state are significantly shorter than the periods spent in light and dark, so

the steady states are (almost) attained between the transitions. In summary, it can be deduced that the OS length, and concentrations of oxygen and glucose are coupled to the light-dark cycle.

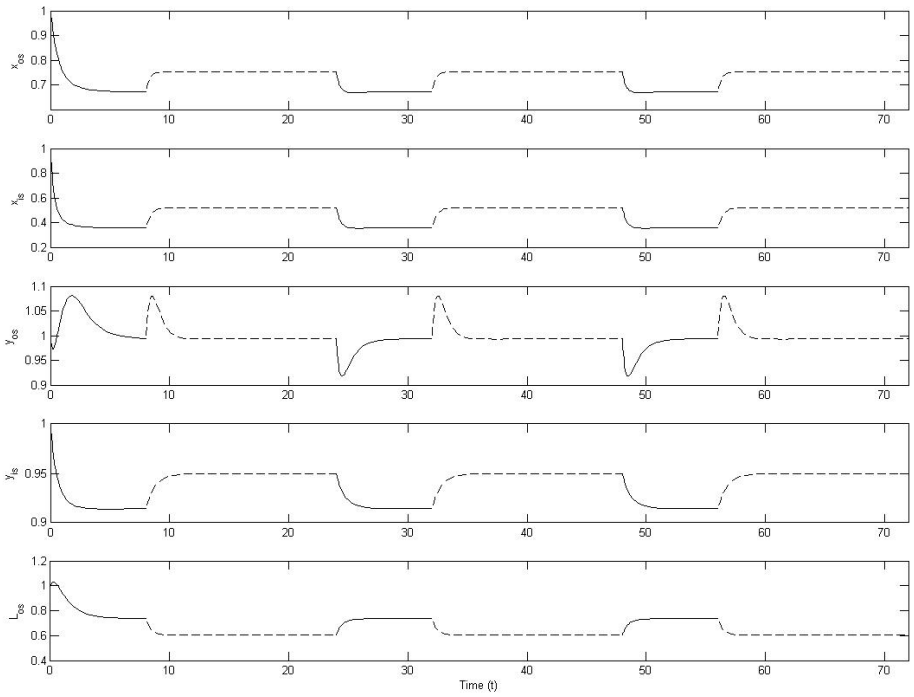

Figure 2.7: Time courses show how oxygen and glucose levels and the length of the OS vary for a **normal** person (eight hours in dark and 16 hours in light per day). Simulations obtained by solving the full model under dark and light conditions and assuming continuity of the transitions from light to dark (and vice versa) with parameter values and initial conditions as shown in Figure 2.6. Key: solid line (dark periods); dashed line (light periods).

We now reduce our model system (2.2.1)-(2.2.5) in order to investigate how oxygen and glucose, taken individually, can affect the growth rate of the OS length on its own. The resulting systems will be called the oxygen and glucose submodels.

2.3.2 The Oxygen Submodel

If we set the glucose concentration to be constant in equations (2.2.12)-(2.2.16) and ignore equations (2.2.14) and (2.2.15), then we obtain our (dimensionless) oxygen submodel under dark conditions:

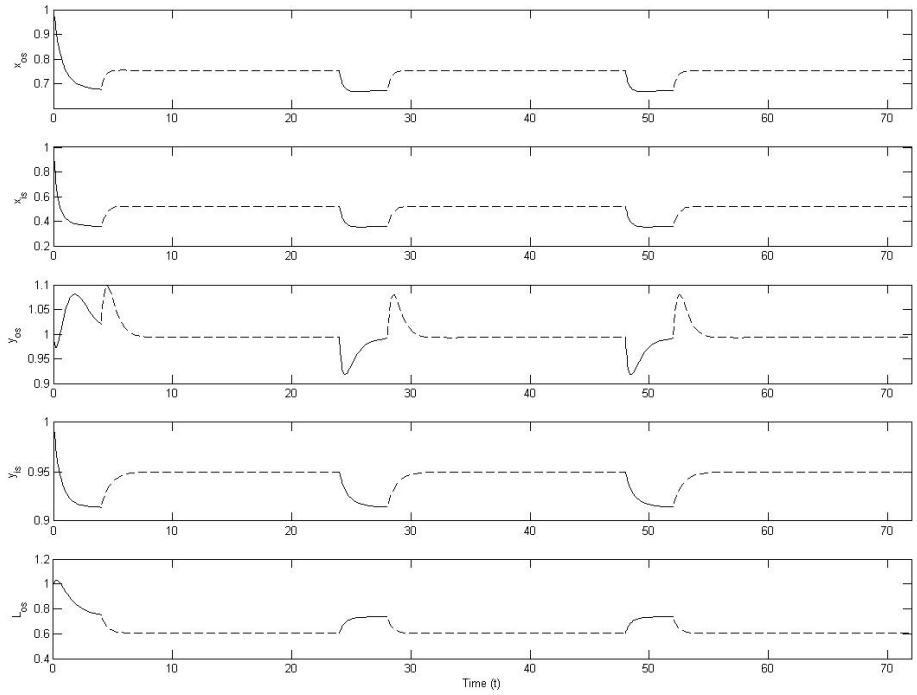

Figure 2.8: Time courses show how oxygen and glucose levels and the length of the OS vary for an **insomniac** (four hours in dark and 20 hours in light per day). Simulations obtained by solving the full model under dark and light conditions and assuming continuity of the transitions from light to dark (and vice versa) with parameter values and initial conditions as shown in Figure 2.6. Key: solid line (dark periods); dashed line (light periods).

$$\frac{dx_{os}}{dt} = \frac{k_{os}}{L_{os}}(1 - x_{os}) - \frac{1}{L_{os}}(x_{os} - x_{is}) - k_r x_{os} - \frac{x_{os}}{L_{os}}\frac{dL_{os}}{dt}, \tag{2.3.17}$$

$$\frac{dx_{is}}{dt} = (x_{os} - x_{is}) - (k_d y_{id} + k_{rr})x_{is}, \tag{2.3.18}$$

$$\frac{dL_{os}}{dt} = \frac{(k_1 x_{is} - k_2 x_d - k_3 x_2 L_{os})}{(k_4 x_{is} + 1)} + \frac{(g_1 y_{id} - g_2 y_d - g_3 y_2 L_{os})}{(g_4 y_{id} + 1)}, \tag{2.3.19}$$

where y_{id} is the assumed constant glucose concentration under dark conditions in the IS (0.9143).

Steady-State Analysis

By setting the time-derivatives to zero in equations (2.3.17)-(2.3.19) it is possible to show that at steady state

$$x_{os}^d = (1 + k_d y_{id} + k_{rr}) x_{is}^d \equiv (1 + \mathrm{b}_1) x_{is}^d, \tag{2.3.20}$$

$$L_{os}^d = \frac{(k_1 x_{is}^d - k_2 x_d)(g_4 y_{id} + 1) + (g_1 y_{id} - g_2 y_d)(k_4 x_{is}^d + 1)}{k_3 x_2 (g_4 y_{id} + 1) + g_3 y_2 (k_4 x_{is}^d + 1)}, \tag{2.3.21}$$

$$L_{os}^d = \frac{k_{os} - (\mathrm{b}_1(1 + k_{os}) + k_{os}) x_{is}^d}{k_r (1 + \mathrm{b}_1) x_{is}^d}, \tag{2.3.22}$$

where $\mathrm{b}_1 = k_d y_{id} + k_{rr} > 0$.

Equations (2.3.21) and (2.3.22) are a pair of simultaneous equations for L_{os}^d and x_{is}^d. Therefore we have the quadratic equation:

$$B_1 (x_{is}^d)^2 + B_2 x_{is}^d + B_3 = 0, \tag{2.3.23}$$

where

$$\begin{aligned}
B_1 &= [k_1(g_4 y_{id} + 1) + g_1 y_{id} k_4 - g_2 y_d k_4] k_r (1 + \mathrm{b}_1) + (k_{os}(1 + \mathrm{b}_1) + \mathrm{b}_1)\, g_3 y_2 k_4, \\
B_2 &= (1 + g_4 y_{id})(k_r k_2 x_d \mathrm{b}_1 - \mathrm{b}_1 k_3 x_2 + k_r k_2 x_d) + (1 + \mathrm{b}_1)(k_r g_2 y_d - k_r g_1 y_{id}) \\
&\quad - g_3 y_2 (k_{os} + \mathrm{b}_1) - k_{os} k_3 x_2 (1 + \mathrm{b}_1 g_4 y_{id} + \mathrm{b}_1 - g_4 y_{id}) - k_{os} g_3 y_2 (\mathrm{b}_1 - k_4), \\
B_3 &= k_{os} k_3 x_2 g_4 y_{id} + k_{os} k_3 x_2 + k_{os} g_3 y_2 > 0.
\end{aligned}$$

Once x_{is}^d is known, x_{os}^d and L_{os}^d can be determined by using equations (2.3.20) and (2.3.21), respectively. Therefore the steady-state values of the other dependent variables rely on x_{is}^d. We remark that if x_{is}^d and L_{os}^d are greater than zero, x_{os}^d is also greater than zero, which is required for the steady state to be physically meaningful.

By applying the Descartes' rule of signs in quadratic equation (2.3.23) we obtain that if

$$B_1 < 0, \tag{2.3.24}$$

then the equation (2.3.23) has only one positive real root for x_{is}^d. Thus the oxygen submodel has a unique positive steady-state solution. If $B_1 > 0$, then there can be three possible cases: two positive real roots, two negative real roots or two complex conjugate roots, and this submodel would not have unique positive steady-state solution. In

practice, however, we can find only one physical steady-state solution.

We determine the behaviour of the system under light conditions by changing k_d, x_d, y_d and y_{id} to k_l, x_l, y_l and y_{il}, respectively (where y_{il} is the assumed constant glucose concentration under light conditions in the IS).

Numerical Results

We determine the dimensionless and dimensional steady-state values (x_{os}, x_{is}, L_{os}) of the oxygen submodel under dark and light conditions for the parameter values shown in Table 2.3, with $y_{id} = 0.9143$ and $y_{il} = 0.9501$ (these are the dimensionless steady-state values of the glucose concentration under dark and light conditions, respectively, in the IS of the full model (see Table 2.4)). Both dimensionless and dimensional steady-state values of the oxygen submodel correspond to those obtained for the full model (see Table 2.5 for the steady-state values of the oxygen submodel).

	Dimensionless		Dimensional	
	Dark	Light	Dark	Light
x_{os}	0.6716	0.7534	0.0451 mM	0.0506 mM
x_{is}	0.3559	0.5222	0.0239 mM	0.0351 mM
L_{os}	0.7376	0.6064	23.60×10^{-6}m	19.41×10^{-6}m

Table 2.5: Steady-state values of the dependent variables for the oxygen submodel under dark and light conditions. Results presented in terms of dimensionless and dimensional values.

We plot time series of the dimensionless full model against the dimensionless oxygen submodel under dark and light conditions to show how they differ before reaching their steady-state values (see Figure 2.9). In Figure 2.9, there is good agreement between simulations for the oxygen submodel and the full model as follows. The oxygen levels for the oxygen submodel are slightly less than their levels for the full model at the beginning before they reach their steady-state values in both the OS and IS. Moreover, the length of the OS for the oxygen submodel is slightly greater than its length for the full model before reaching its same steady-state values under dark and light conditions. A reason for their differences might be that we set the constant glucose concentration under dark conditions ($y_{id} = 0.9143$) and under light conditions ($y_{il} = 0.9501$) in the IS for the oxygen submodel to be greater than the initial value for glucose concentration in the IS (0.8 under both light and dark conditions) in the full model. It is noted that when the glucose concentrations, both under dark and light conditions, are fixed in the IS for the oxygen submodel, the dynamics of the oxygen submodel do not differ sub-

stantially from those of the full model. The oxygen submodel approximates well the behaviour of the full model.

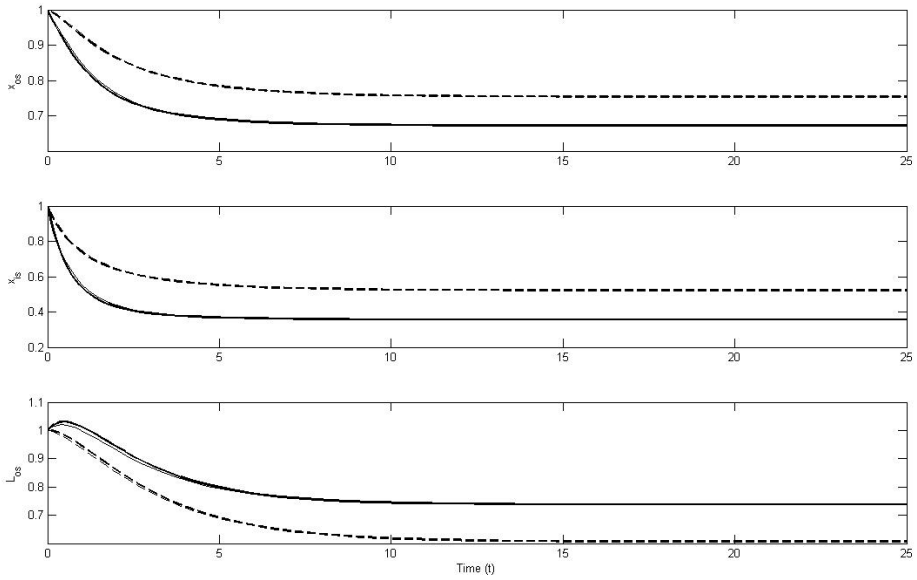

Figure 2.9: Time courses for the dimensionless full model and oxygen submodel under dark and light conditions with parameter values as shown in Table 2.3 together with $y_{id} = 0.9143$ and $y_{il} = 0.9501$.Key: bold solid line (for the full model under dark conditions); bold dashed line (for the full model under light conditions); solid line (for the oxygen submodel under dark conditions); dashed line (for the oxygen submodel under light conditions).

2.3.3 The Glucose Submodel

We obtain the glucose submodel by fixing the oxygen concentration in the OS and IS of the full model system (2.2.1)-(2.2.5). In this way, we find that the (dimensionless) glucose submodel under dark conditions is

$$\frac{dy_{os}}{dt} = \frac{k_{in}}{L_{os}}(1 - y_{os}) - (r_d x_{od} + k_g)y_{os} - \frac{y_{os}}{L_{os}}\frac{dL_{os}}{dt}, \tag{2.3.25}$$

$$\frac{dy_{is}}{dt} = k_{in}(1 - y_{is}) - (q_d x_{id} + p_d + k_a)y_{is}, \tag{2.3.26}$$

$$\frac{dL_{os}}{dt} = \frac{(k_1 x_{id} - k_2 x_d - k_3 x_2 L_{os})}{(k_4 x_{id} + 1)} + \frac{(g_1 y_{is} - g_2 y_d - g_3 y_2 L_{os})}{(g_4 y_{is} + 1)}, \tag{2.3.27}$$

where x_{od} and x_{id}, are the assumed constant oxygen concentrations under dark conditions in the OS and IS, respectively ($x_{od} = 0.6642$ and $x_{id} = 0.3520$).

Steady-State Analysis

We determine the steady state of equations (2.3.25)-(2.3.27) by setting the time-derivatives to zero.

$$y_{is}^d = \frac{k_{in}}{(k_{in} + q_d x_{id} + p_d + k_a)} > 0, \tag{2.3.28}$$

$$L_{os}^d = \frac{(k_1 x_{id} - k_2 x_d)(g_4 y_{is}^d + 1) + (g_1 y_{is}^d - g_2 y_d)(k_4 x_{id} + 1)}{k_3 x_2 (g_4 y_{is}^d + 1) + g_3 y_2 (k_4 x_{id} + 1)}, \tag{2.3.29}$$

$$y_{os}^d = \frac{k_{in}}{(k_{in} + (r_d x_{od} + k_g) L_{os}^d)}. \tag{2.3.30}$$

We find L_{os}^d and y_{os}^d by substituting (2.3.28) into (2.3.30) and (2.3.29). As $y_{is}^d > 0$, we find that if $L_{os} > 0$ when

$$k_1 x_{id}(g_4 y_{is}^d + 1) + g_1 y_{is}^d (k_4 x_{id} + 1) > k_2 x_d (g_4 y_{is}^d + 1) + g_2 y_d (k_4 x_{id} + 1),$$

then we will have only one positive steady-state solution for the dimensionless glucose submodel under dark conditions.

We determine the behaviour of the glucose submodel under light conditions by changing r_d, q_d, p_d, x_d, y_d x_{od} and x_{id} in equations (2.3.30)-(2.3.29) to r_l, q_l, p_l, x_l, y_l x_{ol} and x_{il}, respectively (where x_{ol} and x_{il} are the assumed constant oxygen concentrations under light conditions in the OS and IS, respectively).

Numerical Results

The dimensionless and dimensional steady-state values of (y_{os}, y_{is}, L_{os}) under dark and light conditions are determined by using the parametric values in Table 2.3. In addition, we fix $x_{od} = 0.6642$, $x_{id} = 0.3520$, $x_{ol} = 0.7484$ and $x_{il} = 0.5187$ (these are the dimensionless steady-state values of the oxygen levels under dark and light conditions in the OS and IS, respectively, of the full model, as shown in Table 2.4). Both dimen-

	Dimensionless		Dimensional	
	Dark	Light	Dark	Light
y_{os}	0.9934	0.9932	4.4703 mM	4.4694 mM
y_{is}	0.9143	0.9501	4.1144 mM	4.2754 mM
L_{os}	0.7347	0.6038	23.51×10^{-6}m	19.32×10^{-6}m

Table 2.6: Steady-state values of the dependent variables for the glucose submodel under dark and light conditions in term of dimensionless and dimensional values.

sionless and dimensional steady-state values for the glucose submodel, presented in Table 2.6, correspond to those values for the full model.

Figure 2.10 shows how time dependent solutions for the dimensionless full model and glucose submodel under dark and light conditions are different before they reach their steady-state values. The simulations between the glucose submodel and the full model are not in good agreement. The glucose levels in the OS for the glucose submodel are higher at the beginning and then shorter than their levels for the full model before they tend towards their steady-state values. Moreover, the glucose levels in the IS change slightly between the glucose submodel and the full model. The OS lengths for the glucose submodel both under dark and light conditions decrease quickly, before tending to their steady-state values. The OS lengths, moreover, are shorter for the glucose submodel than their lengths for the full model. It is noted that, at the beginning, the length of the OS for the glucose submodel under dark conditions decreases while its length for the full model increases. These behaviours might be explained by the fact that, in both the OS and the IS, the constant oxygen concentrations under dark conditions ($x_{od} = 0.6642$ and $x_{id} = 0.3520$) and under light conditions ($x_{ol} = 0.7484$ and $x_{il} = 0.5187$) for the glucose submodel are less than the initial values for the oxygen concentrations in the IS and OS (0.8 both under light and dark conditions) in the full model. When the oxygen concentrations (under both dark and light conditions) are fixed in the OS and the IS for the glucose submodel, the dynamics of the glucose submodel differ in terms of the glucose level in the OS and the OS length, compared to those of the full model.

2.4 Summary of Light/Dark Regulation of the OS Length Model

In this chapter we have developed a mathematical model to study metabolism of rod photoreceptors. The resulting model consists of a system of nonlinear ordinary differential equations that describe how oxygen and glucose levels in the OS and IS change over time and also how the length of the OS evolves. We distinguished between dark and light conditions, because consumption rates of oxygen and glucose are different in each situation.

Analysis of the rod system has been carried out by studying the steady-state solution for the full model and for two submodels in which either oxygen and glucose is assumed to be the rate-limiting metabolite. Although our model of light/dark regulation

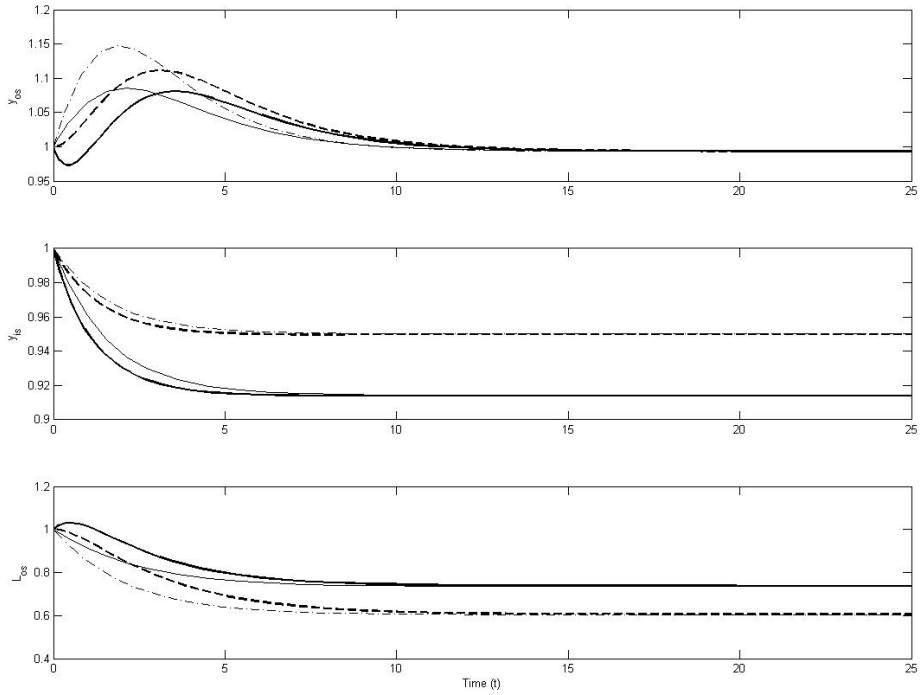

Figure 2.10: Time courses for the dimensionless full model and glucose submodel under dark and light conditions with parameter values as shown in Table 2.3 together with $x_{od} = 0.6642$, $x_{id} = 0.3520$, $x_{ol} = 0.7484$ and $x_{il} = 0.5187$. Key: bold solid line (for the full model under dark conditions); bold dashed line for the full model under light conditions); solid line (for the glucose submodel under dark conditions); dashed line (for the glucose submodel under light conditions).

of length of the OS has predicted what the OS length and the concentration of oxygen and glucose should be under dark and light conditions the same as the vivo results (for more details see §2.3.1), the length of the OS under both conditions are not in close agreement with the lengths from the literature (28 mm) [69]. This disagreement might be that in our model only oxygen and glucose regulate the OS length. In practice, however, Cr, CP, ATP and ADP also play important roles. When we compare both the oxygen and glucose submodels with the full models we have found that oxygen, rather than glucose, is the growth rate-limiting metabolite of our model.

Our models have some weaknesses. In particular in our present model only glucose and oxygen regulate the OS length. Moreover, we do not account for energy exchange from the IS to the OS. It is known that the human eyes form part of the nervous system. There is some evidence [41] supporting that glutamate (an essential amino acid) involves with a mechanism by which retina ganglion cells die in the glaucoma, an

eye disease causing gradual loss of sight. In Chapters 3 and 4 we shall consider the metabolism of the nervous system. The nervous system consists mainly of two cell types: the neuronal cells and the glial cells [2, 12–14]. Both cells play essential roles in the life of the system. The neuronal cells are excitable cells that generate and carry electrical signals. Such a signal molecule is called a neurotransmitter. The glial cells however provide support and protection for the neuronal cells. The neuronal and glial cells are separated from each other by the extracellular space [15, 16].

The metabolism of the neurotransmitters is regulated by a cycle in which substrates such as glutamate and glutamine are exchanged between neuronal and glial cells. This cycle is known as the glutamate-glutamine cycle. We will focus on the glutamate-glutamine cycle in the nervous system which is divided into three compartments: the neuronal cell, the extracellular space and the glial cell. We investigate whether changes in metabolic demand of the rates of glutamate and glutamine in the extracellular space can avoid excitotoxic neuron cell damage.

CHAPTER 3

Model of the Glutamate-Glutamine Cycle

In this chapter a model describing the Glu-Gln cycle within the nervous system is presented. This is of interest since the human eyes form part of the nervous system. We start with a brief explanation of the relevant biology and then develop a mathematical model, comprising a system of time-dependent ordinary differential equations. In this system Glu and Gln are assumed to be the rate-limiting substrates and all other chemicals such as ammonia, aspartate, ATP and a $-$ Ketoglutarate are assumed to be present in abundance. We use our model to investigate whether the rates at which Glu and Gln are released into (or out of) the extracellular space (ECS) change the metabolic demand of the system and, thereby, enable it to avoid excitotoxic neuronal cell damage. Since excessive amounts of Glu in the ECS are toxic to neurons, high Glu levels may kill neuronal cells. We will study excitotoxicity in more detail in Chapter 4.

3.1 Introduction

As mentioned in §1.1.3, the nervous system consists mainly of two cell types: neuronal cells and glial cells [2, 12–14]. Neurons are excitable cells that generate and transport electrical signals. Such a signal molecule is called a neurotransmitter. The glial cells however provide support and protection for the neuronal cells. The neuronal and glial cells are separated from each other by the synaptic cleft (ECS) [15, 16] (see the three compartments: the neuronal cell, the ECS and the glial cell, in Figure 3.1).

The metabolism of the neurotransmitters is regulated by a cycle in which substrates such as Glu and Gln are exchanged between neuronal and glial cells. This cycle is

known as the Glu-Gln cycle (see Figure 3.1). The steps in the Glu-Gln cycle are briefly explained [15, 16, 18, 20–22, 24, 35] as follows:

- extracellular Glu is actively transported from the neuronal cell to the glial cell via the ECS,
- Glu is converted to Gln in the glial cell by the enzyme GS (see reaction (3.1.1)),

$$\text{Glutamate} + \text{NH}_4^+ + \text{ATP} \xrightarrow{\text{GS}} \text{Glutamine} + \text{ADP} + \text{P}_\text{i}, \tag{3.1.1}$$

- Gln is transported passively to the neuronal cell from the glial cell via the ECS, and
- Gln in neuronal cells is converted to Glu via the action of the enzyme PAG (see reaction (3.1.2)).

$$\text{Glutamine} + \text{H}_2\text{O} \xrightarrow{\text{PAG}} \text{Glutamate} + \text{NH}_4^+. \tag{3.1.2}$$

We note that there is evidence [28] which suggests that Glu can be released from the glial cells back to the ECS. Glu efflux from glial cells acts to reduce ATP production in these cells. In Figure 3.1 we present a schematic diagram of the Glu and Gln concentrations in the three compartments of interest: the neuronal cell, the ECS and the glial cell. Since Gln transport is believed to be passive, it is a reversible, two-way process. By contrast, active transport across membranes uses cellular energy to move molecules up concentration gradients (and is irreversible (one-way process)).

It is well known that the Glu-Gln cycle plays a crucial role in glutamatergic neurotransmission. Disruption of this cycle caused by pathologic conditions such as Alzheimer's disease, Parkinson's disease and Retinitis Pigmentosa, may result in different patterns of brain damage. Observations by Lucas and Newhouse [41] and Choi [52] suggest that after injection of excitatory amino acid into the brain, release of the normal excitatory amino acid transmitter, Glu, can itself cause neuronal damage during a seizure. Because it has been difficult to detect an increase in extracellular Glu during a single prolonged seizure without intervening and full recovery of consciousness, it would appear that the trigger is excessive stimulation of Glu receptors. Hence, it is initially important to understand how the Glu-Gln cycle functions.

In the following section we derive our mathematical model of the Glu-Gln cycle. As

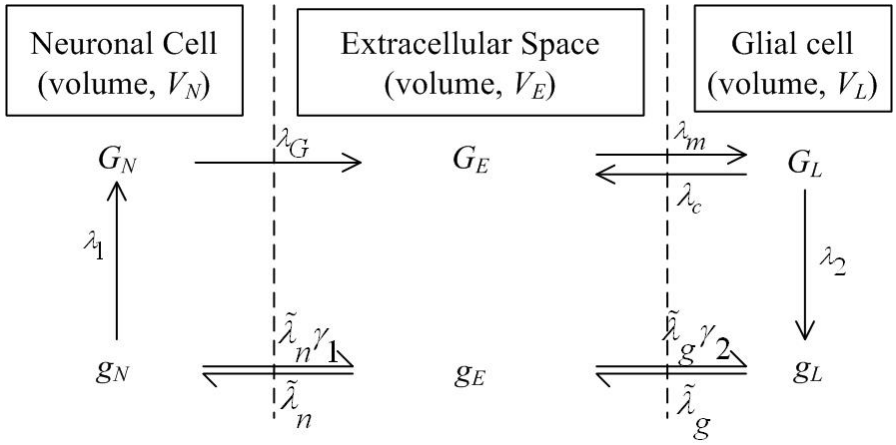

Figure 3.1: A schematic diagram of our model of the Glu-Gln cycle showing how Glu and Gln move during neuronal cells, the ECS and glial cells. GS= the enzyme glutamine synthetase; PAG = the enzyme glutaminase; $\rightleftharpoons$ represents the passive transport; $\rightarrow$ represents the active transport.

stated above, the nervous system is divided into three compartments, namely the neuronal cells, the ECS and the glial cells (see Figure 3.2). In §3.3 numerical simulations and an asymptotic analysis of our model are presented. In §3.4 we summarise our results, and discuss the model shortcomings and possible extensions.

3.2 Model Development and Nondimensionalisation

In this section we present our model of the Glu-Gln cycle in which we focus on three tissue compartments (see Figure 3.2). We assume that Glu and Gln are the rate-limiting substrates: all other chemicals such as aspartate, ammonia and ATP, are assumed to be present in abundance. We investigate how the rates at which Glu and Gln exchange with the ECS influence the metabolic demand of the system and enable it to avoid excitotoxic neuronal damage.

When developing our model we denote by G and g the concentrations (in millimolar, mM) of Glu and Gln, respectively. The model consists of a system of coupled ODEs and the tissue is decomposed into three compartments: the neuronal cells, the ECS and the glial cells. We do not distinguish between the mitochondria and cytosol in the neuronal and glial cells. We use the subscripts N, E and L to represent neuronal, ECS and glial quantities, respectively. We introduce G_N, g_N, G_E, g_E, G_L and g_L to denote the concentrations of Glu and Gln in each compartment. l_i's are reaction rates, and g_i's are positive constants; for more detail about the physical meaning of the parameters

see Table 3.1. We use the principle of mass balance [73] to derive evolution equations for the six time-dependent variables and the law of mass action [73] to deduce functional forms for the production or loss terms of the concentrations of Glu and Gln in the neuronal and glial cell (see reactions (3.1.1) and (3.1.2)). We note that the concentrations of the other reactants that appear in reactions (3.1.1) and (3.1.2) are assumed to be constant.

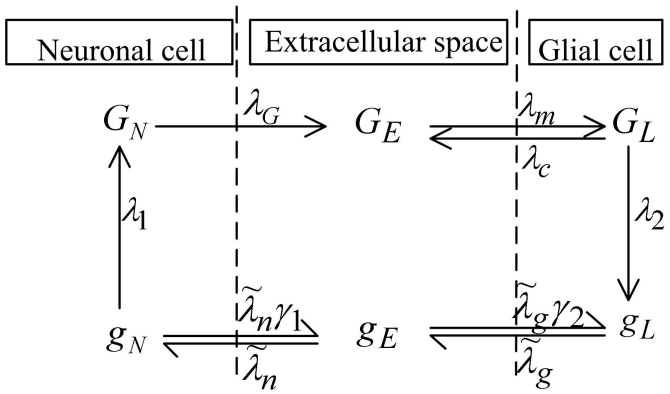

Figure 3.2: A schematic diagram of our model of the Glu-Gln cycle showing how Glu and Gln move between the neuronal cells, the ECS and the glial cells. l_i's are reaction rates, and g_i's are constants; for more detail about the physical meaning of the parameters, see Table 3.1.

3.2.1 The Principle of Mass Balance and the Law of Mass Action

We apply the principle of mass balance to Glu and Gln in each compartment to derive ODEs for their time evolution. Then the law of mass action, stating that the rate of reaction is proportional to the product of the concentrations of the reactants [73], is applied in reactions (3.1.1) and (3.1.2).

We assume that the volume of a neuronal cell is V_N (μm^3), the volume of a glial cell is V_L (μm^3) and the volume of the ECS is V_E (μm^3). We note that the total amounts of Glu and Gln in the various compartments are given by $V_N G_N$, $V_N g_N$, $V_E G_E$, $V_E g_E$, $V_L G_L$ and $V_L g_L$, respectively.

Therefore, the dimensional system is

$$\frac{d(V_N G_N)}{dt} = \mathrm{l}_1 V_N g_N - \mathrm{l}_G V_N G_N, \tag{3.2.1}$$
$$\frac{d(V_N g_N)}{dt} = \tilde{\mathrm{l}}_n A_2(g_E - \mathrm{g}_1 g_N) - \mathrm{l}_1 V_N g_N, \tag{3.2.2}$$
$$\frac{d(V_E G_E)}{dt} = \mathrm{l}_G V_N G_N - \mathrm{l}_m V_E G_E + \mathrm{l}_c V_L G_L, \tag{3.2.3}$$
$$\frac{d(V_E g_E)}{dt} = \tilde{\mathrm{l}}_g A_2(g_L - \mathrm{g}_2 g_E) - \tilde{\mathrm{l}}_n A_2(g_E - \mathrm{g}_1 g_N), \tag{3.2.4}$$
$$\frac{d(V_L G_L)}{dt} = \mathrm{l}_m V_E G_E - \mathrm{l}_2 V_L G_L - \mathrm{l}_c V_L G_L, \tag{3.2.5}$$
$$\frac{d(V_L g_L)}{dt} = \mathrm{l}_2 V_L G_L - \tilde{\mathrm{l}}_g A_2(g_L - \mathrm{g}_2 g_E), \tag{3.2.6}$$

where the l_i's are rate constants, the g_i's are positive constants and A_2 is the cross-sectional area of the nervous system (mm^2).

Summing equations (3.2.1)-(3.2.6) we note that there is a conserved quantity

$$\frac{d(V_N G_N)}{dt} + \frac{d(V_N g_N)}{dt} + \frac{d(V_E G_E)}{dt} + \frac{d(V_E g_E)}{dt} + \frac{d(V_L G_L)}{dt} + \frac{d(V_L g_L)}{dt} = 0,$$

so that

$$V_N G_N + V_N g_N + V_E G_E + V_E g_E + V_L G_L + V_L g_L = V_T G_T(\text{constant}),$$

where $V_T G_T$ is the total amount of Glu and Gln (mm^3) within the presented system.

We can use this result to eliminate g_E in terms of the other model variables and in this way reduce equations (3.2.1)-(3.2.6) to five ODEs. As stated in §1.1.4, glial cells are approximately one-tenth the size of neuronal cells [2] and the ECS comprises approximately 20% of brain tissue volume [17]. However, there are approximately 10 times more glial cells than neurons, therefore neuronal and glial cells take up equal space. The volumes V_N, V_E and V_L that appear in equations (3.2.1)-(3.2.6) are assumed to be constant. We estimate that

$$V_N = V_L, \ \frac{V_E}{V_T} = 0.2, \ \frac{V_L}{V_T} = \frac{V_N}{V_T} = 0.4. \tag{3.2.7}$$

We note that

$$\frac{V_E}{V_L} = \frac{1}{2}, \ \frac{V_E}{V_T} = \frac{1}{5}. \tag{3.2.8}$$

Parameters	Physical Meanings	Units
l_1	rate constant for enzyme PAG	per minute (min^{-1})
l_2	rate constant for enzyme GS	min^{-1}
l_G	rate at which the neuronal cell secrets Glu into the ECS	min^{-1}
l_c	rate at which the glial cell releases Glu back to the ECS	min^{-1}
l_m	rate at which the ECS transports Glu into the glial cell	min^{-1}
$\tilde{l}_n$	rate at which the ECS releases Gln into the neuronal cell	(mm) min^{-1}
$\tilde{l}_g$	rate at which the glial cell releases Gln into the ECS assumed to be equation (3.2.14)	(mm) min^{-1}
l_{go}	a maximum rate of Glu at which it causes Gln to be released from the glial cell to the ECS	min^{-1}
l_h	the concentration of Glu in the ECS at which the rate is half of l_{go}	mM
G_T	total amount of Glu and Gln in the three compartments	mM
V_N, V_E, V_L	volume of the neuronal cell, the ECS and the glial cell, respectively	$(mm)^3$
A_2	the cross-sectional area of nervous system,	$(mm)^2$
g_1	Gln efflux from the neuronal cell to the ECS coefficient	-
g_2	Gln uptake from the ECS to the glial cell coefficient	-

Table 3.1: Parameters appearing for the equations (3.2.1)-(3.2.6) and their estimated values will be shown in Table 3.2.

We can rewrite our model equations as follows:

$$\frac{dG_N}{dt} = l_1 g_N - l_G G_N, \tag{3.2.9}$$

$$\frac{dg_N}{dt} = l_n((\frac{V_T}{V_E}G_T - \frac{V_N}{V_E}(G_N + g_N + G_L + g_L) - G_E) - g_1 g_N) - l_1 g_N, \tag{3.2.10}$$

$$\frac{dG_E}{dt} = \frac{V_N}{V_E} l_G G_N - l_m G_E + \frac{V_L}{V_E} l_c G_L, \tag{3.2.11}$$

$$\frac{dG_L}{dt} = \frac{V_E}{V_L} l_m G_E - (l_2 + l_c) G_L, \tag{3.2.12}$$

$$\frac{dg_L}{dt} = l_2 G_L - l_g(g_L - g_2(\frac{V_T}{V_E}G_T - \frac{V_N}{V_E}(G_N + g_N + G_L + g_L) - G_E)). \tag{3.2.13}$$

where $l_n = \dfrac{\tilde{l}_n A_2}{V_N}$ and $l_g = \dfrac{\tilde{l}_g A_2}{V_L}$.

In what follows we assume that all rates have constant coefficients, except for the rate at which the glial cells secrete Gln into the ECS (l_g). As mentioned above, Gln released from the glial cell is transported back to the neuron via the ECS where it is a main precursor of neurotransmitter pools of Glu. Moreover, the Glu level in the ECS (G_E) is an important indicator of excitotoxicity in the nervous system. We assume that l_g, the rate at which the glial cell releases Gln into the ECS, is a saturating function of G_E,

$$l_g = \frac{l_{go} G_E}{l_h + G_E}, \tag{3.2.14}$$

where l_{go} represents the maximum rate (in min^{-1}) at which Glu can be transported from the glial cells to the ECS, and l_h is the concentration of Glu in the ECS (in mM) at which the rate is half-maximal.

With $l_g = l_g(G_E)$ defined by (3.2.14), our model of the Glu-Gln cycle becomes:

$$\frac{dG_N}{dt} = l_1 g_N - l_G G_N, \tag{3.2.15}$$

$$\frac{dg_N}{dt} = l_n[(\frac{V_T}{V_E} G_T - \frac{V_N}{V_E}(G_N + g_N + G_L + g_L) - G_E) - g_1 g_N] - l_1 g_N, \tag{3.2.16}$$

$$\frac{dG_E}{dt} = \frac{V_N}{V_E} l_G G_N - l_m G_E + \frac{V_L}{V_E} l_c G_L, \tag{3.2.17}$$

$$\frac{dG_L}{dt} = \frac{V_E}{V_L} l_m G_E - (l_2 + l_c) G_L, \tag{3.2.18}$$

$$\frac{dg_L}{dt} = l_2 G_L - \frac{l_{go} G_E}{l_h + G_E}[g_L - g_2(\frac{V_T}{V_E} G_T - \frac{V_N}{V_E}(G_N + g_N + G_L + g_L) - G_E)]. \tag{3.2.19}$$

Estimates of Initial Conditions

Where possible we obtain estimates for the initial conditions from the literature (see [16, 18, 23, 29, 46, 74]). Typical Glu levels are high in the mammalian brain, with an average value of 12.5 mM which is considerably greater (by two-three fold) than levels of Gln. Thus the total Gln concentration in the three compartments is assumed to be 5.5 mM. Therefore, the total amount of both amino acids, Glu and Gln, in the three compartments, G_T, is approximately 18 mM. Most Glu is found in neurons and its extracellular concentration is normally maintained in the low micromolar range in order to avoid excitotoxic nerve cell damage: if the Glu level in the ECS rises to 0.06 mM, neuronal cells get damaged. For Gln, its concentration in the glial cells is higher than elsewhere and Gln is normally present in the ECS at higher levels than other amino acids in the ECS. Accordingly, we fix the dimensional initial values of Glu and Gln in

each compartment as follows:

$$\begin{aligned} G_N(0) &= 4, & g_N(0) &= 0.5, & G_E(0) &= 10^{-3}, \\ G_L(0) &= 0.1, & g_L(0) &= 1. \end{aligned} \tag{3.2.20}$$

In summary, our dimensional model comprises system (3.2.15)-(3.2.20). The physical meaning of all model parameters is given in Table 3.1.

3.2.2 Nondimensionalisation

We now nondimensionalise equations (3.2.15)-(3.2.19) by setting the following dimensionless variables:

$$G_N^* = \frac{G_N}{G_T}, \quad g_N^* = \frac{g_N}{G_T}, \quad G_E^* = \frac{G_E}{G_T}, \quad G_L^* = \frac{G_L}{G_T}, \quad g_L^* = \frac{g_L}{G_T}, \quad t^* = \frac{t}{T}, \tag{3.2.21}$$

where G_T and T are respectively typical values of Glu and Gln in the three compartments, and time, and starred variables denote dimensionless variables.

We use the rate constant that models the conversion of Gln to Glu in the neuronal cell to fix the timescale so that $T = \frac{1}{\mathrm{l}_1}$. Substituting these scalings into equations (3.2.15)-(3.2.19) and (because of exactly estimating the volumes of the three compartments above) introducing the small parameter e such that

$$\mathrm{e} = \frac{V_E}{V_L} \quad \text{and} \quad \mathrm{e}^2 = \frac{V_E}{V_T}, \tag{3.2.22}$$

and the following dimensionless parameters

$$\begin{aligned} \mathrm{l}_G^* &= \frac{\mathrm{l}_G}{\mathrm{l}_1}, & \mathrm{l}_n^* &= \frac{\mathrm{l}_n}{\mathrm{l}_1}, & \mathrm{l}_2^* &= \frac{\mathrm{l}_2}{\mathrm{l}_1}, & \mathrm{l}_h^* &= \frac{\mathrm{l}_h}{G_T}, \\ \mathrm{l}_m^* &= \frac{\mathrm{l}_m}{\mathrm{l}_1}, & \mathrm{l}_c^* &= \frac{\mathrm{l}_c}{\mathrm{l}_1}, & \mathrm{l}_{go}^* &= \frac{\mathrm{l}_{go}}{\mathrm{l}_1}, \end{aligned}$$

(dropping the stars for notational simplicity) gives

$$\begin{aligned}
\frac{dG_N}{dt} &= g_N - \mathrm{l}_G G_N, && (3.2.23)\\
\frac{dg_N}{dt} &= \mathrm{e}^{-2}\mathrm{l}_n[1-\mathrm{e}(G_N+g_N+G_L+g_L)-\mathrm{e}^2 G_E-\mathrm{e}^2\mathrm{g}_1 g_N]-g_N, && (3.2.24)\\
\mathrm{e}\frac{dG_E}{dt} &= \mathrm{l}_G G_N - \mathrm{e}\,\mathrm{l}_m G_E + \mathrm{l}_c G_L, && (3.2.25)\\
\frac{dG_L}{dt} &= \mathrm{e}\,\mathrm{l}_m G_E - (\mathrm{l}_2+\mathrm{l}_c)G_L, && (3.2.26)\\
\frac{dg_L}{dt} &= \mathrm{l}_2 G_L - \frac{\mathrm{l}_{go}G_E}{\mathrm{l}_h+G_E}[g_L-\mathrm{e}^{-2}\mathrm{g}_2(1-\mathrm{e}(G_N+g_N+G_L+g_L) \\
&\quad -\mathrm{e}^2 G_E)], && (3.2.27)
\end{aligned}$$

with initial conditions (appealing to equations (3.2.20) and (3.2.21) with $G_T = 18$):

$$\begin{aligned}
G_N(0) &= \frac{2}{9}, & g_N(0) &= \frac{1}{36}, & G_E(0) &= \frac{1}{1.8\times 10^4},\\
G_L(0) &= \frac{1}{1.8\times 10^2}, & g_L(0) &= \frac{1}{18}. && (3.2.28)
\end{aligned}$$

We have now presented our dimensionless model of the Glu-Gln cycle (3.2.23)-(3.2.28).

3.2.3 Steady-State Analysis

Here we construct the steady-state solutions of equations (3.2.23)-(3.2.27). By setting the time-derivatives to zero in equations (3.2.23)-(3.2.27), it is possible to show that at steady-state

$$\begin{aligned}
g_N &= \mathrm{l}_G G_N, && (3.2.29)\\
G_L &= \frac{\mathrm{l}_G}{\mathrm{l}_2}G_N, && (3.2.30)\\
G_E &= \frac{\mathrm{l}_G(\mathrm{l}_2+\mathrm{l}_c)}{\mathrm{e}\,\mathrm{l}_m\mathrm{l}_2}G_N, && (3.2.31)\\
g_L &= \mathrm{e}^{-1}(1-\mathrm{e}\tilde{b}_1 G_N), && (3.2.32)\\
G_N &= \frac{1-\mathrm{e}^2\mathrm{l}_2\mathrm{l}_m\mathrm{l}_h/\mathrm{l}_{go}(\mathrm{l}_2+\mathrm{l}_c)}{\mathrm{e}\tilde{b}_1+\mathrm{e}\tilde{b}_2/\mathrm{l}_{go}(\mathrm{l}_2+\mathrm{l}_c)}, && (3.2.33)
\end{aligned}$$

where

$$\begin{aligned}
\tilde{b}_1 &= [1+\mathrm{l}_G(1+\frac{1}{\mathrm{l}_2})+\mathrm{l}_G(\frac{(\mathrm{l}_2+\mathrm{l}_c)}{\mathrm{l}_m\mathrm{l}_2}+\frac{\mathrm{e}}{\mathrm{l}_n}+\mathrm{e}\mathrm{g}_1)], && (3.2.34)\\
\tilde{b}_2 &= \mathrm{l}_G(\mathrm{l}_2+\mathrm{l}_c)[1+\mathrm{l}_{go}\mathrm{g}_2(\frac{1}{\mathrm{l}_n}+\mathrm{g}_1)]. && (3.2.35)
\end{aligned}$$

For physically realistic solutions we require $G_N > 0$, and hence, from (3.2.33) we deduce that the model parameters must satisfy the following inequality:

$$l_{go}(l_2 + l_c) \;>\; e^2 l_2 l_m l_h. \tag{3.2.36}$$

As $g_L > 0$, we get

$$G_N \;<\; \frac{1}{e\tilde{b}_1}. \tag{3.2.37}$$

Additionally, as mentioned above, Glu concentration in the neuron cell (G_N) and Gln concentration in the glial cell (g_L) are higher than the concentrations in any other compartments, and we also know:

$$G_N > g_L.$$

We deduce that

$$G_N > \frac{1}{1 + e\tilde{b}_1}. \tag{3.2.38}$$

Combining inequalities (3.2.37)-(3.2.38), we obtain the following necessary condition for $G_N > g_L > 0$:

$$\frac{1}{1 + e\tilde{b}_1} < \frac{l_{go}(l_2 + l_c) - e^2 l_2 l_m l_h}{e\, l_{go}(l_2 + l_c)\tilde{b}_1 + e\tilde{b}_2} < \frac{1}{e\tilde{b}_1}. \tag{3.2.39}$$

Inequalities (3.2.37) and (3.2.39) are necessary conditions for the existence of a physically realistic steady-state.

3.2.4 Estimates of Parameters

Using available data, we have estimated $e = \frac{V_E}{V_L} = 0.5$ [2, 17]. While the appropriate data required to determine other parameter values are not yet available, we do possess information about how influential certain reactions are in relation to others. We anticipate that the values of l_G, l_c, l_m and l_2 will be important in determining whether the system is excitotoxic. As stated in §3.1, when Glu is released from the neuronal cell by the efflux rate l_G, it is rapidly transported (l_m) to the glial cell in order to keep extracellular Glu levels low. Glu efflux from the glial cell to the ECS (l_c) increases as the rate of ATP production decreases. If l_m is low or l_c is high, then the level of Glu in the ECS may exceed typical healthy values of 0.06 mM [16, 18]. We assume that $l_m \gg l_c$, $l_2 \gg l_G$ to ensure that our model does not exhibit excitotoxicity. The re-

maining default parameters are selected in order to ensure that inequalities (3.2.36) and (3.2.39) hold (see the default values of all dimensionless parameters in Table 3.2).

Nondimensional Parameter	Default Value
l_m	48
g_1, l_c, l_2	2
l_{go}	0.5
l_n	0.125
g_2	0.0625
l_G, l_h	0.025

Table 3.2: The default parameter set that is used in equations (3.2.23)-(3.2.27).

3.2.5 Numerical Results

In this section we construct numerical solutions of equations (3.2.23)-(3.2.28) with parameters from Table 3.2. We integrate the ODEs using the ode15s solver in MATLAB v.7.1. Typical solutions of equations (3.2.23)-(3.2.28) are presented in Figure 3.3. In Figure 3.3, since the system rapidly evolves to a steady-state, we plot the dependent variables against $\log(t)$.

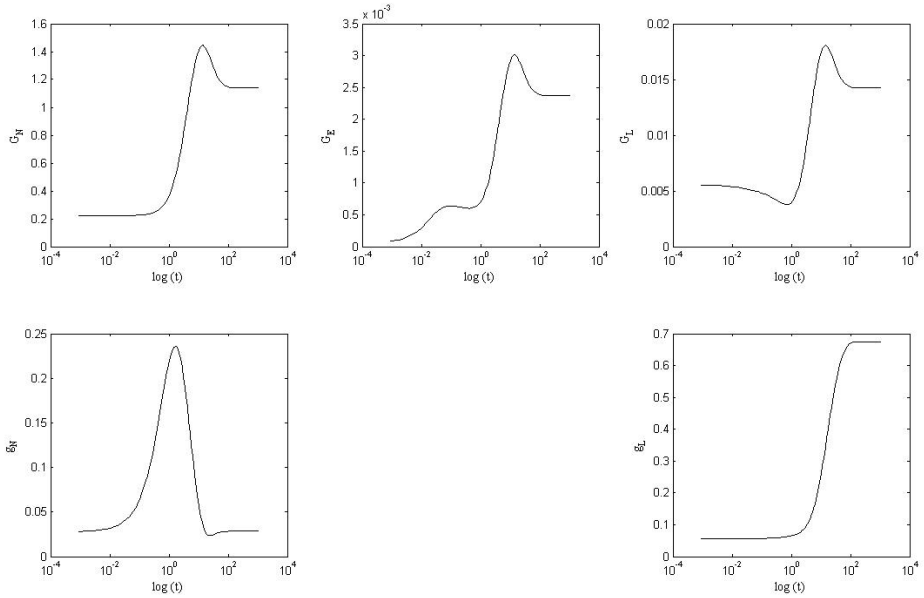

Figure 3.3: Series of semilog plots showing how, for a typical choice of parameter values in Table 3.2, the solution to equations (3.2.23)-(3.2.27) evolves over time.

In Figure 3.3, we can see clearly that G_E changes dramatically throughout the time of the simulation, firstly increasing until $t \sim 10^{-3}$, following a shortly decreasing line and then increasing before tending to a steady-state. G_L decreases slightly until $t \sim 1$ and then increases before settles to a steady-state. Additionally, g_N increases until $t \sim 1$, and then decreases rapidly before settles to a steady-state. By contrast, G_N and g_L increase rapidly for $1 < t < 10$ and for $1 < t < 10^2$, respectively, an then tend to their steady-state.

We note that e $= 0.5$ is not a small enough value to perform asymptotic analysis. We show below that the system behaviour is not affected by whether e $= 0.5$ or e $\ll 1$ (see Figure 3.4). When e is reduced, all variables become greater (this is consistent with the analytical expressions for the steady-state solutions (3.2.29)-(3.2.33)). In order to perform asymptotic analysis in §3.3.5 we focus on a case for which e $= 0.05$ (which is less than ten times the original epsilon) since then the analysis is tractable and the behaviour is qualitatively similar to that when e $= 0.5$.

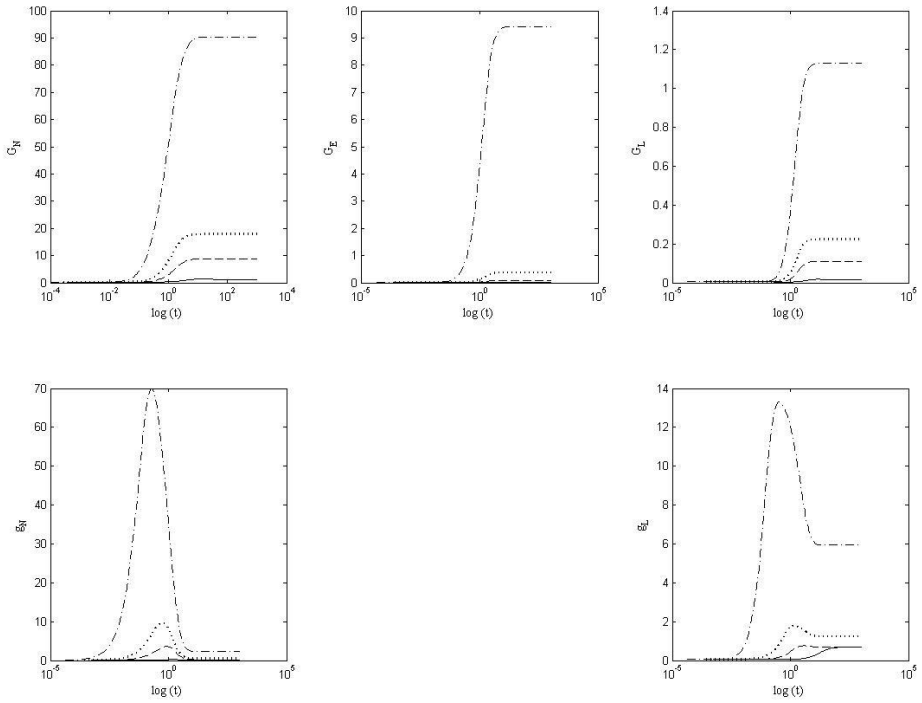

Figure 3.4: A comparison of the numerical solutions for all variables of system (3.2.23)-(3.2.27) when e is varied, while other parameter values and initial conditions are held fixed at the values used in Figure 3.3 (e $= 0.5$: solid lines; e $= 0.1$: dashed lines; e $= 0.05$: dotted lines; and e $= 0.01$: dashed-dotted lines).

In the next section we perform an asymptotic analysis of system (3.2.23)-(3.2.28) in order to understand fully its behaviour.

3.3 Model Analysis and Simulations

In this section we exploit the appearance of a small parameter (e) in equations (3.2.23)-(3.2.28) to construct approximate model solutions valid on different timescales. We start by estimating the dimensionless parameters and then motivate our re-scaling of the dependent variables by inspecting the steady-state solutions. Finally numerical simulations are presented and compared with the asymptotic solutions of our dimensionless system (3.2.23)-(3.2.28).

3.3.1 Parameter Scaling

Initially we estimate our dimensionless parameters as shown in Table 3.2. At the end of this section we present numerical solutions of equations (3.2.23)-(3.2.28) after re-scaling all parameters and varying e (e $= 0.5,\ 0.1,\ 0.05,\ 0.01$). These simulations motivate the re-scaling of the dependent variables that we consider in the next section.

As stated in §3.1 the nervous system can protect itself from neurotoxicity by restricting Glu concentrations in the ECS (via the Glu transporter) and by converting Glu into Gln (via the enzyme GS) in the glial cells. Parameters in our model which are therefore directly important to neurotoxicity are l_m, l_c and l_2. Since Glu uptake from the ECS to the glial cell is an active process and limits the Glu concentration in the ECS, we suppose that l_m, the rate at which Glu, in the ECS, is transported to the glial cell is greater than the rate at which the glial cell releases Glu back to the ECS (l_c) and also the rate at which Glu is converted to Gln by the enzyme GS in the glial cell (l_2). In particular we rescale l_m, l_c, l_2 and g_1 as follows

$$\mathrm{l}_m = \mathrm{e}^{-2}\bar{\mathrm{l}}_m, \tag{3.3.1}$$

$$\mathrm{l}_c = O(1),\ \ \mathrm{l}_2 = O(1)\ \text{ and }\ \mathrm{g}_1 = O(1). \tag{3.3.2}$$

In (3.3.2) we assume that g_1, the rate of Gln removal from the neuronal cell to the ECS coefficient, is $O(1)$ so that the rates of influx and efflux to the neuronal cell are similar in magnitude.

In addition, we choose

$$l_G = e^2 \bar{l}_G, \qquad l_{go} = e^2 \bar{l}_{go} \qquad \text{and} \qquad l_h = e^2 \bar{l}_h. \tag{3.3.3}$$

These parameters are assumed to scale with e^2 in order to prevent excitotoxicity by maintaining extracellular Glu at low levels (see Table 3.1 for definitions of all the parameters).

Finally, we assume that

$$l_n = e^3 \bar{l}_n, \text{ and } g_2 = e^4 \bar{g}_2. \tag{3.3.4}$$

We choose l_n, the Gln influx rate from the ECS to the neuronal cell, and g_2, Gln uptake from the neuronal cell to the ECS coefficient, to be the small as Gln levels are not related to occurring excitotoxicity. The above scaling which guarantees that $l_n \gg g_2$ ensures that there is sufficient Gln for Glu production in the neuronal cells (see reaction (3.1.2)).

Unless otherwise stated, all dimensionless parameters for the remainder of this chapter (except e) will be taken to be unity, with physically realistic $e = 0.5$. The associated default values of the unbarred dimensionless parameters are displayed in Table 3.2.

In Figure 3.5, we compare the numerical solutions of equations (3.2.23)-(3.2.28) when all parameters are scaled as above (3.3.1)-(3.3.4) with the associated default parameters in Table 3.2 (when e is varied). We see that with the new scaling parameters G_N and g_L become higher, while g_N, G_E and G_L become smaller when e is reduced. This motivates the scaling of the dependent variables that is presented in the next section.

3.3.2 Variable Scaling

We scale the dependent variables as follows:

$$G_N, g_L = O(e^{-1}) >> g_N, G_L = O(e) >> G_E = O(e^2). \tag{3.3.5}$$

As stated in §3.2.1, the total value of Glu and Gln in mammalian brain is approximately 12.5 and 5.5 mM, respectively. The Glu concentration is high in the neuron and in the ECS its concentration must not exceed approximately 0.06 mM to prevent excitotoxic

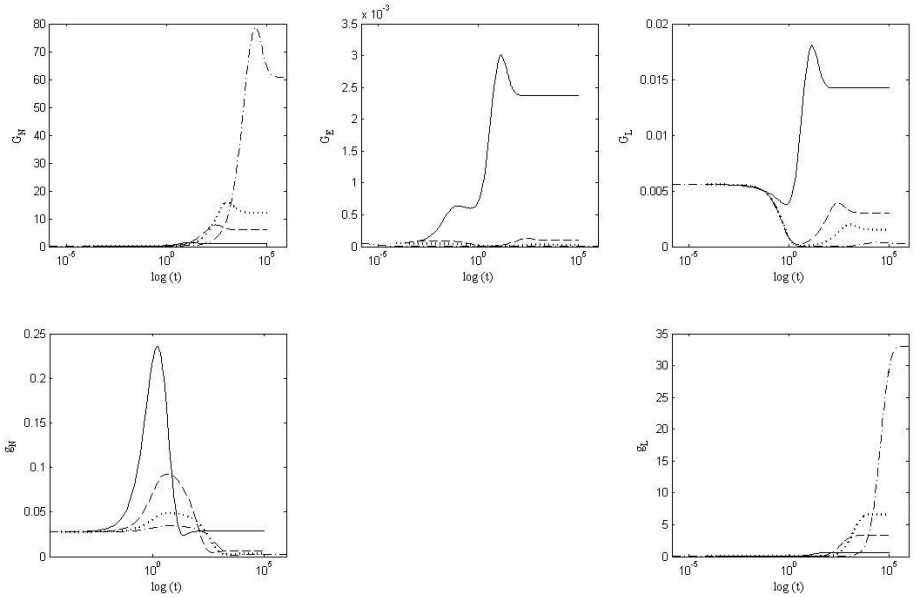

Figure 3.5: A comparison of the numerical solutions for all variables of system (3.2.23)-(3.2.28) when all parameters are scaled as shown in (3.3.1)-(3.3.4) and the associated default parameters are shown in Table 3.2 with e is varied, (e = 0.5: solid lines; e = 0.1: dashed lines; e = 0.05: dotted lines; and e = 0.01: dashed-dotted lines).

neuronal damage. The Gln concentration is higher in the glial cells than elsewhere. From this we can deduce that the levels of Glu in the neuronal cell (G_N) and Gln in the glial cell (g_L) are higher than the concentrations in any other compartments. We scale

$$G_N, g_L = O(\mathrm{e}^{-1}).$$

The Glu concentration is least in the ECS, so we scale

$$G_E = O(\mathrm{e}^2).$$

Finally, we scale the Gln concentration in both the neuronal and glial cell to be intermediate:

$$g_N, G_L = O(\mathrm{e}).$$

Guided by (3.3.5) we rescale the dependent variables as follows

$$G_N = \frac{1}{\mathrm{e}}\bar{G}_N, \qquad g_N = \mathrm{e}\bar{g}_N, \qquad G_E = \mathrm{e}^2\bar{G}_E, \qquad G_L = \mathrm{e}\bar{G}_L, \qquad g_L = \frac{1}{\mathrm{e}}\bar{g}_L. \tag{3.3.6}$$

Inserting the associated rescalings in the governing ODEs, equations (3.2.23)-(3.2.20)

transform to give (dropping the bars for notational simplicity):

$$\begin{aligned}
e^{-2}\frac{dG_N}{dt} &= g_N - l_G G_N, && (3.3.7)\\
\frac{dg_N}{dt} &= l_n[1-(G_N+g_L)-e^2(g_N+G_L)-e^4 G_E - e^3 g_1 g_N] - g_N, && (3.3.8)\\
e^2\frac{dG_E}{dt} &= l_G G_N - l_m G_E + l_c G_L, && (3.3.9)\\
\frac{dG_L}{dt} &= l_m G_E - (l_2 + l_c) G_L, && (3.3.10)\\
e^{-2}\frac{dg_L}{dt} &= l_2 G_L - \frac{l_{go} G_E}{l_h + G_E}[g_L - e^3 g_2(1-(G_N+g_L)-e^2(g_N+G_L) \\
&\quad -e^4 G_E)], && (3.3.11)
\end{aligned}$$

with initial conditions

$$\begin{aligned}
&G_N(0) = G_N^{(0)}, \qquad g_N(0) = g_N^{(0)}, \qquad G_E(0) = G_E^{(0)}, \\
&G_L(0) = G_L^{(0)}, \qquad g_L(0) = g_L^{(0)}.
\end{aligned} \tag{3.3.12}$$

We notice that estimates of the rescaled initial conditions derive from equations (3.2.28) and (3.3.6).

As stated above, we focus on a case for which $e = 0.05$ so that the analysis is tractable (our earlier numerical simulations indicate that the behaviour when $e = 0.05$ is qualitatively similar to that when $e = 0.5$).

3.3.3 Steady-State Analysis

The steady-state solutions of equations (3.2.23)-(3.2.27) (before scaling parameters and variables) are presented in equations (3.2.29)-(3.2.33). Here we state the equivalent steady-state solutions of the rescaled equations (3.3.7)-(3.3.11):

$$G_N = \frac{L_0}{L_1} + e^2\frac{L_0 L_2}{L_1^2} + e^3\frac{L_0 L_3}{L_1^2} + O(e^4), \tag{3.3.13}$$

where

$$\begin{aligned} L_0 &= l_{go}(l_2 + l_c) - l_2 l_m l_h, \\ L_1 &= (l_2 + l_c)[l_G + l_{go} + l_{go}\frac{l_G}{l_n}], \\ L_2 &= -l_{go} l_G (l_2 + l_c)(1 + \frac{1}{l_2}), \\ L_3 &= -l_{go} l_G (l_2 + l_c)(g_1 + \frac{g_2}{l_n}), \end{aligned}$$

together with

$$g_L = 1 - (\frac{L_0}{L_1})b_{10} - e^2(\frac{L_0}{L_1})b_{12} - e^3(\frac{L_0}{L_1})b_{13} + O(e^4), \tag{3.3.14}$$

$$g_N = l_G G_N, \tag{3.3.15}$$

$$G_L = \frac{l_G}{l_2} G_N, \tag{3.3.16}$$

$$G_E = \frac{l_G(l_2 + l_c)}{\bar{l}_m l_2} G_N, \tag{3.3.17}$$

where

$$\begin{aligned} b_{10} &= (1 + \frac{l_G}{l_n}), \\ b_{12} &= (l_G(1 + \frac{1}{l_2}) + \frac{L_2}{L_1} b_{10}), \\ b_{13} &= (g_1 l_G + \frac{L_3}{L_1} b_{10}). \end{aligned}$$

We note that in the above expressions for the steady-state solutions (see equations (3.3.13)-(3.3.17)) the coefficient of $O(e)$ vanishes.

3.3.4 Numerical Simulations

In this section we construct numerical solutions of equations (3.3.7)-(3.3.11) with $e = 0.05$, and all parameters and initial conditions as per Figure 3.5 and $e = 0.05$.

To identify clearly the relevant timescales of interest, we plot the dependent variables against $\log(t)$ in Figure 3.6. Figure 3.6 reveals that G_E changes dramatically throughout the course of the simulation, initially increasing until $t \approx 10^{-4}$, following a rapidly decreasing line until $t \approx 1$ and then increasing before settling to a steady-state. G_L decreases rapidly for $10^{-4} < t < 1$ and then increasing before setting to a steady-state. In addition, the variable g_N increases for $10^{-3} < t < 1$, and then decreases

rapidly before tending to its steady-state. By contrast, G_N and g_L increase rapidly for $1 < t < 10^3$ and for $10^2 < t < 10^3$, respectively, and then settle to their steady-states. Guided by these numerical results, we suppose that our dimensionless system (3.3.7)-(3.3.12) evolves on three distinct timescales, namely $t = O(\mathrm{e}^2)$, $t = O(1)$ and $t = O(\mathrm{e}^{-2})$.

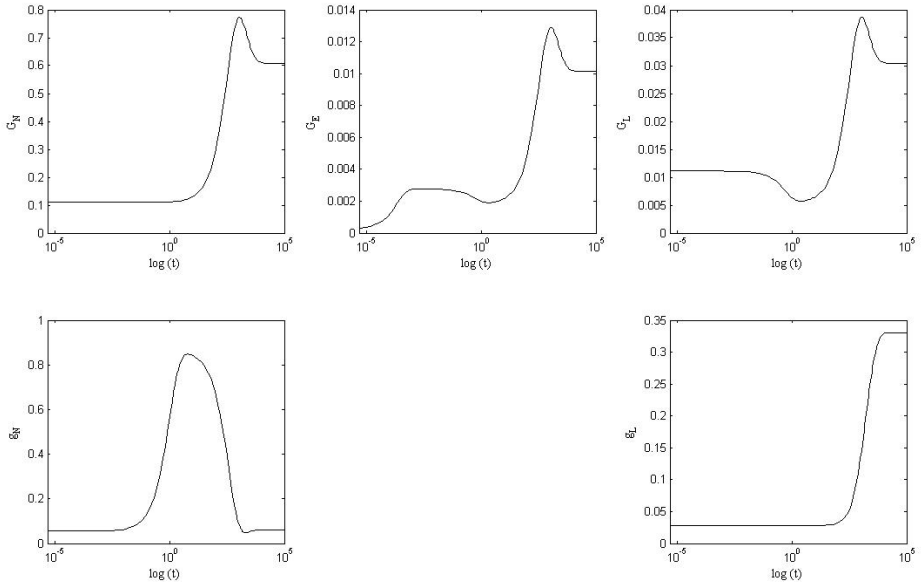

Figure 3.6: Semilog plots of the dimensionless solutions in equations (3.3.7)-(3.3.11) with $\mathrm{e} = 0.05$, other parameter values and initial conditions as performed in Figure 3.5.

In the next section we consider how the system behaves on each of these timescales. When comparing the numerical solutions and the asymptotic approximations we fix the parameters and initial conditions as per Figure 3.6.

3.3.5 Asymptotic Expansions

In this section we construct asymptotic solutions of equations (3.3.7)-(3.3.11) for the three timescales of interest.

Timescale I: $t = O(\mathrm{e}^2)$

To study this fast timescale, we re-scale $t = \mathrm{e}^2 t_1$. Equations (3.3.7)-(3.3.11) then become

$$\frac{1}{\mathrm{e}^4}\cdot\frac{dG_N}{dt_1} = g_N - \mathrm{l}_G G_N, \tag{3.3.18}$$

$$\frac{1}{\mathrm{e}^2}\cdot\frac{dg_N}{dt_1} = \mathrm{l}_n[1-(G_N+g_L)-\mathrm{e}^2(g_N+G_L)-\mathrm{e}^4 G_E-\mathrm{e}^3\mathrm{g}_1 g_N]-g_N, \tag{3.3.19}$$

$$\frac{dG_E}{dt_1} = \mathrm{l}_G G_N - \mathrm{l}_m G_E + \mathrm{l}_c G_L, \tag{3.3.20}$$

$$\frac{1}{\mathrm{e}^2}\cdot\frac{dG_L}{dt_1} = \mathrm{l}_m G_E - (\mathrm{l}_2+\mathrm{l}_c)G_L, \tag{3.3.21}$$

$$\frac{1}{\mathrm{e}^4}\cdot\frac{dg_L}{dt_1} = \mathrm{l}_2 G_L - \frac{\mathrm{l}_{go} G_E}{\mathrm{l}_h + G_E}[g_L - \mathrm{e}^3\mathrm{g}_2(1-(G_N+g_L)-\mathrm{e}^2(g_N+G_L) -\mathrm{e}^4 G_E)], \tag{3.3.22}$$

and the initial conditions are as stated in equation (3.3.12). Recalling that the coefficient of $O(\mathrm{e})$ of all variables equals zero (see equations (3.3.13)-(3.3.17)), we seek solutions which are regular power series expansions of the form

$$G_N(\mathrm{e}) = G_{N0} + \mathrm{e}^2 G_{N2} + O(\mathrm{e}^3), \tag{3.3.23}$$

$$g_N(\mathrm{e}) = g_{N_0} + \mathrm{e}^2 g_{N_2} + O(\mathrm{e}^3), \tag{3.3.24}$$

$$G_E(\mathrm{e}) = G_{E0} + \mathrm{e}^2 G_{E2} + O(\mathrm{e}^3), \tag{3.3.25}$$

$$G_L(\mathrm{e}) = G_{L0} + \mathrm{e}^2 G_{L2} + O(\mathrm{e}^3), \tag{3.3.26}$$

$$g_L(\mathrm{e}) = g_{L_0} + \mathrm{e}^2 g_{L_2} + O(\mathrm{e}^3), \tag{3.3.27}$$

where $0 < \mathrm{e} \ll 1$. Substituting equations (3.3.23)-(3.3.27) into (3.3.18)-(3.3.22) and equating powers of e, we obtain at leading order:

$$\frac{dG_{N0}}{dt_1} = 0, \tag{3.3.28}$$

$$\frac{dg_{N0}}{dt_1} = 0, \tag{3.3.29}$$

$$\frac{dG_{E0}}{dt_1} = \mathrm{l}_G G_{N0} - \mathrm{l}_m G_{E0} + \mathrm{l}_c G_{L0}, \tag{3.3.30}$$

$$\frac{dG_{L0}}{dt_1} = 0, \tag{3.3.31}$$

$$\frac{dg_{L_0}}{dt_1} = 0. \tag{3.3.32}$$

Solving the leading order system (3.3.28)-(3.3.32), we have that G_{N0}, g_{N_0}, G_{L0} and g_{L_0} are constant and therefore equal to their initial values. Solving equation (3.3.30), we

obtain

$$G_{E0}(t_1) = (G_E^{(0)} - \frac{l_G G_N^{(0)} + l_c G_L^{(0)}}{l_m})e^{-l_m t_1} + (\frac{l_G G_N^{(0)} + l_c G_L^{(0)}}{l_m}). \quad (3.3.33)$$

It is noted that when we consider the next order of e, the $O(e)$ coefficients for all dependent variables are equal to zero as we have mentioned in §3.3.3. Then we continue our analysis by focussing on terms that are $O(e^2)$ and equating coefficients of $O(e^2)$ yields:

$$\frac{dG_{N2}}{dt_1} = 0, \quad (3.3.34)$$
$$\frac{dg_{N2}}{dt_1} = l_n[1 - (G_{N0} + g_{L0})] - g_{N0}, \quad (3.3.35)$$
$$\frac{dG_{E2}}{dt_1} = l_G G_{N2} - l_m G_{E2} + l_c G_{L2}, \quad (3.3.36)$$
$$\frac{dG_{L2}}{dt_1} = l_m G_{E0} - (l_2 + l_c) G_{L0}, \quad (3.3.37)$$
$$\frac{dg_{L2}}{dt_1} = 0. \quad (3.3.38)$$

We can see from equations (3.3.34) and (3.3.38) that G_{N2} and g_{L2} are constant. Matching their initial values, we obtain $G_{N2} = 0$ and $g_{L2} = 0$. Solving (3.3.35), we see

$$g_{N2}(t_1) = [l_n(1 - G_N^{(0)} - g_L^{(0)}) - g_N^{(0)}]t_1, \quad (3.3.39)$$

and solving (3.3.37), we get

$$G_{L2}(t_1) = (G_E^{(0)} - \frac{l_G G_N^{(0)} + l_c G_L^{(0)}}{l_m})(1 - e^{-l_m t_1}) + (l_G G_N^{(0)} - l_2 G_L^{(0)})t_1. \quad (3.3.40)$$

Finally, substituting from (3.3.40) into (3.3.36), and noting that $G_{N2} = 0$, we have

$$\begin{aligned} G_{E2}(t_1) = & -l_c(G_E^{(0)} - \frac{l_G G_N^{(0)} + l_c G_L^{(0)}}{l_m})e^{-l_m t_1} t_1 \\ & - \frac{l_c}{l_m}[G_E^{(0)} + \frac{l_2}{l_m} G_L^{(0)} - \frac{2 l_G G_N^{(0)} + l_c G_L^{(0)}}{l_m}]e^{-l_m t_1} \\ & + \frac{l_c}{l_m}(l_G G_N^{(0)} - l_2 G_L^{(0)})t_1 \\ & + \frac{l_c}{l_m}[G_E^{(0)} + \frac{l_2}{l_m} G_L^{(0)} - \frac{2 l_G G_N^{(0)} + l_c G_L^{(0)}}{l_m}]. \end{aligned} \quad (3.3.41)$$

Combining the solutions of all variables from $O(1)$ to $O(e^2)$, we can see that only G_N and g_L remain constant (their initial values) over this entire timescale. The solutions of

$g_N(t_1)$,$G_L(t_1)$ and $G_E(t_1)$ are

$$\begin{aligned} g_N(t_1) &\approx g_N^{(0)} + \mathrm{e}^2 \hat{g}_{N2} t_1, && (3.3.42)\\ G_L(t_1) &\approx G_L^{(0)} + \mathrm{e}^2(\hat{G}_{E0} - \hat{G}_{E0} e^{-\mathrm{l}_m t_1} + \hat{G}_{L2} t_1), && (3.3.43)\\ G_E(t_1) &\approx G_E^{(0)} - \hat{G}_{E0} + \hat{G}_{E0} e^{-\mathrm{l}_m t_1} \\ &\quad + \mathrm{e}^2(\hat{G}_{E2} - \hat{G}_{E2} e^{-\mathrm{l}_m t_1} - \mathrm{l}_c \hat{G}_{E0} e^{-\mathrm{l}_m t_1} t_1 + \frac{\mathrm{l}_c}{\mathrm{l}_m} \hat{G}_{L2} t_1), && (3.3.44) \end{aligned}$$

where

$$\begin{aligned} \hat{g}_{N2} &= (\mathrm{l}_n(1 - G_N^{(0)} - g_L^{(0)}) - g_N^{(0)}),\\ \hat{G}_{E0} &= (G_E^{(0)} - \frac{\mathrm{l}_G G_N^{(0)} + \mathrm{l}_c G_L^{(0)}}{\mathrm{l}_m}),\\ \hat{G}_{L2} &= (\mathrm{l}_G G_N^{(0)} - \mathrm{l}_2 G_L^{(0)}),\\ \hat{G}_{E2} &= \frac{\mathrm{l}_c}{\mathrm{l}_m}(\hat{G}_{E0} - \frac{\hat{G}_{L2}}{\mathrm{l}_m}). \end{aligned}$$

When $t_1 \approx O(\mathrm{e}^{-2})$ (i.e. when $t \approx O(1)$), the expansions for g_N, G_E and G_L break down. This can motivate analysis on the intermediate timescale which is presented in next section. As $t_1 \approx O(\mathrm{e}^{-2})$, we get:

$$\begin{aligned} g_N &\approx \mathrm{l}_n(1 - G_N^{(0)} - g_L^{(0)}),\\ G_L &\approx \mathrm{l}_G G_N^{(0)} + (1 - \mathrm{l}_2) G_L^{(0)}, && (3.3.45)\\ G_E &\approx \frac{\mathrm{l}_G}{\mathrm{l}_m}(1 - \mathrm{l}_c) G_N^{(0)} + \frac{\mathrm{l}_c}{\mathrm{l}_m}(1 - \mathrm{l}_2) G_L^{(0)}. \end{aligned}$$

(3.3.45) will be used as the initial (or matching) conditions for g_N, G_L and G_E on the following timescale.

Figure 3.7 illustrates those variables whose approximations change over this timescale. The resulting solutions of $g_N(t_1)$, $G_E(t_1)$ and $G_L(t_1)$ from (3.3.42)-(3.3.44) are plotted (notice that we have plotted both the numerical solutions of the full system and the approximate solutions against $\log(t)$). We see unbounded growth of g_N, G_E and G_L, and note that there is good agreement between the analytical and numerical solutions of all variables for $0 \leq t \leq 10^{-1}$.

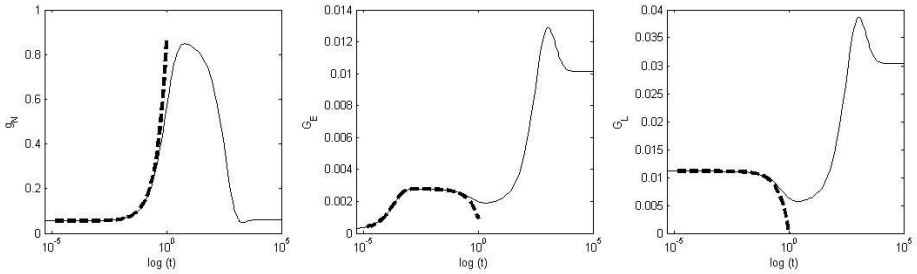

Figure 3.7: A comparison of the asymptotic and numerical solutions of g_N, G_E and G_L on the initial timescale. The numerical solutions to the dimensionless model (3.3.7)-(3.3.11) are represented by the solid line, while the asymptotic approximations (3.3.42)-(3.3.44) are given by the dashed line with all parameter values and initial conditions as used in Figure 3.6.

Timescale II: $t = O(1)$

We next consider the intermediate timescale $t = O(1)$. Letting $t = t_2$ [1], the governing equations are given by (3.3.7)-(3.3.11) which we re-state below in terms of t_2:

$$e^{-2}\frac{dG_N}{dt_2} = g_N - l_G G_N, \tag{3.3.46}$$

$$\frac{dg_N}{dt_2} = l_n[1 - (G_N + g_L) - e^2(g_N + G_L) - e^4 G_E - e^3 g_1 g_N] - g_N, \tag{3.3.47}$$

$$e^2\frac{dG_E}{dt_2} = l_G G_N - l_m G_E + l_c G_L, \tag{3.3.48}$$

$$\frac{dG_L}{dt_2} = l_m G_E - (l_2 + l_c) G_L, \tag{3.3.49}$$

$$e^{-2}\frac{dg_L}{dt_2} = l_2 G_L - \frac{l_{go} G_E}{l_h + G_E}[g_L - e^3 g_2(1 - (G_N + g_L) - e^2(g_N + G_L) - e^4 G_E)]. \tag{3.3.50}$$

Matching to the previous timescale, we note that the initial conditions of G_N and g_L on timescale II are the same as those on timescale I since their approximation was simply constant on this first timescale. By contrast, since the dynamics of $g_N(t_1)$, $G_E(t_1)$ and $G_L(t_1)$ change on the timescale I, we use the matching conditions at $t_2 = 0$ given by

[1] We notice that we have renamed t as t_2 in order to make it clear we are examining the intermediate timescale, but we could equally have simply written t.

equation (3.3.45) as their initial conditions as follows:

$$\begin{aligned} g_N^{(0,t_2)} &= l_n(1 - G_N^{(0)} - g_L^{(0)}), \\ G_L^{(0,t_2)} &= l_G G_N^{(0)} + (1 - l_2) G_L^{(0)}, \\ G_E^{(0,t_2)} &= \frac{l_G}{l_m}(1 - l_c) G_N^{(0)} + \frac{l_c}{l_m}(1 - l_2) G_L^{(0)}, \end{aligned} \tag{3.3.51}$$

where $G_N^{(0)}$, $g_L^{(0)}$ and $G_L^{(0)}$ are the original initial conditions (see equation (3.3.12)), and $g_N^{(0,t_2)}$, $G_L^{(0,t_2)}$ and $G_E^{(0,t_2)}$ are the matching conditions on this second timescale. For the remainder of this timescale (for notational simplicity), we write

$$g_N^{(0,t_2)} = g_N^{(0)}, \quad G_L^{(0,t_2)} = G_L^{(0)} \quad \text{and} \quad G_E^{(0,t_2)} = G_E^{(0)}.$$

After substituting the expansions (3.3.23)-(3.3.27) into equations (3.3.46)-(3.3.50), and equating powers of e, we have at leading order:

$$\frac{dG_{N0}}{dt_2} = 0, \tag{3.3.52}$$

$$\frac{dg_{N0}}{dt_2} = l_n(1 - G_{N0} - g_{L_0}) - g_{N0}, \tag{3.3.53}$$

$$0 = l_G G_{N0} - l_m G_{E0} + l_c G_{L0}, \tag{3.3.54}$$

$$\frac{dG_{L0}}{dt_2} = l_m G_{E0} - (l_2 + l_c) G_{L0}, \tag{3.3.55}$$

$$\frac{dg_{L0}}{dt_2} = 0. \tag{3.3.56}$$

From equations (3.3.52) and (3.3.56), we see that G_{N0} and g_{L_0} remain constant on this timescale. Equations (3.3.53) and (3.3.55) can be integrated with respect to t_2 and combined with (3.3.54) in order to determine g_{N_0}, G_{E0} and G_{L0}.

Integrating equation (3.3.53), we obtain

$$g_{N0}(t_2) = l_n(1 - G_N^{(0)} - g_L^{(0)}) + [g_N^{(0)} - l_n(1 - G_N^{(0)} - g_L^{(0)})]e^{-t_2}, \tag{3.3.57}$$

where, as before, the superscript (0) denotes the initial value of a particular variable.

Adding equations (3.3.54) and (3.3.55), we obtain

$$\frac{dG_{L0}}{dt_2} = l_G G_N^{(0)} - l_2 G_{L0}, \tag{3.3.58}$$

giving

$$G_{L0}(t_2) = \frac{l_G}{l_2} G_N^{(0)} + (G_L^{(0)} - \frac{l_G}{l_2} G_N^{(0)}) e^{-l_2 t_2}. \tag{3.3.59}$$

Substituting equation (3.3.59) into (3.3.54), we have

$$G_{E0}(t_2) = \frac{l_G}{l_m}(1 + \frac{l_c}{l_2}) G_N^{(0)} + \frac{l_c}{l_m}(G_L^{(0)} - \frac{l_G}{l_2} G_N^{(0)}) e^{-l_2 t_2}. \tag{3.3.60}$$

We note that

$$G_{E0}(t_2) \to \frac{l_G}{l_m} G_N^{(0)} + \frac{l_c}{l_m} G_L^{(0)} \text{ as } t \to 0. \tag{3.3.61}$$

Since the $O(\mathrm{e})$ coefficients of all variables are equal to zero (see §3.3.3), we equate coefficients of $O(\mathrm{e}^2)$ and obtain:

$$\frac{dG_{N2}}{dt_2} = g_{N0} - l_G G_{N0}, \tag{3.3.62}$$

$$\frac{dg_{N2}}{dt_2} = -l_n(G_{N2} + g_{L2} + g_{N0} + G_{L0}) - g_{N2}, \tag{3.3.63}$$

$$\frac{dG_{E0}}{dt_2} = l_G G_{N2} - l_m G_{E2} + l_c G_{L2}, \tag{3.3.64}$$

$$\frac{dG_{L2}}{dt_2} = l_m G_{E2} - (l_2 + l_c) G_{L2}, \tag{3.3.65}$$

$$\frac{dg_{L2}}{dt_2} = l_2 G_{L0} - \frac{l_{go} G_{E0}}{l_h + G_{E0}} g_{L0}. \tag{3.3.66}$$

Recalling that G_{N0} is constant and g_{N0} is defined by equation (3.3.57), we can integrate (3.3.62) to obtain

$$\begin{aligned} G_{N2}(t_2) = {} & [l_n(1 - G_N^{(0)} - g_L^{(0)}) - l_G G_N^{(0)}] t_2 - [g_N^{(0)} - l_n(1 - G_N^{(0)} - g_L^{(0)})] e^{-t_2} \\ & + [g_N^{(0)} - l_n(1 - G_N^{(0)} - g_L^{(0)})]. \end{aligned} \tag{3.3.67}$$

Differentiating equation (3.3.60), we have

$$\frac{dG_{E0}}{dt_2} = -\frac{l_2 l_c}{l_m}(G_L^{(0)} - \frac{l_G}{l_2} G_N^{(0)}) e^{-l_2 t_2}. \tag{3.3.68}$$

Adding (3.3.64) and (3.3.65) by using (3.3.68), then integrating it, we have

$$\begin{aligned} G_{L2}(t_2) &= \frac{l_c l_2}{l_m}(G_L^{(0)} - \frac{l_G}{l_2}G_N^{(0)})e^{-l_2 t_2}t_2 + \frac{l_G}{l_2}(l_n(1-G_N^{(0)}-g_L^{(0)}) - l_G G_N^{(0)})t_2 \\ &\quad - l_G(\frac{g_N^{(0)} - l_n(1-G_N^{(0)}-g_L^{(0)})}{l_2-1})e^{-t_2} + l_G[\frac{l_n(1-G_N^{(0)}-g_L^{(0)}) - l_G G_N^{(0)}}{l_2^2} \\ &\quad + (g_N^{(0)} - l_n(1-G_N^{(0)}-g_L^{(0)}))(\frac{1}{l_2-1} - \frac{1}{l_2})]e^{-l_2 t_2} \\ &\quad + l_G(\frac{g_N^{(0)} - l_n(1-G_N^{(0)}-g_L^{(0)})}{l_2} - \frac{l_n(1-G_N^{(0)}-g_L^{(0)}) - l_G G_N^{(0)}}{l_2^2}). \end{aligned} \quad (3.3.69)$$

Substituting (3.3.68) into (3.3.64), and then integrating with respect to t_2, we have

$$G_{E2}(t_2) = \frac{1}{l_m}[l_G G_{N2} + l_c G_{L2} + \frac{l_c l_2}{l_m}(G_L^{(0)} - \frac{l_G}{l_2}G_N^{(0)})e^{-l_2 t_2}], \quad (3.3.70)$$

where G_{N2} and G_{L2} are defined by (3.3.67) and (3.3.69).

Equations (3.3.63) and (3.3.66) can be integrated numerically with respect to t_2 to determine g_{N2} and g_{L2}.

The solutions of each variable on the intermediate timescale consist of a leading order term and an $O(\mathrm{e}^2)$ contribution. When $t_2 \approx O(\mathrm{e}^{-2})$ (i.e. when $t \approx O(\mathrm{e}^{-2})$) the expansions for all variables break down (for example, see equation (3.3.67)). Similarly to on timescale I, this motivates the analysis on the final timescale for which $t = O(\mathrm{e}^{-2})$. We note that taking the limit as $t_2 = O(\mathrm{e}^{-2})$, enables us to calculate all the matching conditions for this subsequent timescale.

Figure 3.8 shows good agreement between the numerical and analytical solutions for all variables in the range $10^{-1} \leq t \leq 10^2$. In Figure 3.8, G_N, G_E, G_L and g_L display unbounded growth as $t_2 \to ¥$, while g_N shows unbounded decay.

The final timescale sees the system behaviour finally achieving its steady-state.

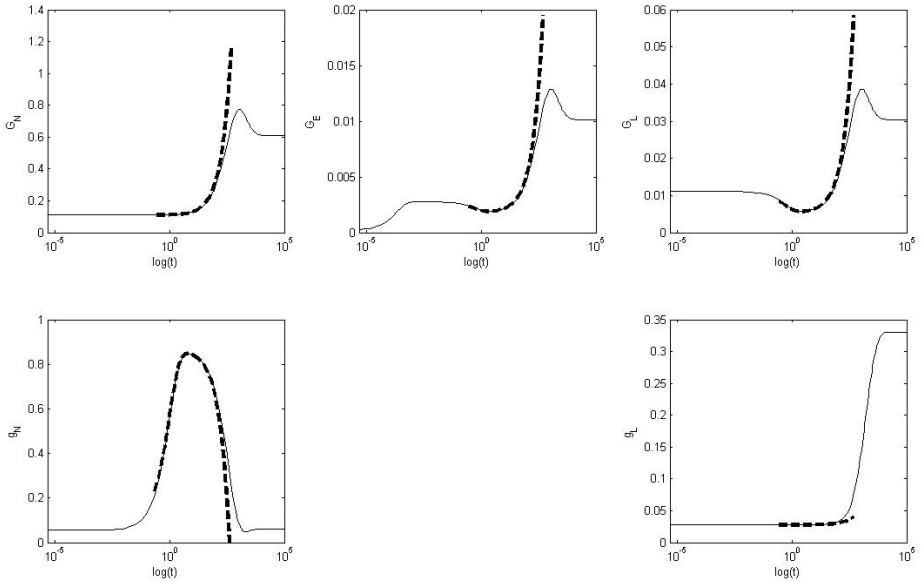

Figure 3.8: A comparison of the asymptotic and numerical solutions on the second timescale ($t = O(1)$). All numerical and asymptotic solutions of variables match perfectly in the range $10^{-1} \leq t \leq 10^2$.

Timescale III: $t = O(\mathrm{e}^{-2})$

When $t = O(1)$, all variables evolve with time. We now consider the dynamics on the long timescale, $t = \mathrm{e}^{-2}t_3$ for which the governing equations become

$$\frac{dG_N}{dt_3} = g_N - \mathrm{l}_G G_N, \tag{3.3.71}$$

$$\mathrm{e}^2\frac{dg_N}{dt_3} = \mathrm{l}_n[1 - (G_N + g_L) - \mathrm{e}^2(g_N + G_L) - \mathrm{e}^4 G_E - \mathrm{e}^3 \mathrm{g}_1 g_N] - g_N, \tag{3.3.72}$$

$$\mathrm{e}^4\frac{dG_E}{dt_3} = \mathrm{l}_G G_N - \mathrm{l}_m G_E + \mathrm{l}_c G_L, \tag{3.3.73}$$

$$\mathrm{e}^2\frac{dG_L}{dt_3} = \mathrm{l}_m G_E - (\mathrm{l}_2 + \mathrm{l}_c) G_L, \tag{3.3.74}$$

$$\frac{dg_L}{dt_3} = \mathrm{l}_2 G_L - \frac{\mathrm{l}_{go} G_E}{\mathrm{l}_h + G_E}[g_L - \mathrm{e}^3 \mathrm{g}_2(1 - (G_N + g_L) - \mathrm{e}^2(g_N + G_L) - \mathrm{e}^4 G_E)]. \tag{3.3.75}$$

The initial conditions on this timescale are matched to the approximations on the previous timescale when $t_2 = O(\mathrm{e}^{-2})$ (i.e. when $t_3 \to 0$). Substituting series expansions of the form (3.3.23)-(3.3.27) into equations (3.3.71)-(3.3.75) and equating like powers of e,

we get at leading order:

$$\begin{aligned}
\frac{dG_{N0}}{dt_3} &= g_{N0} - l_G G_{N0}, && (3.3.76)\\
0 &= l_n(1 - G_{N0} - g_{L0}) - g_{N0}, && (3.3.77)\\
0 &= l_G G_{N0} - l_m G_{E0} + l_c G_{L0}, && (3.3.78)\\
0 &= l_m G_{E0} - (l_2 + l_c) G_{L0}, && (3.3.79)\\
\frac{dg_{L0}}{dt_3} &= l_2 G_{L0} - \frac{l_{go} G_{E0}}{l_h + G_{E0}} g_{L0}. && (3.3.80)
\end{aligned}$$

Adding equations (3.3.78) and (3.3.79), we get

$$G_{L0}(t_3) = \frac{l_G}{l_2} G_{N0}. \tag{3.3.81}$$

Using equations (3.3.79) and (3.3.81), we get

$$G_{E0}(t_3) = (\frac{l_c + l_2}{l_m}) \frac{l_G}{l_2} G_{N0}. \tag{3.3.82}$$

Solving equation (3.3.77), we obtain

$$g_{N0}(t_3) = l_n(1 - G_{N0} - g_{L0}). \tag{3.3.83}$$

Substituting (3.3.83) into (3.3.76), and substituting (3.3.81) and (3.3.82) into (3.3.80), we have

$$\begin{aligned}
\frac{dG_{N0}}{dt_3} &= l_n(1 - g_{L0}) - (l_n + l_G) G_{N0}, && (3.3.84)\\
\frac{dg_{L0}}{dt_3} &= l_G G_{N0} - \frac{l_{go}(l_2 + l_c) l_G G_{N0} g_{L0}}{l_2 l_m l_h + l_{go}(l_2 + l_c) l_G G_{N0}}. && (3.3.85)
\end{aligned}$$

It remains to solve equations (3.3.84)-(3.3.85) numerically: equations (3.3.81)-(3.3.83) can then be used to determine the solution of the other system variables.

As for the two previous timescales, the $O(\mathrm{e})$ coefficients of all variables vanish. Equat-

ing power of e, we have at $O(e^2)$:

$$\frac{dG_{N2}}{dt_3} = g_{N2} - l_G G_{N2}, \tag{3.3.86}$$

$$\frac{dg_{N0}}{dt_3} = -l_n(G_{N2} + g_{L2} + g_{N0} + G_{L0}) - g_{N2}, \tag{3.3.87}$$

$$0 = l_G G_{N2} - l_m G_{E2} + l_c G_{L2}, \tag{3.3.88}$$

$$\frac{dG_{L0}}{dt_3} = l_m G_{E2} - (l_2 + l_c) G_{L2}, \tag{3.3.89}$$

$$\frac{dg_{L_2}}{dt_3} = l_2 G_{L2} - \frac{l_{go}}{2(l_h + G_{E0})}(G_{E0} g_{L2} + G_{E2} g_{L0} - \frac{G_{E0} g_{L0} G_{E2}}{l_h + G_{E0}}). \tag{3.3.90}$$

Adding equations (3.3.88) and (3.3.89), we get

$$\frac{dG_{L0}}{dt_3} = l_G G_{N2} - l_2 G_{L2}. \tag{3.3.91}$$

Differentiating equations (3.3.81) and (3.3.83), we respectively have

$$\frac{dG_{L0}}{dt_3} = \frac{l_G}{l_2}(g_{N0} - l_G G_{N0}), \tag{3.3.92}$$

$$\frac{dg_{N0}}{dt_3} = -l_n(g_{N0} - l_G G_{N0} + l_2 G_{L0} - \frac{l_{go} G_{E0}}{l_h + G_{E0}} g_{L_0}). \tag{3.3.93}$$

Substituting (3.3.93) into (3.3.87) and (3.3.92) into (3.3.89) and solving, we get

$$g_{N2}(t_3) = -l_n(G_{N2} + g_{L2} + G_{L0} + l_G G_{N0} - l_2 G_{L0} + \frac{l_{go} G_{E0}}{l_h + G_{E0}} g_{L_0}), \tag{3.3.94}$$

$$G_{L2}(t_3) = \frac{l_G}{l_2}[G_{N2} - \frac{1}{l_2}(g_{N0} - l_G G_{N0})]. \tag{3.3.95}$$

Using (3.3.88) and (3.3.95), we have

$$G_{E2}(t_3) = \frac{l_G l_c}{l_2 l_m}[G_{N2}(1 + \frac{l_2}{l_c}) - \frac{1}{l_2}(g_{N0} - l_G G_{N0})]. \tag{3.3.96}$$

Finally, substituting (3.3.94)-(3.3.96) into equations (3.3.86) and (3.3.90) and numerically integrating them, we obtain solutions of G_{N2} and g_{L2}. When G_{N2} and g_{L2} are known, g_{N2}, G_{L2} and G_{E2} are determined from equations (3.3.94)-(3.3.96).

Combining the leading-order solutions and the $O(e^2)$-solutions for each variable, we compare the numerical and asymptotic results for all variables on the $O(e^{-2})$-timescale in Figure 3.9. We note the good agreement between the numeric and the asymptotic results and in particular that the approximate solutions evolve to the correct steady-state solutions.

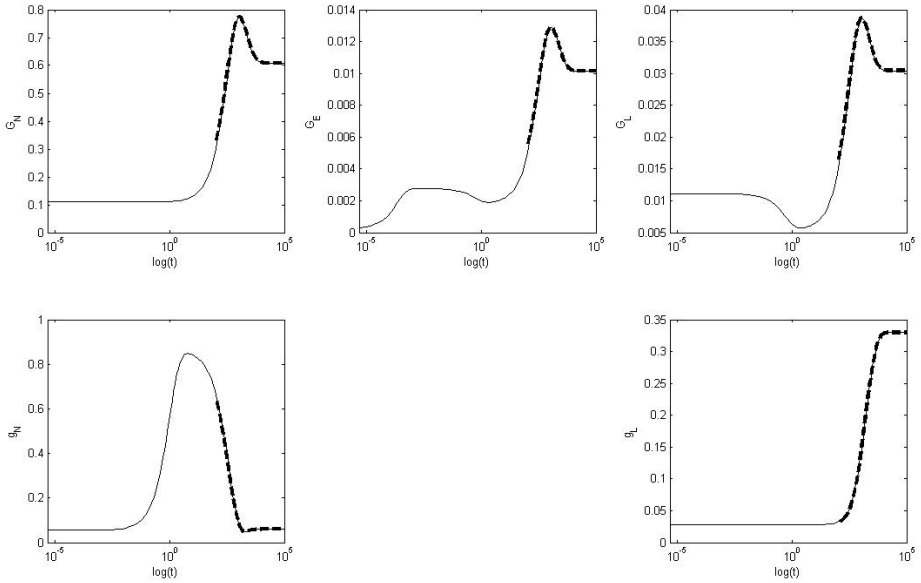

Figure 3.9: A comparison of the asymptotic and numerical solutions at the final $t = O(\mathrm{e}^{-2})$ for all variables against $\log(t)$.

We have presented a model of the glutamate-glutamine cycle. The numerical solutions of equations (3.3.7)-(3.3.11) and the asymptotic approximations on each timescale are in excellent agreement (see Figures 3.7-3.9) when $\mathrm{e} = 0.05$.

We conclude our asymptotic analysis by comparing the numerical solutions of system (3.3.7)-(3.3.12): solid line; with the asymptotic solutions from the three different timescales of interest. The results are presented in Figure 3.10 for different choices of e. As expected, the agreement between the approximate solutions and the numerical simulations improves as e is decreased, the smaller value (epsilon) being used to validate the asymptotic approximations.

3.4 Summary of Glutamate-Glutamine Model

In this chapter we have developed a mathematical model using the principle of mass balance and the law of mass action [73] (for reactions (3.1.1) and (3.1.2)) to study the metabolism of the Glu and Gln cycle in the nervous system. The resulting model consists of six nonlinear ordinary differential equations that describe how Glu and Gln levels in three different compartments (the neuron (N), ECS (E) and glial cell (L))

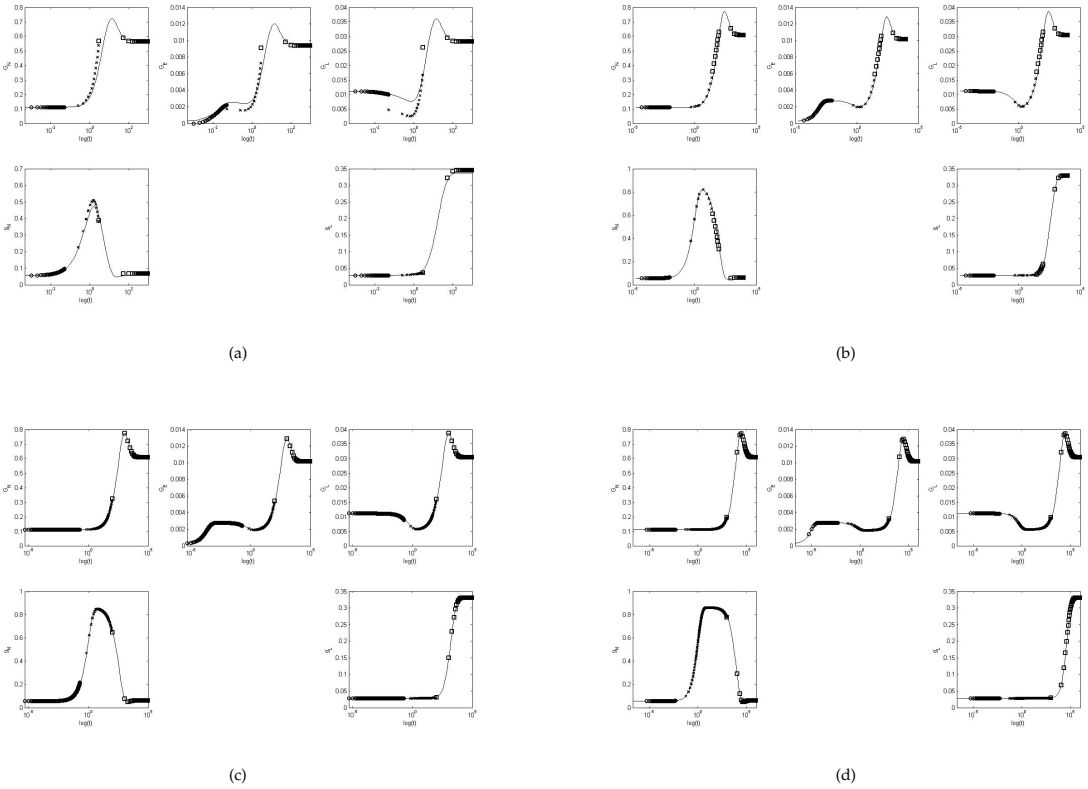

Figure 3.10: Comparisons of the asymptotic and numerical solutions at all timescales (timescale I: circle line; timescale II: cross line; and timescale III: square line) for all variables when e is varied. (a): $e = 0.5$; (b): $e = 0.1$; (c): $e = 0.05$; and (d): $e = 0.01$.

change over time. We used estimates from the literature to infer that the size of these three compartments are such that $V_E < V_N \approx V_L$ [2, 17]. We have also found that there is a conserved quantity in the model, allowing us to reduce it to five ODEs. We then nondimensionalised the governing equations.

We estimated all parameters using inequalities (3.2.36) and (3.2.39) hold for physically realistic steady-state solutions with $\mathrm{e} = 0.5$ from physical realistic value [2, 17]. Numerical simulations performed for a range of values of e (from the physically realistic $\mathrm{e} = 0.5$ to $\mathrm{e} = 0.05 \ll 1$) reveal that the qualitative dynamics do not change as e varies. We exploited this qualitative agreement to justify performing an asymptotic analysis of the governing equations in the limit for which $\mathrm{e} \ll 1$.

After suitably rescaling the system parameters and variables, we analysed equations (3.3.7)-(3.3.12), showing there to be three timescales of interest. This analysis gave insight into processes that controlled the different stages of the Glu-Gln cycle: $t = O(\mathrm{e}^2)$, $t = O(1)$ and $t = O(\mathrm{e}^{-2})$.

Initially, on the short timescale $t = O(\mathrm{e}^2)$ (i.e. we introduced the scaling $t = \mathrm{e}^2 t_1$), adding the leading order terms for each variable to those at $O(\mathrm{e}^2)$, we derived expressions for g_N, G_E and G_L. These broke down as $t_1 = O(\mathrm{e}^{-2})$ (i.e. $t = O(1)$), see Figure 3.7. This was used to motivate the analysis on the intermediate timescale. Taking the limit as $t_1 = O(\mathrm{e}^{-2})$, we were able to calculate the matching conditions for all variables.

On the intermediate timescale $t = O(1)$ (or $t = t_2$). After matching to the initial timescale and combining the leading-order and $O(\mathrm{e}^2)$ solutions for each variable, we found that all approximations broke down when $t_2 = O(\mathrm{e}^{-2})$ (see Figure 3.8). We were once again able to obtain the matching conditions for the subsequent timescale by taking the limit as $t_2 = O(\mathrm{e}^{-2})$.

On the final timescale $t = O(\mathrm{e}^{-2})$ (or $t = \mathrm{e}^{-2} t_3$). After matching to the intermediate timescale and combining both the leading-order and the $O(\mathrm{e}^2)$ solutions for each variable, we found there was good agreement between the numerical and the asymptotical solutions. In particular the approximations tended to the steady-state solutions of the full system (3.3.7)-(3.3.12), see Figure 3.9.

Finally, we compared the numerical solutions of our system (3.3.7)-(3.3.12) with the asymptotic solutions from the three different timescales of interest ($t = O(\mathrm{e}^2)$, $t = O(1)$ and $t = O(\mathrm{e}^{-2})$) for different choices of e (see Figure 3.10). There was perfectly good agreement with sufficient small e. Reducing e improved the agreement, thus validating our asymptotic approximations.

Despite being the dominant excitatory neurotransmitter in mammalian brain, Glu can be toxic to neurons. After Gln is converted to Glu in the neuronal cell, Glu is stored in the synaptic vesicle. When there is an influxes of calcium through the calcium channels and the Glu receptors, the neuronal calcium triggers fusion of the synaptic vesicle and Glu efflux occurs. However, the excess Glu in the ECS chronically over-activates Glu receptors, causing the release of excess intracellular calcium and leading to neuronal cell death. This process is known as excitotoxicity. As the intracellular calcium level is one of the causes of the excitotoxicity, in the next chapter the model of Glu-Gln cycle is extended to include intracellular calcium.

CHAPTER 4

Calcium Signalling in the Glutamate-Glutamine Cycle

In the previous chapter, we developed a dimensionless model formulated as a system of ODEs in order to study the Glu-Gln cycle within the central nervous system. Both analytical and numerical solutions were presented. Numeric solutions imply that qualitative dynamics of system do not change as e varies from physically realistic value ($e = 0.5$) to asymptotically small value ($e = 0.05 \ll 1$). We exploit this qualitative agreement to motivate performing asymptotic analysis of governing equations in asymptotic limit ($e \ll 1$). This analysis provides insight into processes that regulate different stages of the Glu-Gln cycle. In this chapter we focus on the role of calcium signalling in the Glu-Gln cycle. We start by explaining how calcium interacts with the Glu-Gln cycle and how it triggers excitotoxicity in §4.1. In §4.2, the model of the Glu-Gln cycle in Chapter 3 is then modified to investigate how calcium interacts with the Glu-Gln cycles. Model analysis and simulations are presented in §4.3. In §4.4 we consider when our system affects excitotoxicity by adding a toxic source to the extracellular Glu. In the last section, we summarise our findings and discuss the recent model.

4.1 Introduction

Glu is the key excitatory neurotransmitter in the mammalian brain. After being released from neuronal cells, extracellular Glu is rapidly transported to glial cells by the glutamate-aspartate transporter GLAST (for details see §1.1.4) in order to prevent Glu neurotoxicity or excitotoxicity (excitotoxicity is explained below). In glial cells, Glu is converted to Gln via the enzyme glutamine synthetase. Gln is then released to the neuronal cells via the ECS (extracellular space). In the neuronal cells Gln is converted to

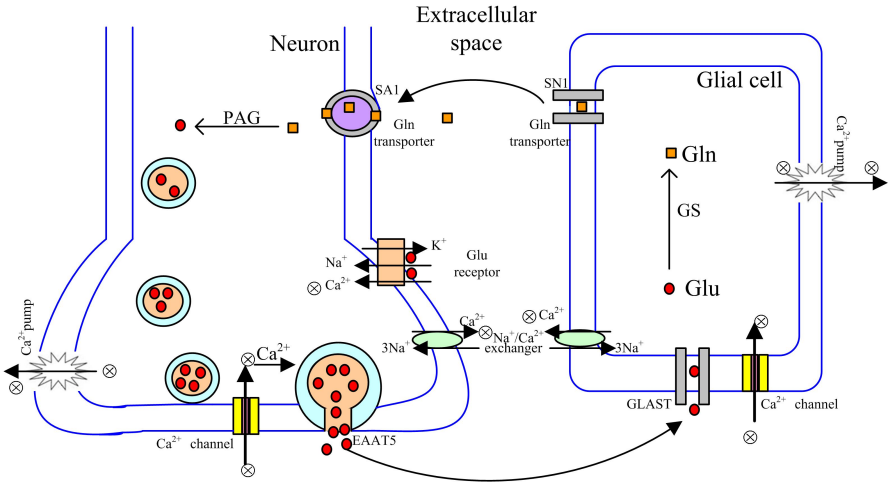

Figure 4.1: A schematic diagram of the release of a neurotransmitter (Glu) from a synaptic vesicle. Gln is released back to the neurons where Glu is regenerated via PAG. Neuronal Glu is stored in the synaptic vesicle and released to the ECS when Ca^{2+} influx through voltage-gated channels and glutamate receptor triggers fusion of the synaptic vesicle with the plasma membrane. Transported to the glial cells via GLAST, Glu is converted to Gln via GS. Ca^{2+} is released from the cells via Ca^{2+} pump and Na^{+}/Ca^{2+} exchanger. Glu (◯) = glutamate; Gln (□) = glutamine; Ca^{2+} (⊗) = calcium; GS = the enzyme glutamine synthetase; PAG = the enzyme glutaminase; GLAST = glutamate aspartate transporter; EAAT5 = excitatory amino acid transporter 5; SN1 = system N transporter 1; SA1 = system A transporter 1; Na^{+} = sodium; K^{+} = potassium.

Glu via the enzyme glutaminase and the resulting Glu is stored in synaptic vesicles. The concentration of Glu in the vesicles can be very high (in excess of 20 mM) [36]. Glu release then occurs by exocytosis (i.e. the release of cellular substances contained in cell vesicles). The vesicle moves toward the presynaptic membrane and waits for Glu release. When an action potential arrives at the terminal (see Figure 4.1), there is an influx of calcium (Ca^{2+}) through voltage-gated channels and Glu receptors. This triggers fusion of the synaptic vesicle with the plasma membrane and Glu efflux occurs [36–40]. This process constitutes the Glu-Gln cycle.

It is believed that Ca^{2+} influx is necessary for the release of neurotransmitters [39]. Thus we consider calcium dynamics in order to understand clearly its roles in the Glu-Gln cycle. Calcium is maintained at a very low level inside resting cells (0.1 mM) but may rise to 5 mM when cells are stimulated. By contrast, extracellular calcium is approximately 2 mM [37, 40, 65]. Since the internal concentration is low, there is a steep concentration gradient across the cell membrane. As there are different levels, the cells

are able to raise their calcium concentration rapidly by opening calcium voltage-gated channels (see Figure 4.1) and relying on passive flow down a steep concentration gradient. In addition to the action of the voltage-gated channels, calcium can enter neuronal cells via the Glu receptor (NMDA, n-methyl-d-aspartic acid). When the Glu receptor is activated by extracellular Glu, ion channels on the cell membrane open. This allows sodium (Na^+) and small amounts of Ca^{2+} to flow into the cells and potassium (K^+) to flow out of the cells [36–40].

Calcium is removed from the cells in two principal ways [40, 58]. Firstly, it is pumped out of a cell, a process that requires expenditure of energy by a calcium ATPase that uses energy stored in ATP. Secondly, there is also a Na^{2+}/Ca^{2+} exchanger in the cell membrane that uses the energy of the Na^{2+} electrochemical gradient to remove calcium from the cell at the expense of Na^{2+} entry (see Figure 4.1).

We note that the calcium dynamics within a glial cell are similar to those within a neuron except there is no calcium influx via the Glu receptor. The glial Glu receptor (AMPA, alpha-amino-3-hydroxy-5-methyl-4-isoxazole-propionic acid) allows Na^+ to flow into the cells and K^+ to flow out [37, 40].

Several studies support the hypothesis that Glu and calcium play important roles in excitotoxicity [40, 53, 75]. Frequently, the Glu concentration released into the ECS rises to high levels (1 mM), but it remains at this level for only a few milliseconds. If abnormally high levels of Glu accumulate in the ECS, the excessive activation of neuronal Glu receptors allows high levels of calcium to enter the neuronal cells. This influx activates a number of enzymes which damage cell structures and cause the cells die. This is the process of excitotoxicity.

The aim of this chapter is to study the role of calcium of the Glu-Gln cycle and in particular the influence of intracellular calcium dynamics on excitotoxicity. In the remainder of this chapter we extend the model of the Glu-Gln cycle developed in Chapter 3 to account for calcium levels in the compartment of interest which is the neuronal cell, since the excitotoxicity occurs only in the neuronal cell. We also present asymptotic analysis and numerical simulations of a system. The excitotoxicity will be presented. The chapter concludes with a summary of our results.

4.2 Model Motivation and Nondimensionalisation

In this section we start by developing an ODE which describes how intracellular levels of Ca^{2+} change over time. We then couple this ODE to our model of the Glu-Gln cycle (see equations (3.2.15)-(3.2.19) in Chapter 3), assuming that intracellular Ca^{2+} within the neuronal cell is the rate-limiting substrate (i.e. the glial and extracellular calcium concentrations are assumed to be present in abundance). We notice that only the neuronal calcium level is considered in here differing from the Glu and Gln levels in Chapter 3 that they occur in three compartments. This is because the excitotoxicity occurs only in the neuronal cell. After nondimensionalising the full model, we use it to study how the rate of calcium influx influences the metabolic demand of the neurotransmitters.

As for Chapter 3, we use the principle of mass balance [73] to derive an ODE which describes the evolution of C_N, the concentration of neuronal calcium (in mM). In what follows we denote by C^E and g_3 the assumed constant concentration of extracellular calcium and the rate of calcium uptake from the neuronal cell to the ECS.

When considering the evolution of C_N, we suppose that the dominant factors are:

- the rate at which extracellular calcium enters via the calcium channel (a passive process),
- the rate at which it enters via the Glu receptor (this requires activation of extracellular Glu and is assumed to be an active process),
- the rate of calcium efflux via the calcium pump and the Na^{2+}/Ca^{2+} exchanger (an active process).

We assume that the rate at which calcium passes from the ECS via the calcium channel to the neuronal cell is proportional to $(C^E - g_3 C_N)$. Combining the above and noting that the total amount of the neuronal calcium is given by $V_N C_N$ (V_N is the volume of the neuronal cell), we deduce that the evolution of C_N satisfies:

$$\frac{d(V_N C_N)}{dt} = \tilde{h}_0 A_2 (C^E - g_3 C_N) + h_1 V_E C^E - h_2 V_N C_N, \tag{4.2.1}$$

where A_2 and V_E represent respectively the cross-sectional area of nervous system and the volume of the ECS. In equation (4.2.1), the positive constants $\tilde{h}_0$, h_1 and h_2 represent the rate at which calcium enters the neuronal via the calcium channel, its rate of influx

via the Glu receptor and its rate of efflux, respectively. The physical interpretation and units of all parameters that appear in (4.2.1) are given in Table 4.1.

Parameters	Physical Meanings	Units
$\tilde{h}_0$	Ca^{2+} influx rate into the neuronal cell via the calcium channel and the exchanger	$(\mathtt{mm})\mathrm{min}^{-1}$
h_1	Ca^{2+} influx rate into the neuronal cell via the glutamate receptor	min^{-1}
h_2	Ca^{2+} efflux rate from the neuronal cell via calcium pump	min^{-1}
C^E	the extracellular Ca^{2+} concentration	mM
V_N, V_E	volume of the neuronal cell and the ECS, respectively	$(\mathtt{mm})^3$
A_2	the cross-sectional area of nervous system,	$(\mathtt{mm})^2$
g_3	Ca^{2+} uptake from the neuronal cell to the ECS coefficient	-

Table 4.1: Interpretation of the parameters that appear in equation (4.2.1).

Recalling that V_N and V_E assumed to be constant, we can rewrite the equation (4.2.1) as follows:

$$\frac{dC_N}{dt} = h_0(C^E - g_3 C_N) + h_1 \frac{V_E}{V_N} C^E - h_2 C_N, \tag{4.2.2}$$

where $h_0 = \dfrac{\tilde{h}_0 A_2}{V_N}$.

Initial Conditions

As stated above, intracellular levels of Ca^{2+} can vary markedly in comparison with C^E, the extracellular calcium concentration. For example, under normal physiological conditions we anticipate $C^E \sim 2$ mM while C_N can vary from 0.1 mM for a resting cell to 5 mM for an activated cell [37, 40, 65]. Accordingly, we prescribe the initial value of the neuronal calcium (in mM) to be

$$C_N(0) = 10^{-3}. \tag{4.2.3}$$

In summary, equations (4.2.2) and (4.2.3) describe how the neuronal calcium concentration changes in neuronal cells. In the next section, we couple an equation (4.2.2) to our earlier model of the Glu-Gln cycle (3.2.15)-(3.2.19).

4.2.1 Calcium Signalling in the Glutamate-Glutamine Cycle

Before nondimensionalising the neuronal calcium equation, we couple the equation (4.2.2) to the dimensional equations (3.2.15)-(3.2.19) from Chapter 3. Thus our dimensional full model becomes

$$\frac{dG_N}{dt} = \mathrm{l}_1 g_N - \mathrm{l}_G G_N, \tag{4.2.4}$$

$$\frac{dg_N}{dt} = \mathrm{l}_n[(\frac{V_T}{V_E}G_T - \frac{V_N}{V_E}(G_N + g_N + G_L + g_L) - G_E) - \mathrm{g}_1 g_N] - \mathrm{l}_1 g_N, \tag{4.2.5}$$

$$\frac{dG_E}{dt} = \frac{V_N}{V_E}\mathrm{l}_G G_N - \mathrm{l}_m G_E + \frac{V_L}{V_E}\mathrm{l}_c G_L, \tag{4.2.6}$$

$$\frac{dG_L}{dt} = \frac{V_E}{V_L}\mathrm{l}_m G_E - (\mathrm{l}_2 + \mathrm{l}_c)G_L, \tag{4.2.7}$$

$$\frac{dg_L}{dt} = \mathrm{l}_2 G_L - \frac{\mathrm{l}_{g^o} G_E}{\mathrm{l}_h + G_E}[g_L - \mathrm{g}_2(\frac{V_T}{V_E}G_T - \frac{V_N}{V_E}(G_N + g_N + G_L + g_L) - G_E)], \tag{4.2.8}$$

$$\frac{dC_N}{dt} = h_0(C^E - \mathrm{g}_3 C_N) + h_1\frac{V_E}{V_N}C^E - h_2 C_N, \tag{4.2.9}$$

We note that l_G, the rate at which the neuronal Glu is released to the ECS depends on the intracellular calcium levels (see §4.1). By contrast, h_1, the calcium influx via the Glu receptor, and h_2, the calcium efflux, depend on the extracellular Glu levels and the intracellular calcium levels, respectively. Therefore, we define the parameters which involve with calcium signalling based on biological information [36–39] as follows. Increase of extracellular Glu (G_E) activates Glu receptors, so high intracellular calcium (C_N) occurs. However, increasing of C_N leads to G_N (neuronal Glu) decreasing but G_E increasing. Thus, it is positive feedback that regulates the calcium signalling in the Glu-Gln cycle.

We assume that the rate of influx of Ca^{2+} via the calcium channel (h_0) is constant. By contrast, the rate of influx via the Glu receptor (h_1) and the rate of efflux (h_2) have typically been medelled as saturating functions of G_E and C_N, respectively. Ca^{2+} influx via the Glu receptor (h_1) relies on the extracellular Glu level (G_E) for activation. Thus, we set

$$h_1 = \frac{h_{10}G_E}{h_{11} + G_E}, \tag{4.2.10}$$

where h_{10} represents the maximum rate (in min^{-1}) at which Ca^{2+} can be actively transported from the ECS to the neuronal cell, and h_{11} is the concentrations of Ca^{2+} in the neuronal cell (in mM) at which this rate is half-maximal.

As in [40], we assume that the rate of efflux of Ca^{2+} (h_2) depends on the intracellular calcium level, in a similar manner, so that

$$h_2 = \frac{h_{20}C_N}{h_{21}+C_N}, \tag{4.2.11}$$

where h_{20} represents the maximum rate (in $\min^{-1}$) at which Ca^{2+} can be secreted to the ECS from the neuronal cell and h_{21} is the concentration of Ca^{2+} in the neuronal (in mM) at which the rate is half-maximal.

In addition, since Glu release from the neuronal cell depends on the intracellular calcium concentration, we assume that the rate at which Glu is released to the ECS (l_G) is a saturating function of the intracellular calcium level:

$$\mathrm{l}_G = \frac{\mathrm{l}_{G0}C_N}{\mathrm{l}_{G1}+C_N}, \tag{4.2.12}$$

where l_{G0} represents the maximum rate (in $\min^{-1}$) at which intracellular Glu can be secreted to the ECS from the neuronal cell and l_{G1} is the concentration of Glu in the neuronal cell (in mM) at which the rate is half-maximal .

Thus the Ca^{2+} dynamics and the Glu-Gln cycle are coupled through $\mathrm{l}_G = \mathrm{l}_G(C_N)$, $h_1 = h_1(G_E)$ and $h_2 = h_2(C_N)$. Substituting from (4.2.10)-(4.2.12) into the equations (4.2.4)-(4.2.9), our model now becomes:

$$\frac{dG_N}{dt} = \mathrm{l}_1 g_N - \frac{\mathrm{l}_{G0}C_N}{\mathrm{l}_{G1}+C_N}G_N, \tag{4.2.13}$$

$$\frac{dg_N}{dt} = \mathrm{l}_n[(\frac{V_T}{V_E}G_T - \frac{V_N}{V_E}(G_N+g_N+G_L+g_L)-G_E) - \mathrm{g}_1 g_N] - \mathrm{l}_1 g_N, \tag{4.2.14}$$

$$\frac{dG_E}{dt} = (\frac{V_N}{V_E})\frac{\mathrm{l}_{G0}C_N}{\mathrm{l}_{G1}+C_N}G_N - \mathrm{l}_m G_E + \frac{V_L}{V_E}\mathrm{l}_c G_L, \tag{4.2.15}$$

$$\frac{dG_L}{dt} = (\frac{V_E}{V_L})\mathrm{l}_m G_E - (\mathrm{l}_2+\mathrm{l}_c)G_L, \tag{4.2.16}$$

$$\frac{dg_L}{dt} = \mathrm{l}_2 G_L - \frac{\mathrm{l}_{go}G_E}{\mathrm{l}_h+G_E}[g_L - \mathrm{g}_2(\frac{V_T}{V_E}G_T - \frac{V_N}{V_E}(G_N+g_N+G_L+g_L) - G_E)], \tag{4.2.17}$$

$$\frac{dC_N}{dt} = h_0(C^E - \mathrm{g}_3 C_N) + (\frac{V_E}{V_N})\frac{h_{10}G_E}{h_{11}+G_E}C^E - \frac{h_{20}C_N}{h_{21}+C_N}C_N. \tag{4.2.18}$$

4.2.2 Nondimensionalisation

The calcium equation (4.2.18) and the new term of l_G ($\mathrm{l}_G = \dfrac{\mathrm{l}_{G0}C_N}{\mathrm{l}_{G1}+C_N}$) shown in equations (4.2.13) and (4.2.15) are nondimensionalised using a similar process to that used for the model of the Glu-Gln model in Chapter 3. The other variables and parameters are nondimensionalised as shown in §3.2.2. We rescale variable C_N with C^E, time t with $\dfrac{1}{\mathrm{l}_1}$ (l_1 represents the rate constant that converts Gln to Glu via enzyme PAG in the neuronal cell). We recall that we have estimated $V_N \approx V_L$, and $\mathrm{e} = \dfrac{V_E}{V_N} = 0.5$, being the ratio of the ECS volume and the neuronal cell volume.

In addition, we introduce the following new dimensionless parameter groupings

$$\mathrm{l}^*_{G0} = \frac{\mathrm{l}_{G0}}{\mathrm{l}_1}, \qquad \mathrm{l}^*_{G1} = \frac{\mathrm{l}_{G1}}{C^E}, \qquad h^*_0 = \frac{h_0}{\mathrm{l}_1}, \qquad h^*_{10} = \frac{h_{10}}{\mathrm{l}_1},$$
$$h^*_{11} = \frac{h_{11}}{G^T}, \qquad h^*_{20} = \frac{h_{20}}{\mathrm{l}_1}, \qquad h^*_{21} = \frac{h_{21}}{C^E},$$

(G^T is the total amounts of Glu and Gln in the three compartments) and recall the following dimensionless parameters which were introduced in Chapter 3

$$\mathrm{l}^*_n = \frac{\mathrm{l}_n}{\mathrm{l}_1}, \qquad \mathrm{l}^*_2 = \frac{\mathrm{l}_2}{\mathrm{l}_1}, \qquad \mathrm{l}^*_h = \frac{\mathrm{l}_h}{G_T},$$
$$\mathrm{l}^*_m = \frac{\mathrm{l}_m}{\mathrm{l}_1}, \qquad \mathrm{l}^*_c = \frac{\mathrm{l}_c}{\mathrm{l}_1}, \qquad \mathrm{l}^*_{go} = \frac{\mathrm{l}_{go}}{\mathrm{l}_1}.$$

Under the above rescaling, the governing equations simplify to give (dropping the stars for notational simplicity)

$$\frac{dG_N}{dt} = g_N - \frac{\mathrm{l}_{G0}C_N}{\mathrm{l}_{G1}+C_N}G_N, \tag{4.2.19}$$
$$\frac{dg_N}{dt} = \mathrm{e}^{-2}\mathrm{l}_n[1-\mathrm{e}(G_N+g_N+G_L+g_L)-\mathrm{e}^2G_E-\mathrm{e}^2\mathrm{g}_1g_N]-g_N, \tag{4.2.20}$$
$$\mathrm{e}\frac{dG_E}{dt} = \frac{\mathrm{l}_{G0}C_N}{\mathrm{l}_{G1}+C_N}G_N - \mathrm{e}\,\mathrm{l}_m G_E + \mathrm{l}_c G_L, \tag{4.2.21}$$
$$\frac{dG_L}{dt} = \mathrm{e}\,\mathrm{l}_m G_E - (\mathrm{l}_2+\mathrm{l}_c)G_L, \tag{4.2.22}$$
$$\frac{dg_L}{dt} = \mathrm{l}_2 G_L - \frac{\mathrm{l}_{go}G_E}{\mathrm{l}_h+G_E}[g_L - \mathrm{e}^{-2}\mathrm{g}_2(1-\mathrm{e}(G_N+g_N+G_L+g_L) -\mathrm{e}^2G_E)], \tag{4.2.23}$$
$$\frac{dC_N}{dt} = h_0(1-\mathrm{g}_3C_N) + \mathrm{e}\frac{h_{10}G_E}{h_{11}+G_E} - \frac{h_{20}C_N}{h_{21}+C_N}C_N. \tag{4.2.24}$$

We solve (4.2.19)-(4.2.24) subject to the following initial conditions (see equation (3.2.20)

for Glu and Gln, and (4.2.3) for C_N (rescaling C_N with C^E ($C^E = 2$))):

$$\begin{aligned} G_N(0) &= G_N^{(0)}, & g_N(0) &= g_N^{(0)}, & G_E(0) &= G_E^{(0)}, \\ G_L(0) &= G_L^{(0)}, & g_L(0) &= g_L^{(0)}, & C_N(0) &= C_N^{(0)}. \end{aligned} \tag{4.2.25}$$

4.2.3 Numerical Results

Before constructing the numerical solutions of the equations (4.2.19)-(4.2.25), we note that we could not find the explicitly steady-state solutions of equations (4.2.19)-(4.2.25). The default parameter values in (4.2.19)-(4.2.24) are fixed at the same values used to solve (3.2.23)-(3.2.27) in Chapter 3 (see Table 4.2). Moreover, the default values of the new parameters are stated in Table 4.3. We note that we set $\mathrm{l}_{G1} < \mathrm{l}_{G0}$ and keep $\mathrm{l}_{G0} = 0.025$ which is the same as l_G in Chapter 3. We assume that h_{20} and g_3 are greater than other remainder parameters to ensure that our model does not exhibit excitotoxicity.

Nondimensional Parameter	Default Value
l_m	48
g_1, l_c, l_2	2
l_{go}	0.5
l_n	0.125
g_2	0.0625
l_h	0.025

Table 4.2: The default parameter set that is used in equations (3.2.23)-(3.2.27).

Nondimensional Parameter	Default Value
h_{20}	5
g_3	1
h_{21}, h_{10}, h_{11},	0.25
l_{G0}, h_0	0.025
l_{G1}	0.01

Table 4.3: The new default parameter set.

In Figure 4.2, we show a comparison of numerical solutions of equations (4.2.19)-(4.2.25) by the solid line, and those of equations (3.2.23)-(3.2.27) by the dashed line against $\log(t)$ since the system rapidly tends to a steady-state with parameters from Tables 4.2 and 4.3, and $\mathrm{e} = \dfrac{V_E}{V_L} = 0.5$ [2, 17]. These Glu and Gln behaviours are qualitatively similar on both systems, while C_N increases until $t \sim 1$ and settles to a steady-state.

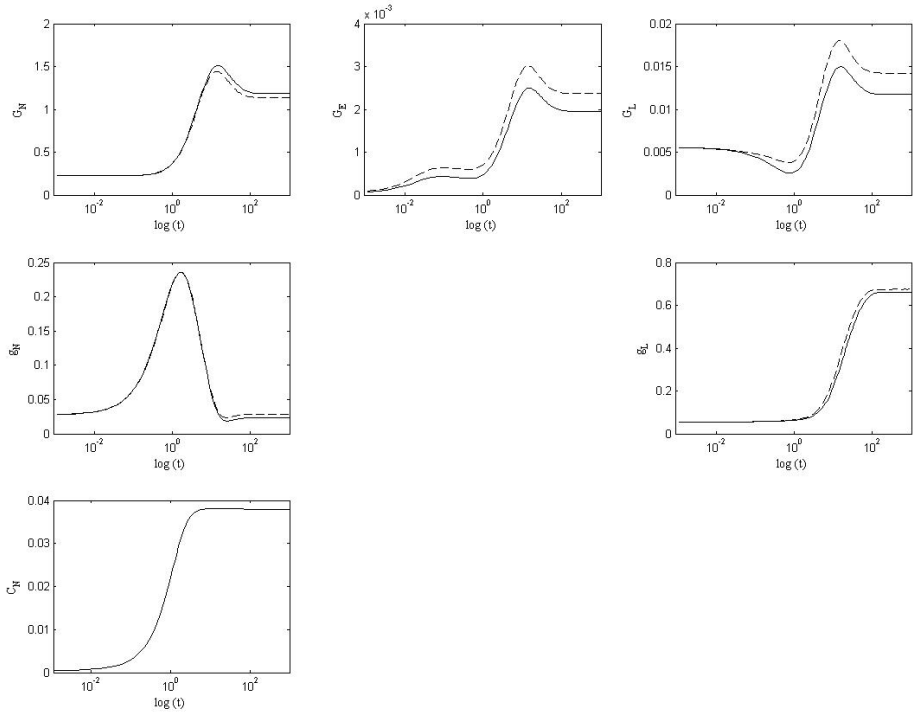

Figure 4.2: A comparison of numerical solutions (4.2.19)-(4.2.24) by the solid line, and (3.2.23)-(3.2.27) by the dashed line with e $= 0.5$ and other parameters as shown in Tables 4.2 and 4.3.

In the next section we present an asymptotic analysis of system (4.2.19)-(4.2.25) by starting with rescaling all parameters and variables in term of the physically realistic value, e $= 0.5$. As for Chapter 3, e $= 0.5$ is not small enough to perform asymptotic analysis. In addition, to avoid the repetitive process from showing the qualitative dynamics of equations (4.2.19)-(4.2.24) do not change when e varies, as for Chapter 3, we use e $= 0.05 \ll 1$ that the analysis is tractable.

4.3 Model Analysis

We start by estimating the dimensionless parameters in equations (4.2.19)-(4.2.24) and then motivate our scaling of the dependent variable C_N, based on the physically realistic value e $= 0.5$. We fix some estimated parameters and the scaling of Glu and Gln as used in Chapter 3. We note that the new rate of release of G_N (i.e. $\dfrac{l_{G0}C_N}{l_{G1}+C_N}$ in (4.2.19) and (4.2.21)) is also estimated below.

4.3.1 Parameter and Variable Scaling

As for Chapter 3, we recall that some Glu-Gln parameters and variables scale with e (for more details see §3.3) as follows:

$$\mathrm{l}_c, \mathrm{l}_2, \mathrm{g}_1 = O(1), \qquad \mathrm{l}_{go} = O(\mathrm{e}), \qquad \mathrm{l}_h = O(\mathrm{e}^2), \qquad \mathrm{l}_n = O(\mathrm{e}^3), \qquad \mathrm{g}_2 = O(\mathrm{e}^4),$$

and

$$G_N, g_L = O(\mathrm{e}^{-1}) >> g_N, G_L = O(\mathrm{e}) >> G_E = O(\mathrm{e}^2).$$

We next scale the new parameters (l_{G0}, l_{G1}, h_0, g_3, h_{10}, h_{11}, h_{20}, h_{21}) which are introduced in this chapter. As mentioned in §4.1, in order to prevent excitotoxicity, intracellular calcium must be maintained at low levels. Therefore, we suppose that all parameters involving the rates of Ca^{2+} efflux (namely g_3, h_{20} and h_{21}) are considerably greater than the correspondence rates of influx (h_0, h_{10} and h_{11}). We thus choose

$$\mathrm{g}_3 = O(1), \qquad h_{20} = O(1) \qquad \text{and} \qquad h_{21} = \mathrm{e}^2\bar{h}_{21}. \tag{4.3.1}$$

We note that h_{21} is scaled with e^2 in order to ensure that the Ca^{2+} efflux rate (i.e. $\dfrac{h_{20}C_N}{h_{21}+C_N}$, note that h_{21} appears in the denominator) is greater than the Ca^{2+} influx rate. In addition, we choose

$$h_0 = \mathrm{e}^2\bar{h}_0, \qquad h_{11} = \mathrm{e}^2\bar{h}_{11} \qquad \text{and} \qquad h_{10} = \mathrm{e}\bar{h}_{10}. \tag{4.3.2}$$

We choose h_{11} to have the same magnitude as G_E, and the calcium influx rate via the Glu receptor (i.e. $\dfrac{h_{10}G_E}{h_{11}+G_E}$) to be higher than that rate via the calcium channel (h_0), in order to give influx via the Glu receptor more influence.

As stated above, calcium is normally maintained at very low levels inside cells [37, 65]. We deduce that $C_N = O(G_E)$ (note that G_E is scaled to be the smallest in Chapter 3). Recalling from above that $G_E = O(\mathrm{e}^2)$, we consequently obtain the following scaled dependent variable

$$C_N = \mathrm{e}^2\bar{C}_N. \tag{4.3.3}$$

Finally, we choose

$$\mathrm{l}_{G0} = \mathrm{e}^2 \bar{\mathrm{l}}_{G0} \qquad \text{and} \qquad \mathrm{l}_{G1} = \mathrm{e}^2 \bar{\mathrm{l}}_{G1} \tag{4.3.4}$$

in order to ensure that the values of l_{G0} and l_{G1} that we use in (4.2.13) and (4.2.15) are such that the nonlinear intracellular Ca^{2+}-dependent term (see (4.2.12)) is similar in magnitude l_G to that is used in Chapter 3.

Combining the above assumptions and inserting the associated rescalings in the governing ODEs we deduce that the equations (4.2.19)-(4.2.25) transform to give (dropping the bars for notational simplicity):

$$\begin{aligned}
\mathrm{e}^{-2}\frac{dG_N}{dt} &= g_N - \frac{\mathrm{l}_{G0}C_N}{\mathrm{l}_{G1}+C_N}G_N, && (4.3.5)\\
\frac{dg_N}{dt} &= \mathrm{l}_n[1-(G_N+g_L)-\mathrm{e}^2(g_N+G_L)-\mathrm{e}^4G_E-\mathrm{e}^3\mathrm{g}_1g_N]-g_N, && (4.3.6)\\
\mathrm{e}^2\frac{dG_E}{dt} &= \frac{\mathrm{l}_{G0}C_N}{\mathrm{l}_{G1}+C_N}G_N - \mathrm{l}_m G_E + \mathrm{l}_c G_L, && (4.3.7)\\
\frac{dG_L}{dt} &= \mathrm{l}_m G_E - (\mathrm{l}_2+\mathrm{l}_c)G_L, && (4.3.8)\\
\mathrm{e}^{-2}\frac{dg_L}{dt} &= \mathrm{l}_2 G_L - \frac{\mathrm{l}_{go}G_E}{\mathrm{l}_h+G_E}[g_L - \mathrm{e}^3\mathrm{g}_2(1-(G_N+g_L)-\mathrm{e}^2(g_N+G_L)\\
&\quad -\mathrm{e}^4G_E)], && (4.3.9)\\
\frac{dC_N}{dt} &= h_0(1-\mathrm{e}^2\mathrm{g}_3C_N) + \frac{h_{10}G_E}{h_{11}+G_E} - \frac{h_{20}C_N}{h_{21}+C_N}C_N, && (4.3.10)
\end{aligned}$$

with

$$\begin{aligned}
&G_N(0) = G_N^{(0)}, \qquad g_N(0) = g_N^{(0)}, \qquad G_E(0) = G_E^{(0)},\\
&G_L(0) = G_L^{(0)}, \qquad g_L(0) = g_L^{(0)}, \qquad C_N(0) = C_N^{(0)}.
\end{aligned} \tag{4.3.11}$$

We note that exact values for the rescaled-initial conditions are stated in equations (3.3.12), and (4.2.3) when applied to the new scaling of C_N (see (4.3.3)).

4.3.2 Numerical Simulations

In this section we present numerical solutions of equations (4.3.5)-(4.3.11) against $\log(t)$ by using the associated default parameters, as shown in Table 4.2 and 4.3. Typical solutions of equations (4.3.5)-(4.3.11) are shown in Figure 4.3.

As in Chapter 3, we note that all dimensionless parameters for the remainder of this chapter (except e) will be taken to be unity with the physically realistic value $\mathrm{e} = 0.5$ being the focus of attention. Figure 4.3 shows a series of semilog plots of the numerical solutions of equations (4.3.5)-(4.3.11) with the asymptotically small value $\mathrm{e} = 0.05$: these provide guidance for the small e asymptotic analysis.

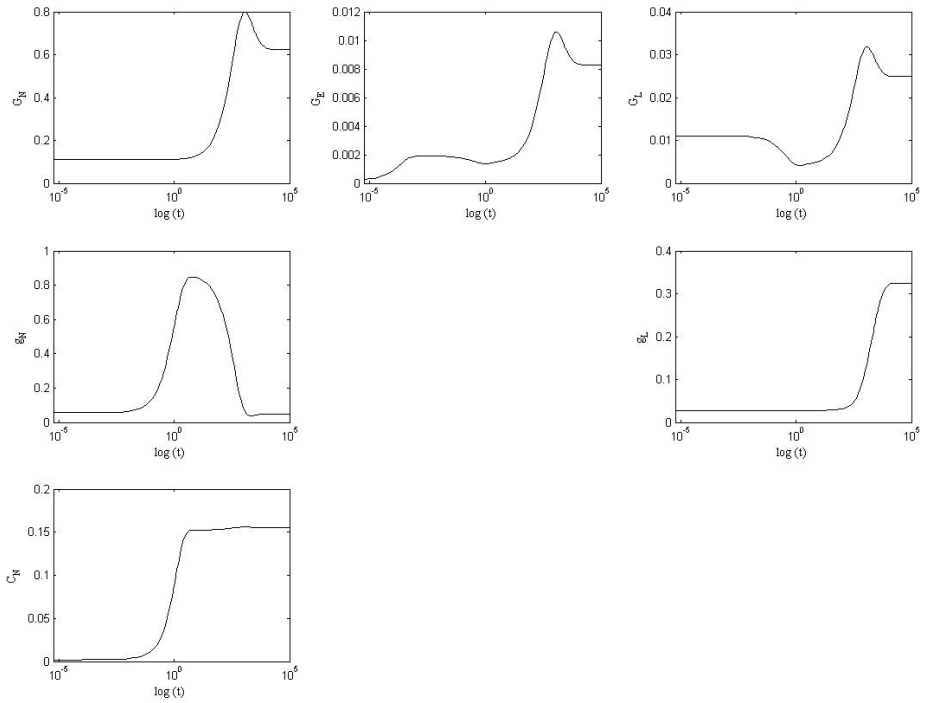

Figure 4.3: Series of semilog plots of numerical solutions of equations (4.3.5)-(4.3.11) with $\mathrm{e} = 0.05$ and the associated default values as shown in Tables 4.2 and 4.3.

From Figure 4.3, the neuronal Ca^{2+}, C_N, increases dramatically for $10^{-3} < t < 1$, before slowly tending to a steady-state. As the behaviour of G_N, g_N, G_E, G_L and g_L in equations (4.3.5)-(4.3.11) is qualitatively similar to that in equations (3.3.7)-(3.3.12), we are guided by the asymptotic analysis from Chapter 3 and that presented later in this chapter. In particular, in terms of what varies when $t = O(\mathrm{e}^2)$, when $t = O(1)$ and when $t = O(\mathrm{e}^{-2})$, these results are similar to what happens in Chapter 3.

In the next section we perform a time-dependent asymptotic analysis of equations (4.3.5)-(4.3.11).

4.3.3 Asymptotic Expansions

Guided by the numerical simulations presented in §4.3.2 and the analysis from Chapter 3, in this section we construct asymptotic expansions of equations (4.3.5)-(4.3.10) on three distinct timescales: $t = O(\mathrm{e}^2)$, $t = O(1)$ and $t = O(\mathrm{e}^{-2})$. We notice that, as for Chapter 3, when we write the steady-state solutions of equations (4.3.5)-(4.3.10) in term of e, there is no $O(\mathrm{e})$ term in any of the variables.

Timescale I: $t = O(\mathrm{e}^2)$

On the initial timescale, we re-scale $t = \mathrm{e}^2 t_1$. Equations (4.3.5)-(4.3.10) transform to give

$$\begin{aligned}
\frac{1}{\mathrm{e}^4}\cdot\frac{dG_N}{dt_1} &= g_N - \frac{\mathrm{l}_{G0}C_N}{\mathrm{l}_{G1}+C_N}G_N, && (4.3.12)\\
\frac{1}{\mathrm{e}^2}\cdot\frac{dg_N}{dt_1} &= \mathrm{l}_n[1-(G_N+g_L)-\mathrm{e}^2(g_N+G_L)-\mathrm{e}^4G_E-\mathrm{e}^3\mathrm{g}_1g_N]-g_N, && (4.3.13)\\
\frac{dG_E}{dt_1} &= \frac{\mathrm{l}_{G0}C_N}{\mathrm{l}_{G1}+C_N}G_N-\mathrm{l}_mG_E+\mathrm{l}_cG_L, && (4.3.14)\\
\frac{1}{\mathrm{e}^2}\cdot\frac{dG_L}{dt_1} &= \mathrm{l}_mG_E-(\mathrm{l}_2+\mathrm{l}_c)G_L, && (4.3.15)\\
\frac{1}{\mathrm{e}^4}\cdot\frac{dg_L}{dt_1} &= \mathrm{l}_2G_L-\frac{\mathrm{l}_{g_o}G_E}{\mathrm{l}_h+G_E}[g_L-\mathrm{e}^3\mathrm{g}_2(1-(G_N+g_L)-\mathrm{e}^2(g_N+G_L)\\
&\quad -\mathrm{e}^4G_E)], && (4.3.16)\\
\frac{1}{\mathrm{e}^2}\cdot\frac{dC_N}{dt_1} &= h_0(1-\mathrm{e}^2\mathrm{g}_3C_N)+\frac{h_{10}G_E}{h_{11}+G_E}-\frac{h_{20}C_N}{h_{21}+C_N}C_N. && (4.3.17)
\end{aligned}$$

We seek regular power series expansions of the dependent variables in terms of the small parameter, e. The leading order equations can be solved to give:

$$\begin{aligned}
&G_{N0}(t_1)=G_N^{(0)}, && g_{N0}(t_1)=g_N^{(0)}, && G_{L0}(t_1)=G_L^{(0)},\\
&g_{L0}(t_1)=g_L^{(0)}, && C_{N0}(t_1)=C_N^{(0)}, && (4.3.18)
\end{aligned}$$

where the superscripts (0) represent their initial conditions, and

$$\begin{aligned}
G_{E0}(t_1) &= \frac{1}{\mathrm{l}_m}\Big(\frac{\mathrm{l}_{G0}C_N^{(0)}}{\mathrm{l}_{G1}+C_N^{(0)}}G_N^{(0)}+\mathrm{l}_cG_L^{(0)}\Big)+\\
&\quad \Big[G_E^{(0)}-\frac{1}{\mathrm{l}_m}\Big(\frac{\mathrm{l}_{G0}C_N^{(0)}}{\mathrm{l}_{G1}+C_N^{(0)}}G_N^{(0)}+\mathrm{l}_cG_L^{(0)}\Big)\Big]e^{-\mathrm{l}_mt_1}. && (4.3.19)
\end{aligned}$$

As in what happens in §3.3.5, the $O(\mathrm{e})$ terms in all dependent variables vanish. Then

we continue our analysis by focussing on $O(\mathrm{e}^2)$ term. Equating coefficients of $O(\mathrm{e}^2)$ and integrating them, the solutions of $g_{N2}(t_1)$, $G_{L2}(t_1)$ and $G_{E2}(t_1)$ are the same as shown in equations (3.3.39)-(3.3.41), respectively, on inserting the constant $\mathrm{l}_G = \dfrac{\mathrm{l}_{G0} C_N^{(0)}}{\mathrm{l}_{G1} + C_N^{(0)}}$.

By contrast, we get

$$C_{N2}(t_1) = \left(\frac{h_{10}(\mathrm{l}_G G_N^{(0)} + \mathrm{l}_c G_L^{(0)})}{\mathrm{l}_m h_{21} + \mathrm{l}_G G_N^{(0)} + \mathrm{l}_c G_L^{(0)}} + h_0 - \frac{h_{20} {C_N^{(0)}}^2}{h_{21} + C_N^{(0)}}\right) t_1. \tag{4.3.20}$$

Combining the solutions of all variables from leading-order to $O(\mathrm{e}^2)$, we can see the expansions of g_N, G_E, G_L and C_N break down when $t_1 = O(\mathrm{e}^{-2})$, or when $t = O(1)$; for on example (of this breaking down) see equation (4.3.20) when $t_1 = O(\mathrm{e}^{-2})$. As $t_1 = O(\mathrm{e}^{-2})$, we have

$$C_N = C_N^{(0)} + \frac{h_{10}(\mathrm{l}_G G_N^{(0)} + \mathrm{l}_c G_L^{(0)})}{\mathrm{l}_m h_{21} + \mathrm{l}_G G_N^{(0)} + \mathrm{l}_c G_L^{(0)}} + h_0 - \frac{h_{20} {C_N^{(0)}}^2}{h_{21} + C_N^{(0)}}. \tag{4.3.21}$$

Equation (4.3.21) will be used as the matching condition for C_N in the following timescale, while the matching conditions for g_N, G_L and G_E are given by equation (3.3.45) on substituting $\mathrm{l}_G = \dfrac{\mathrm{l}_{G0} C_N^{(0)}}{\mathrm{l}_{G1} + C_N^{(0)}}$.

As depicted in Figure 4.4, g_N, G_E, G_L and C_N change over this initial timescale. There is good agreement between the numerical and analytical solutions on this short timescale (e.g. for $0 \leq t \leq 10^{-1}$).

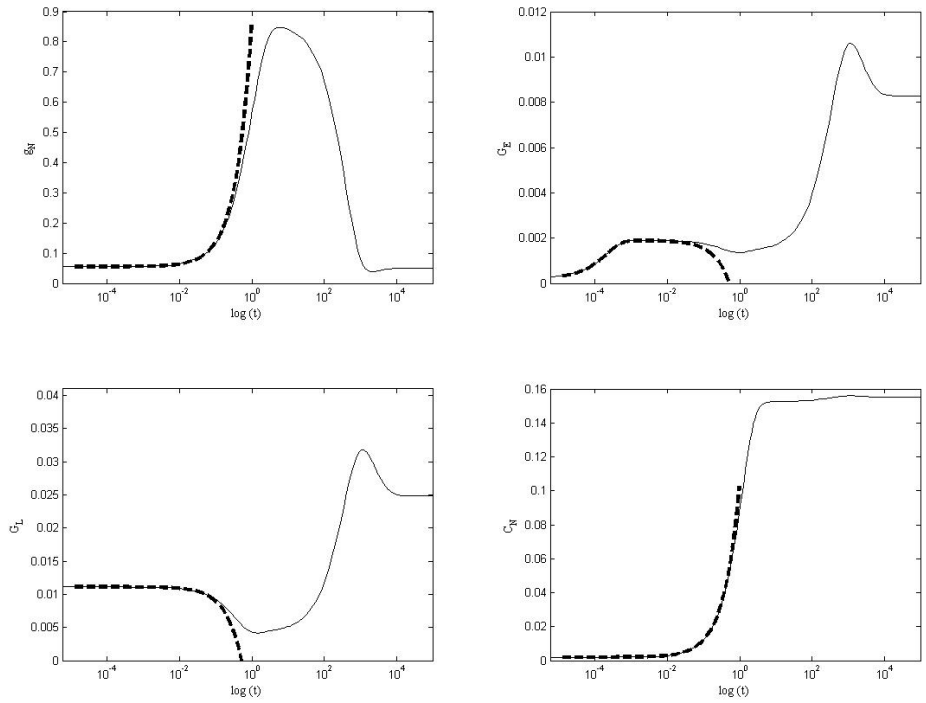

Figure 4.4: A comparison of the asymptotic and numerical solutions on the initial timescale with $\mathrm{e} = 0.05$, other parameter values and initial conditions as used in Figure 4.3. Key: solid line (numerical solutions of the full system (4.3.5)-(4.3.11)), dashed line (asymptotic solutions expanded to $O(\mathrm{e}^2)$ on the first timescale).

Timescale II: $t = O(1)$

On this intermediate timescale, $t = t_2$ [1], and the governing equations are given by equations (4.3.5)-(4.3.10) which we re-state below:

$$\frac{1}{\mathrm{e}^2}\cdot\frac{dG_N}{dt_2} = g_N - \frac{\mathrm{l}_{G0}C_N}{\mathrm{l}_{G1}+C_N}G_N, \tag{4.3.22}$$

$$\frac{dg_N}{dt_2} = \mathrm{l}_n[1-(G_N+g_L)-\mathrm{e}^2(g_N+G_L)-\mathrm{e}^4G_E-\mathrm{e}^3\mathrm{g}_1g_N]-g_N, \tag{4.3.23}$$

$$\mathrm{e}^2\frac{dG_E}{dt_2} = \frac{\mathrm{l}_{G0}C_N}{\mathrm{l}_{G1}+C_N}G_N - \mathrm{l}_mG_E + \mathrm{l}_cG_L, \tag{4.3.24}$$

$$\frac{dG_L}{dt_2} = \mathrm{l}_mG_E - (\mathrm{l}_2+\mathrm{l}_c)G_L, \tag{4.3.25}$$

$$\frac{1}{\mathrm{e}^2}\cdot\frac{dg_L}{dt_2} = \mathrm{l}_2G_L - \frac{\mathrm{l}_{go}G_E}{\mathrm{l}_h+G_E}[g_L-\mathrm{e}^3\mathrm{g}_2(1-(G_N+g_L)-\mathrm{e}^2(g_N+G_L) -\mathrm{e}^4G_E)], \tag{4.3.26}$$

$$\frac{dC_N}{dt_2} = h_0(1-\mathrm{e}^2\mathrm{g}_3C_N)+\frac{h_{10}G_E}{h_{11}+G_E}-\frac{h_{20}C_N}{h_{21}+C_N}C_N. \tag{4.3.27}$$

[1] As for Chapter 3, we note that we have renamed t as t_2 in order to make it clear we are examining the intermediate timescale, but we could equally have simply written t.

Recalling that on the previous timescale $g_N(t_1)$, $G_E(t_1)$, $G_L(t_1)$ and $C_N(t_1)$ changed over time, we apply the matching conditions from the previous timescale at $t_2 = 0$ (i.e. in order to get the initial conditions on this timescale; see more details at the end of the previous timescale). By contrast, the initial conditions for G_N and g_L on this timescale are the same as those on the timescale I.

Taking the leading-order terms of (4.3.22)-(4.3.27) and matching to the previous timescale again gives a system which can be solved sequentially to give

$$G_{N0}(t_2) = G_N^{(0)}, \qquad g_{L0}(t_2) = g_L^{(0)}, \tag{4.3.28}$$

$$g_{N0}(t_2) = 1_n(1 - G_N^{(0)} - g_L^{(0)}) + [g_N^{(0)} - 1_n(1 - G_N^{(0)} - g_L^{(0)})]e^{-t_2}, \tag{4.3.29}$$

$$G_{E0}(t_2) = \frac{1}{1_m}[\frac{1_{G0}G_N^{(0)}C_{N0}(t_2)}{1_{G1} + C_{N0}(t_2)} + 1_c G_{L0}(t_2)]. \tag{4.3.30}$$

We note that the superscript (0) denotes the initial value of a particular variable which differs from the previous timescale, except for $G_N^{(0)}$ and $g_L^{(0)}$.

Substituting (4.3.28) and (4.3.30) into (4.3.25) and (4.3.27), we have

$$\frac{dG_{L0}}{dt_2} = \frac{1_{G0}G_N^{(0)}C_{N0}}{1_{G1} + C_{N0}} - 1_2 G_{L0}, \tag{4.3.31}$$

$$\frac{dC_{N0}}{dt_2} = h_0 + \frac{h_{10}G_{E0}}{h_{11} + G_{E0}} - \frac{h_{20}C_{N0}}{h_{21} + C_{N0}}C_{N0}. \tag{4.3.32}$$

We integrate equations (4.3.35)-(4.3.37) numerically using (4.3.30) to substitute for G_E. In this way we can solve for G_L, C_N and G_E.

Noting that the $O(\mathrm{e})$ terms are 0 for all variables, we move on to $O(\mathrm{e}^2)$. Taking the $O(\mathrm{e}^2)$ terms of (4.3.22)-(4.3.27) gives the system

$$\frac{dG_{N2}}{dt_2} = g_{N0} - \frac{l_{G0}G_N^{(0)}C_{N0}}{l_{G1}+C_{N0}}, \tag{4.3.33}$$

$$\frac{dg_{N2}}{dt_2} = -l_n[G_{N2}+g_{L2}+g_{N0}+G_{L0}]-g_{N2}, \tag{4.3.34}$$

$$\frac{dG_{L2}}{dt_2} = l_m G_{E2}-(l_2+l_c)G_{L2}, \tag{4.3.35}$$

$$\frac{dg_{L2}}{dt_2} = l_2 G_{L0} - \frac{l_{go}g_L^{(0)}G_{E0}}{l_h+G_{E0}}, \tag{4.3.36}$$

$$\begin{aligned}\frac{dC_{N2}}{dt_2} &= -h_0 g_3 C_{N0} + \frac{h_{10}G_{E2}}{2(h_{11}+G_{E0})}(1-\frac{G_{E0}}{h_{11}+G_{E0}}) \\ &\quad -\frac{h_{20}C_{N0}C_{N2}}{h_{21}+C_{N0}}(1-\frac{C_{N0}}{2(h_{21}+C_{N0})}),\end{aligned} \tag{4.3.37}$$

$$\begin{aligned}\frac{dG_{E0}}{dt_2} &= \frac{l_{G0}}{2(l_{G1}+C_{N0})}[C_{N0}G_{N2}+G_N^{(0)}C_{N2}-\frac{G_N^{(0)}C_{N0}C_{N2}}{l_{G1}+C_{N0}}]-l_m G_{E2} \\ &\quad +l_c G_{L2}.\end{aligned} \tag{4.3.38}$$

Differentiating equation (4.3.30) and substituting it into (4.3.38), we have

$$\begin{aligned}G_{E2}(t_2) &= \frac{l_{G0}}{2l_m(l_{G1}+C_{N0})}(C_{N0}G_{N2}+G_N^{(0)}C_{N2}-\frac{G_N^{(0)}C_{N0}C_{N2}}{l_{G1}+C_{N0}})+\frac{l_c}{l_m}G_{L2} \\ &\quad -\frac{1}{l_m^2}[\frac{l_{G0}G_N^{(0)}}{l_{G1}+C_{N0}}(1-\frac{C_{N0}}{l_{G1}+C_{N0}})(h_0+\frac{h_{10}G_{E0}}{h_{11}+G_{E0}}-\frac{h_{20}C_{N0}^2}{h_{21}+C_{N0}}) \\ &\quad +l_c(\frac{l_{G0}G_N^{(0)}}{l_{G1}+C_{N0}}-l_2G_{L0})].\end{aligned} \tag{4.3.39}$$

Substituting (4.3.39) into the equations (4.3.33)-(4.3.37) and integrating numerically those equations, we obtain solutions to equations (4.3.33)-(4.3.38). The solutions of each variable on the intermediate timescale are composed of a leading order term and an $O(e^2)$ contribution. In Figure 4.5, we can see clearly that, when $t_2 \to ¥$, the expansions of all variables break down. Moreover, we can see good agreement between the numerical results and the asymptotic approximations in the range $10^{-1} \leq t \leq 10$ for all variables on this timescale.

Next, we show that the system behaviour finally brings it to its steady state on the final timescale.

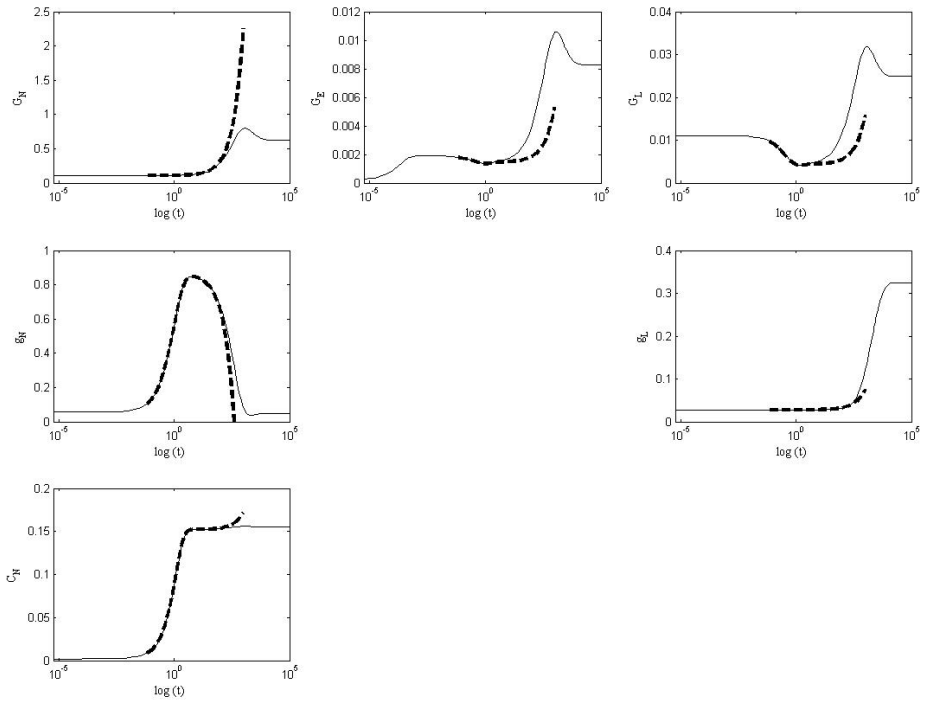

Figure 4.5: A comparison of the numerical (solid line) and asymptotic (dashed line) solutions on the second timescale ($t = O(1)$).

Timescale III: $t = O(\mathrm{e}^{-2})$

The final timescale of interest is the long timescale $t = \mathrm{e}^{-2}t_3$. On this timescale the governing equations become

$$\frac{dG_N}{dt_3} = g_N - \frac{\mathrm{l}_{G0}C_N}{\mathrm{l}_{G1}+C_N}G_N, \tag{4.3.40}$$

$$\mathrm{e}^2\frac{dg_N}{dt_3} = \mathrm{l}_n[1-(G_N+g_L)-\mathrm{e}^2(g_N+G_L)-\mathrm{e}^4G_E-\mathrm{e}^3\mathrm{g}_1g_N]-g_N, \tag{4.3.41}$$

$$\mathrm{e}^4\frac{dG_E}{dt_3} = \frac{\mathrm{l}_{G0}C_N}{\mathrm{l}_{G1}+C_N}G_N - \mathrm{l}_mG_E + \mathrm{l}_cG_L, \tag{4.3.42}$$

$$\mathrm{e}^2\frac{dG_L}{dt_3} = \mathrm{l}_mG_E - (\mathrm{l}_2+\mathrm{l}_c)G_L, \tag{4.3.43}$$

$$\frac{dg_L}{dt_3} = \mathrm{l}_2G_L - \frac{\mathrm{l}_{g0}G_E}{\mathrm{l}_h+G_E}[g_L - \mathrm{e}^3\mathrm{g}_2(1-(G_N+g_L)-\mathrm{e}^2(g_N+G_L) -\mathrm{e}^4G_E)], \tag{4.3.44}$$

$$\mathrm{e}^2\frac{dC_N}{dt_3} = h_0(1-\mathrm{e}^2\mathrm{g}_3C_N) + \frac{h_{10}G_E}{h_{11}+G_E} - \frac{h_{20}C_N}{h_{21}+C_N}C_N. \tag{4.3.45}$$

Since all variables evolve during the second timescale, their initial conditions on this final timescale differ from those used in the previous one. Matching to the previous

timescale (as $t_2 \to$ ¥ and $t_3 \to 0$), we have the initial conditions of this timescale. Taking the leading-order expressions of (4.3.40)-(4.3.45), we have:

$$\frac{dG_{N0}}{dt_3} = g_{N0} - \frac{l_{G0}C_{N0}}{l_{G1}+C_{N0}}G_{N0}, \tag{4.3.46}$$

$$\frac{dg_{L0}}{dt_3} = l_2 G_{L0} - \frac{l_{g^o}G_{E0}}{l_h+G_{E0}}g_{L0}, \tag{4.3.47}$$

$$0 = l_n[1-(G_{N0}+g_{L0})] - g_{N0}, \tag{4.3.48}$$

$$0 = \frac{l_{G0}C_{N0}}{l_{G1}+C_{N0}}G_{N0} - l_m G_{E0} + l_c G_{L0}, \tag{4.3.49}$$

$$0 = l_m G_{E0} - (l_2+l_c)G_{L0}, \tag{4.3.50}$$

$$0 = h_0 + \frac{h_{10}G_{E0}}{h_{11}+G_{E0}} - \frac{h_{20}C_{N0}}{h_{21}+C_{N0}}C_{N0}. \tag{4.3.51}$$

Rearranging equation (4.3.48) gives

$$g_{N0}(t_3) = l_n[1-G_{N0}-g_{L0}]. \tag{4.3.52}$$

Adding equations (4.3.49) and (4.3.50), we get

$$G_{L0}(t_3) = (\frac{l_{G0}C_{N0}}{l_{G1}+C_{N0}})(\frac{G_{N0}}{l_2}). \tag{4.3.53}$$

Combining equations (4.3.50) and (4.3.53), we get

$$G_{E0}(t_3) = (\frac{l_2+l_c}{l_2 l_m})(\frac{l_{G0}C_{N0}}{l_{G1}+C_{N0}})G_{N0}. \tag{4.3.54}$$

From (4.3.51), we have

$$G_{E0}(t_3) = \frac{h_{20}h_{11}C_{N0}^2 - h_0h_{11}(h_{21}+C_{N0})}{(h_{10}+h_0)(h_{21}+C_{N0}) - h_{20}C_{N0}^2}. \tag{4.3.55}$$

We can see that C_{N0} varies with time since $G_{N0} = G_{N0}(t_3)$ satisfies equation (4.3.46). When C_{N0} is known, we can solve for other variables. Equations (4.3.54) and (4.3.55) are a pair of simultaneous equations for G_{E0}. Therefore we have a cubic equation for C_{N0}:

$$F(C_{N0}) \equiv G_0C_{N0}^3 + G_1C_{N0}^2 + G_2C_{N0} + G_3 = 0, \tag{4.3.56}$$

where

$$\begin{aligned}
\mathrm{G}_0 &= -[(\mathrm{l}_2+\mathrm{l}_c)\mathrm{l}_{G0}h_{20}G_{N0}+\mathrm{l}_m\mathrm{l}_2h_{20}h_{11}]<0,\\
\mathrm{G}_1 &= [(\mathrm{l}_2+\mathrm{l}_c)(h_{10}+h_0)\mathrm{l}_{G0}G_{N0}+\mathrm{l}_m\mathrm{l}_2h_{11}(h_0-\mathrm{l}_{G1}h_{20})],\\
\mathrm{G}_2 &= [(\mathrm{l}_2+\mathrm{l}_c)(h_{10}+h_0)\mathrm{l}_{G0}h_{21}G_{N0}+\mathrm{l}_m\mathrm{l}_2h_0h_{11}(\mathrm{l}_{G1}+h_{21})]>0,\\
\mathrm{G}_3 &= [\mathrm{l}_m\mathrm{l}_2\mathrm{l}_{G1}h_0h_{11}h_{21}]>0.
\end{aligned}$$

We note that G_{N0} is greater than zero and all parameter values are positive. Thus, $\mathrm{G}_0<0$, $\mathrm{G}_2>0$ and $\mathrm{G}_3>0$. When applying the Descartes' rule of signs (for example see [72]), the cubic equation (4.3.56) has only one positive real root for whatever sign of G_1 is. The other two roots are negative real roots or complex conjugates.

The cubic equation (4.3.56) will have two distinct negative real roots and one positive real root if

$$4p^3+27q^2<0, \tag{4.3.57}$$

where $p=\dfrac{\mathrm{G}_2}{\mathrm{G}_0}-\dfrac{\mathrm{G}_1^2}{3\mathrm{G}_0^2}$ and $q=\dfrac{\mathrm{G}_3}{\mathrm{G}_0}-\dfrac{\mathrm{G}_1\mathrm{G}_2}{3\mathrm{G}_0^2}+\dfrac{2}{27}\dfrac{\mathrm{G}_1^3}{\mathrm{G}_0^3}$. Therefore if (4.3.57) holds, the one positive real root in term of G_{N0} of equation (4.3.56) is

$$C_{N0}=2\mathrm{D}_0-\frac{\mathrm{G}_1}{3\mathrm{G}_0}, \tag{4.3.58}$$

where

$$\mathrm{D}_0+i\mathrm{D}_1 = \sqrt[3]{-\frac{q}{2}+i\sqrt{-\frac{4p^3+27q^2}{108}}}. \tag{4.3.59}$$

Substituting (4.3.58) into (4.3.53) and (4.3.54), we have G_{E0} and G_{L0} in terms of G_{N0}. When G_{E0} and G_{L0} are known, we can solve a system (4.3.46)-(4.3.47) numerically to get G_{N0} and g_{L0}. In this way, we also solve for g_{N0}, G_{L0}, G_{E0} and C_{N0} from equations (4.3.52), (4.3.53), (4.3.54) and (4.3.58), respectively.

The numerical and asymptotic results for all variables on the final timescale ($t=O(\mathrm{e}^{-2})$) against $\log(t)$ are shown in Figure 4.6. It can be seen that there is good agreement between the numerical and analytical solutions on this timescale. We note that on this final timescale it is sufficient to consider only the leading-order terms.

Here we have presented a model of the calcium signalling in the glutamate-glutamine

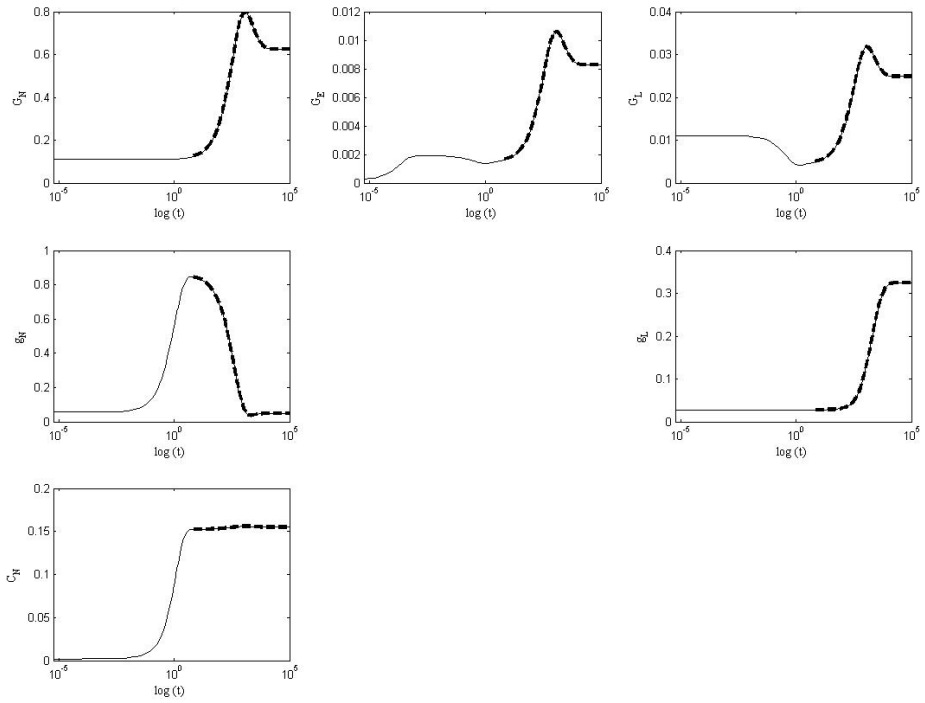

Figure 4.6: A comparison of the asymptotic and numerical solutions on the final timescale ($t = O(\mathrm{e}^2)$).

cycle by adding the neuronal calcium level into the model of the glutamate-glutamine cycle in Chapter 3. The numerical and asymptotic approximations of equations (4.3.5)-(4.3.10) do match perfectly on every timescale (see Figures 4.4-4.6) with the asymptotically small value $\mathrm{e} = 0.05 \ll 1$. In addition, we also show the corresponding results of the numerical and asymptotic approximations for physically realistic value $\mathrm{e} = 0.5$ (see Figure 4.7). This also improve that the higher value of e can not be used to validate the asymptotic approximations.

There is some clinical evidence that injecting Glu can destroy neuronal cells [41, 51, 52]. Lucas and Newhouse [41] say that feeding Glu to infant mice destroys the neuronal retina. Cauquil-Caubère *et al.* [51] propose that, after being injected into the striatum of rats, Glu level rises in the extracellular space. This can lead to progressive dysfunctions of neurotransmitters. In addition, Choi [52] suggests an in vitro study that a 5 minute exposure to 1-100 mM Glu destroys many cultured cortical neurons and by one hour neuronal damage is almost complete. In the following section, we add a toxic source into our recent equations (4.3.5)-(4.3.10) in order to study excitotoxicity.

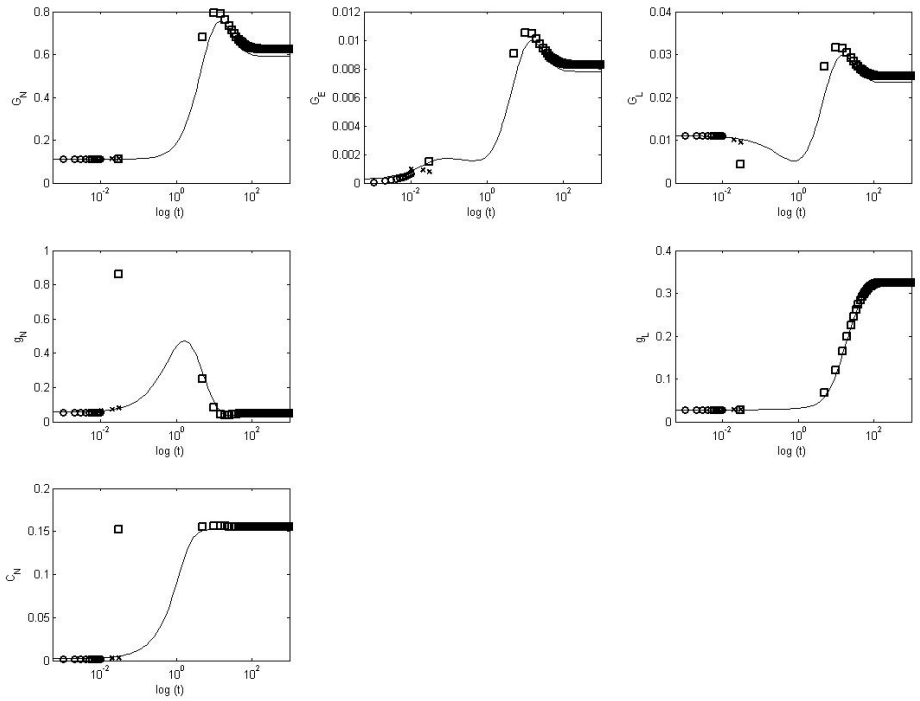

Figure 4.7: A comparison of the numerical solutions of system (4.3.5)-(4.3.10): solid line; and the asymptotic and numerical solutions at all timescales (timescale I: circle line; timescale II: cross line; and timescale III: square line) for e $= 0.5$.

4.4 Excitotoxicity

As mentioned in §4.1, excitotoxicity can occur when there are excessive amounts of G_E. The excessive G_E activates the neuronal Glu receptors and this allows calcium to enter the cell. The neuronal calcium (C_N) triggers fusion of the synaptic vesicle and Glu efflux occurs. However, the high levels of C_N can damage the cell structures and cause cells to die by destruction of a number of cell enzymes [40, 53, 75]. Thus the key for excitotoxicity is G_E and C_N levels.

As stated above, normally the G_E levels are kept below 0.06 mM [16, 18] (corresponding to the value 0.0133 in our system) in order to prevent excitotoxic nerve cell damage. However, the G_E levels can rise to 1 mM when the neuronal cells are activated but it remains at this level for a few milliseconds. If high levels of G_E are maintained for over a few milliseconds, the excessive activation of neuronal Glu receptors allows high levels of calcium to enter the neuronal cells. Excessively neuronal-calcium levels can cause the cells die [52, 53]. This process is called excitotoxicity.

In order to model excitotoxicity, we introduce a constant source of extracellular Glu, G_E^{In}, in equation (4.3.7). Then equations (4.3.5)-(4.3.10) become:

$$\begin{aligned}
e^{-2}\frac{dG_N}{dt} &= g_N - \frac{l_{G0}C_N}{l_{G1}+C_N}G_N, && (4.4.1)\\
\frac{dg_N}{dt} &= l_n[1-(G_N+g_L)-e^2(g_N+G_L)-e^4G_E-e^3g_1g_N]-g_N, && (4.4.2)\\
e^2\frac{dG_E}{dt} &= \frac{l_{G0}C_N}{l_{G1}+C_N}G_N - l_mG_E + l_cG_L + G_E^{In}, && (4.4.3)\\
\frac{dG_L}{dt} &= l_mG_E - (l_2+l_c)G_L, && (4.4.4)\\
e^{-2}\frac{dg_L}{dt} &= l_2G_L - \frac{l_{go}G_E}{l_h+G_E}[g_L - e^3g_2(1-(G_N+g_L)-e^2(g_N+G_L)\\
&\quad -e^4G_E)], && (4.4.5)\\
\frac{dC_N}{dt} &= h_0(1-e^2g_3C_N)+\frac{h_{10}G_E}{h_{11}+G_E}-\frac{h_{20}C_N}{h_{21}+C_N}C_N. && (4.4.6)
\end{aligned}$$

Setting time-derivative of (4.4.6) to zero, we deduce that at steady state

$$C_N = \frac{-\bar{M}_1+\sqrt{\bar{M}_1^2-4\bar{M}_0\bar{M}_2}}{2\bar{M}_0}, \quad (4.4.7)$$

where

$$\begin{aligned}
\bar{M}_0 &= (h_{20}+e^2g_3h_0)(h_{11}+G_E),\\
\bar{M}_1 &= -(h_0(h_{11}+G_E)(1-e^2g_3h_{21})+h_{10}G_E),\\
\bar{M}_2 &= -(h_0h_{11}+(h_0+h_{10})G_E)h_{21}.
\end{aligned}$$

In Figure 4.8, we use (4.4.7) to show how C_N varies with $\log G_E$ with all other parameter values as per Figure 4.3. The point $(G_E, C_N) = (0.0083, 0.1551)$ corresponds to the steady-state of equations (4.3.5)-(4.3.10), while the point $(0.0133, 0.1570)$ denotes the threshold point of G_E for cytotoxicity and the corresponding to value of C_N when we apply (4.4.7). We can see that when G_E increases, C_N increases. When C_N exceeds the maximum value for maintaining healthy neurons leaded to high levels of intracellular calcium, the neuronal cells can be killed. This is entirely consistent with the experimental results [52, 53].

We next look at the steady-state profile of G_E as we vary G_E^{In} for different choices of e. Figure 4.9 shows the resulting solution of equations (4.4.1)-(4.4.6) for G_E when G_E^{In} is varied. We note that the curves of $e = 0.1, 0.05$ and 0.01 are indistinguishable. As

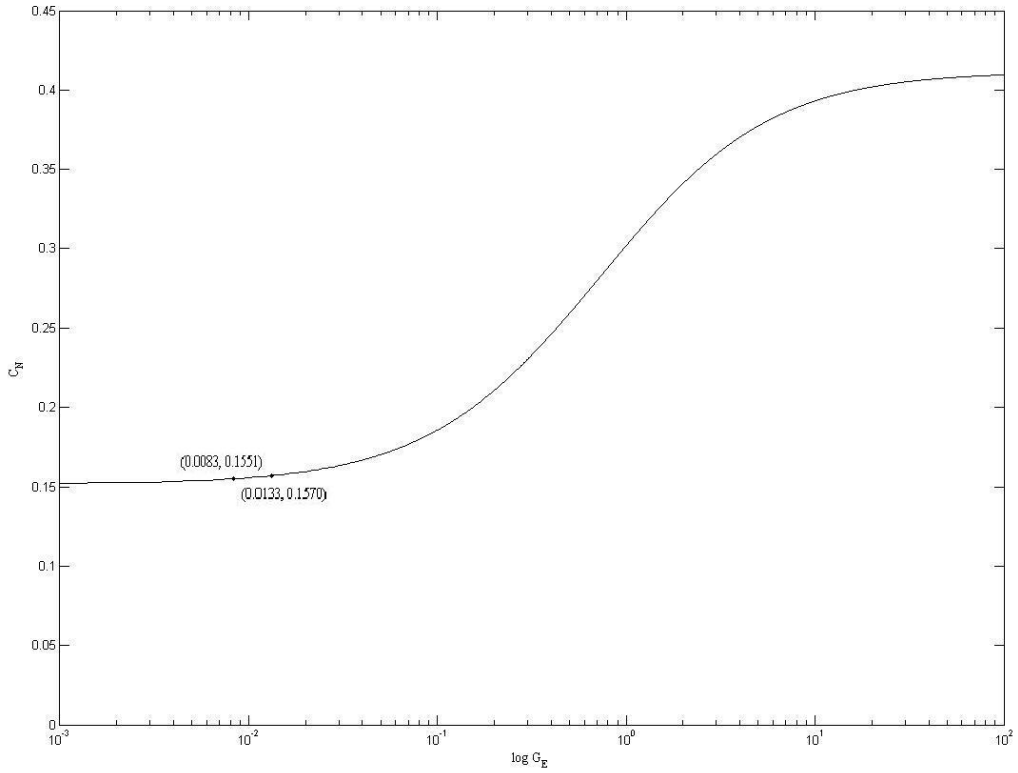

Figure 4.8: The solution curve of (4.4.7) when G_E is varied; the point $(0.0083, 0.1551)$ is the point at steady-state of equations (4.3.5)-(4.3.10) (or when $G_E^{In} = 0$), and the point $(0.0133, 0.1570)$ is the point at the threshold.

stated above, the dimensionless value 0.0133 of G_E in our system is the threshold for excitotoxicity. Thus we can divide our system into two areas: a healthy area and an excitotoxic area. In Figure 4.9, we can see that larger values of e require larger values of G_E^{In} to produce excitotoxicity. We recall that e represents the ratio of the volume fraction of the ECS to that occupied by the neuronal cells.

The results presented in Figure 4.9 are consistent with observations made by Porter and McCarthy [76], and Traynelis and Dingledine [77]. As the extracellular volume fraction is decreased, the concentration of components in the ECS increases. Thus reducing e could lead to an increase in a neuron's responsiveness to a fixed amount of neurotransmitter. It has been said that when the extracellular volume fraction reduces, the excitability of the neurons increases to some extent [76, 77]. In such cases smaller amounts of G_E^{In} will be needed to stimulate excitotoxicity for smaller e.

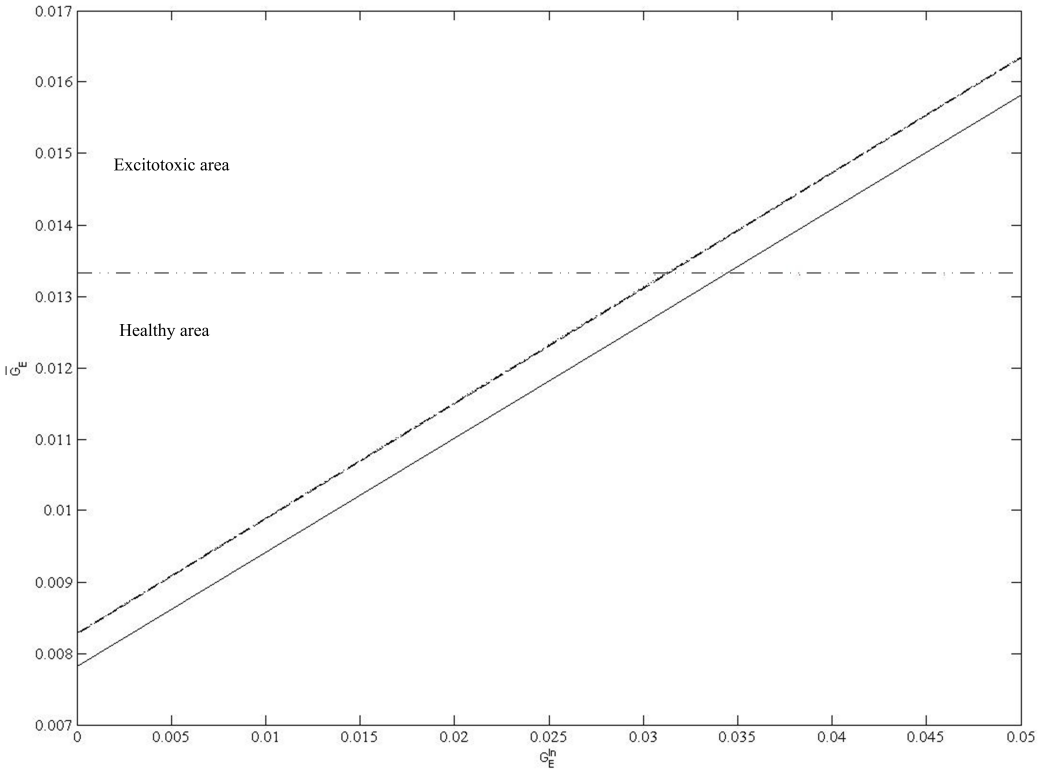

Figure 4.9: The steady-state profile of equations (4.4.1)-(4.4.6) for G_E when G_E^{In} is varied for different choices of e; the solid lines: for e $= 0.5$, the dashed lines: for e $= 0.1$, the dashed-dotted lines: for e $= 0.05$, and the dotted lines: for e $= 0.01$, and other parameter values and initial conditions as per Figure 4.3. We note that e $= 0.1, 0.05$ and 0.01 curves are indistinguishable.

4.5 Summary of Calcium Signalling in the Glutamate-Glutamine cycle

In this chapter we have extended the model from Chapter 3 to examine the role of calcium in the Glu-Gln cycle and investigate how it may stimulate excitotoxicity in our model system. We included an additional equation for intracellular calcium in the neuronal cells into our model of the glutamate-glutamine cycle as excitotoxicity seems to occur only in the neuronal cells. The resulting model consists of a system of six dimensionless nonlinear ordinary differential equations that describe how Glu, Gln and Ca^{2+} levels change over time in the neuronal cell, the ECS and the glial cell.

As in Chapter 3, numerical simulations revealed that the qualitative dynamics of the system do not change when e varies from physically realistic values (e $= 0.5$) to as-

ymptotically small values ($e = 0.05 \ll 1$). We performed an asymptotic analysis of the governing equations in the limit for which $e = 0.05 \ll 1$ and obtained good agreement between the numerical and analytical results for all timescales.

We then used our model to study excitotoxicity caused by addition of extracellular Glu. Excitotoxicity is caused by overstimulation of the neuronal Glu receptors (by G_E) which leads to an increase in intracellular Ca^{2+} and consequently neurodegeneration due to activation of cytotoxic intracellular pathways [40, 53, 75]. As mentioned before, 0.06 mM is the extracellular glutamate threshold for excitotoxicity [16, 18] and this value corresponds to the dimensionless value 0.0133 in our model.

We then introduced a constant toxic source of extracellular Glu, G_E^{In}, into our model. By plotting the solutions of equations (4.4.1)-(4.4.6) for G_E as G_E^{In} varied (and for different choices of e, see Figure 4.9) we showed that smaller values of e need lower levels of G_E^{In} to produce excitotoxicity. This result is consistent with clinical evidence [76, 77] and can be explained as follows. As the extracellular volume fraction decreases, the concentration of components in the ECS increases, and hence a neuron's responsiveness to a fixed amount of neurotransmitter.

CHAPTER 5

Conclusion

Vision is one of the most important sensory systems in humans. The visual system detects and interprets information. The eye focuses the visual image on the receptor cells and a neural component transforms the visual image into a pattern of neural discharges.

When light enters the eye, it impinges on the photoreceptors of a specialised sensory epithelium in the retina. The photoreceptors comprise cones and rods. Cones have high thresholds for detecting light and operate best under daylight conditions. By contrast, rods are sensitive to light and operate best under dark conditions. These photoreceptors communicate via electrical synapses with each other and with second-order neurons in the retina such as bipolar cells and ganglion cells. The output signals are then carried to the brain via the optic nerves [1, 4, 5, 36, 37].

The brain is the control centre of the nervous system. The nervous system controls and maintains diverse biological processes which are essential for maintaining an acceptable quality of life [2, 12]. The nervous system includes neuronal and glial cells. Both cells play important roles in the vitality of the system. However, only neuronal cells can transmit messages from one cell to another. Although the glial cells do not participate directly in the transmission of electrical signals over long distances, they communicate with neurons and with each other via electrical and chemical signals called neurotransmitters. It can be said that the glial cells perform as the connective tissue of the nervous system by helping to support the neuronal cells both physically and metabolically.

The most important excitatory neurotransmitter for the mammalian brain and retina [18, 19] is glutamate (Glu). In the neuronal cells Glu is converted from glutamine (Gln)

via the enzyme glutaminase and then packaged and stored in synaptic vesicles. When there is calcium influx, fusion of the synaptic vesicle with the plasma membrane occurs and Glu is released into the extracellular space (ECS) [36–40]. After it is released from the neuronal cell, extracellular Glu is rapidly transported to the glial cell by the glutamate-aspartate transporter in order to avoid Glu neurotoxicity. In the glial cell, Glu is converted to Gln via enzyme glutamine synthetase. Gln is then released to the neuronal cell via the ECS. This process is called the Glu-Gln cycle.

In this thesis we have applied mathematical techniques to model the photoreceptor cells in order to study whether changes in metabolic demand during periods of light and dark are responsible for the observed variation in the length of the outer segment of the rod. In addition, we have developed an ordinary differential model of the glutamate-glutamine cycle in the nervous system in order to study whether the rates at which glutamate and glutamine released change the metabolic demand of the system. We also extended our model of the glutamate-glutamine cycle to account for calcium signalling in order to develop a more detailed model of the glutamate-glutamine metabolism and to form the basis future studies of excitotoxicity.

We began by developing a nonlinear mathematical model of light/dark regulation of the length of the outer segment of the rod, since it is known that the retinal detachment leads to a reduction in photoreceptor outer segment length. We used our model to predict what the outer segment length and the oxygen and glucose concentrations should be under dark and light conditions, obtaining results which agree with in vivo results. However, the outer segment length under both conditions was shorter than 28 μm which is the rod outer segment length as stated by Duke-Elder and Wybar [69]. Moreover, only oxygen and glucose regulated the length of the rod outer segment in our model. In practice, however, there are other substances such as creatine, creatine phosphate and ATP, playing important roles to the length of the outer segment.

We then moved on to study the glutamate-glutamine cycle in the nervous system as the eyes form the part of the nervous system. The model we developed accounted for glutamate and glutamine concentrations in three compartments: the extracellular space, neuronal and glial cells. We estimated all parameters using inequalities (3.2.36) and (3.2.39) hold for physically realistic steady-state solutions with $e = 0.5$ (the ratio of the volume of the extracellular space to that of the neuronal cell) from physical realistic value [2, 17].

Numerical solutions of the model equations (3.2.23)-(3.2.27) revealed that qualitative dynamics of system did not change as e varied from the physically realistic value e $= 0.5$ to the asymptotically small value (e $= 0.05 \ll 1$). We exploited this qualitative agreement to justify developing asymptotic analysis of the governing equations in the limit e $\to 0$. The resulting analysis revealed three timescales of interest: $t = O(\mathrm{e}^2)$, $t = O(1)$ and $t = O(\mathrm{e}^{-2})$. Both analytical and numerical results matched perfectly on each timescale, from the beginning stage until reaching their steady-state with the asymptotically small value, e $= 0.05$.

Initially, on the short timescale $t = O(\mathrm{e}^2)$ (i.e. we introduced the scaling $t = \mathrm{e}^2 t_1$), adding the leading order terms for each variable to those at $O(\mathrm{e}^2)$, we derived expressions for g_N, G_E and G_L. These broke down as $t_1 = O(\mathrm{e}^{-2})$ (i.e. $t = O(1)$), see Figure 3.7. This was used to motivate the analysis on the intermediate timescale. Taking the limit as $t_1 = O(\mathrm{e}^{-2})$, we were able to calculate the matching conditions for all variables.

On the intermediate timescale $t = O(1)$ (or $t = t_2$). After matching to the initial timescale and combining the leading-order and $O(\mathrm{e}^2)$ solutions for each variable, we found that all approximations broke down when $t_2 = O(\mathrm{e}^{-2})$ (see Figure 3.8). We were once again able to obtain the matching conditions for the subsequent timescale by taking the limit as $t_2 = O(\mathrm{e}^{-2})$.

On the final timescale $t = O(\mathrm{e}^{-2})$ (or $t = \mathrm{e}^{-2} t_3$). After matching to the intermediate timescale and combining both the leading-order and the $O(\mathrm{e}^2)$ solutions for each variable, we found there was good agreement between the numerical and the asymptotical solutions. In particular the approximations tended to the steady-state solutions of the full system (3.3.7)-(3.3.12), see Figure 3.9.

We also compared the numerical solutions of the full system of the glutamate-glutamine cycle with the asymptotic solutions for different choices of e. The excellent agreement when e was small provided independent validation of our asymptotic approximations.

Glutamate is known as the principal excitatory neurotransmitter in the mammalian central nervous system. It is well established that elevated levels of glutamate can result in wide-spread excitotoxicity [52]. Excessive amounts of the extracellular glu-

tamate allow calcium to enter the cell. However, high intracellular calcium levels can damage cell structures and cause the cell die by destruction of a number of cell enzymes [40, 53, 75].

In order to study this process, we extended the model of Chapter 3 to account for intracellular calcium concentration. Moreover, the intracellular calcium level is also important to the neurotransmitter release (glutamate). We set the glutamate efflux from the neuron (l_G) in a saturating term of the intracellular calcium. We found that there were similar dynamics between the full model from Chapter 3 and the model with intracellular calcium in Chapter 4. We also followed this model with a time-dependent asymptotic analysis with the asymptotically small value, $e = 0.05$. Both analytical and numerical solutions matched well on each timescale with $e = 0.05$.

Subsequently, we introduced a constant toxic source into the ODE for extracellular glutamate. Figure 4.9 showed the solutions of excitotoxic equations (4.4.1)-(4.4.6) for G_E as G_E^{In} varied (for different choices of e). Recalling that the extracellular glutamate threshold is 0.06 mM for excitotoxicity [16, 18] corresponding to the dimensionless value 0.0133 in our system, we divided our system into two areas: a healthy area and an excitotoxic area. We found that larger values of toxin are needed for larger values of e to produce excitotoxic effects (see Figure 4.9). This result is consistent with observations made by Porter and McCarthy [76] and Traynelis and Dingledine [77]. As the extracellular volume fraction decreases, the concentration of components in the extracellular space increases. Thus reducing e (our e is the ratio of the volume fraction of the extracellular space to that occupied by the neuronal cell) could lead to an increase in a neuron's responsiveness to a fixed amount of neurotransmitter.

We had, thus far, considered the models of the rod photoreceptors separating into two different models: light/dark regulation of length of the outer segment and the glutamate-glutamine cycle. There are a number of obvious extensions to the work presented in this thesis. Firstly, only glucose and oxygen regulated the rod outer segment length. Future work could account for the energy exchange between the inner and outer segment of other species such as creatine, ATP and ADD.

Secondly, in our model of the glutamate-glutamine cycle additional substances such as aspartate, ammonia and ATP could be included.

In vitro experiments by Choi [52] suggest that five minutes exposure to 1-100 mM glutamate can destroy a large proportion of cortical neurons (1/100th of the tissue concentration normally present in neocortex), with damage almost complete following 60 minutes exposure. It would be interesting to modify the model of Chapter 4 to account for repeated boluses of G_E in order to study how they may cause excitotoxicity.

Finally, extended study could combine the models from Chapter 2 (light/dark regulation of length of the outer segment) and Chapter 4 (calcium signalling in the glutamate-glutamine cycle) in order to develop a more detailed model of glutamate-glutamine metabolism within the rod photoreceptor. A study of the photoreceptor degeneration, retinitis pigmentosa, could also be carried out.

APPENDIX A

Glossary

Active transport. Movement across a membrane that requires the input of energy from ATP.

Adenosine diphosphate (ADP). Precursor of ATP, composed of adenine, ribose and two phosphate groups.

Adenosine triphosphate (ATP). An energy-storing compound composed of adenine, ribose and three phosphate groups.

Alzheimer's disease (AD). A progressive, neurodegenerative disease characterised by loss of function and death of nerve cells in several areas of the brain leading to loss of cognitive function such as memory and language.

Aspartate (Aps). Amino acid that plays a critical part of the enzyme in the liver that transfers nitrogen-containing amino groups, either in building new proteins and amino acids or in breaking down proteins and amino acids for energy and detoxifying the nitrogen in the form of urea.

Cone(s). A photoreceptor for high acuity vision and colour vision during the daytime.

Cyclic guanosine monophosphate (cGMP). A cyclic nucleotide derived from guanosine triphosphate (GTP). cGMP acts as a second messenger much like cyclic AMP, most notably by activating intracellular protein kinases in response to the binding of membrane-impermeable peptide hormones to the external cell surface.

Endoplasmic reticulum (ER). A eukaryotic organelle forms an interconnected network of tubules, vesicles, and cisternae within cells.

Extracellular space (ECS). Interstitial space between cells, occupied by fluid as well as amorphous and fibrous substances.

Exocytosis. The release cellular substances contained in cell vesicles by fusion of the vesicular membrane with the plasma membrane and subsequent release of the contents

to the exterior of the cell.

Excitotoxicity. The pathological process by which nerve cells are damaged and killed by Glu and similar substances.

Glaucoma. An eye disease that causes gradual loss of sight.

Glial cells. Non-excitable support cells of the central nervous system.

Glutaminase (GS). An enzyme that hydrolyzes glutamine to glutamic acid and ammonia.

Glutamine (Gln). Amino acid that is found both free and in proteins in plants and animals and that yields glutamic acid and ammonia on hydrolysis.

Glutamate (Glu). Amino acid that also acts as an excitatory neurotransmitter.

Guanosine monophosphate (GMP). A nucleotide that is found in RNA.

Guanosine triphosphate (GTP). Substrate for the synthesis of RNA during transcription.

Inositol (1,4,5)-triphosphate (IP_3). A secondary messenger molecule used in signal transduction in biological cells.

Krebs cycle. Key metabolic pathway of aerobic respiration. *Synonyms:* citric acid cycle, tricarboxylic cycle, TCA cycle.

Metabolism. All the chemical reactions in the body.

Nerve. A collection of axons running between the central nervous system and the peripheral target cells.

Nervous system. Network of billions or trillions of nerve cells linked together in a highly organized manner to form the rapid control system of the body.

Neuron. A nerve cell, capable of generating and transmitting electrical signals.

Neurotoxicity. Toxic to the nerves or nervous tissue.

Neurotransmitter. A chemical signal released by a neuron that influences the neuron's target cell.

Parkinson's disease (PD). A chronic progressive neurological disease mainly of later life that is linked to decreased dopamine production in the substantia nigra and is marked especially by tremor of resting muscles, rigidity, slowness of movement, impaired balance, and a shuffling gait.

Passive transport. Movement across a membrane that does not depend on an outside source of energy.

Photoreceptor cell. Sensory receptors in the eye that respond primarily to light energy.

Presynaptic cell. The cell releasing neurotransmitter into the chemical synapse.

Postsynaptic cell. The target cell at a synapse.

Retina. Sensory receptors lining the posterior cavity of the eye.

Retinal pigment epithelium (RPE). The retinal pigment epithelium is located just outside the retina and is attached to what is called the choroid, a layer filled with blood vessels that nourish the retina.

Retinitis Pigmentosa. Any of several hereditary progressive degenerative diseases of the eye marked by night blindness in the early stages, atrophy and pigment changes in the retina, constriction of the visual field, and eventual blindness.

Rod(s). A receptor for monochromatic nighttime vision.

Synapse. Region where a neuron meets its target cell.

Synaptic cleft. The space between the pre- and post-synaptic cells.

Synaptic vesicle(s). Small secretory vesicles that release neurotransmitter into the synapse.

References

[1] L. Sherwood, *Fundamentals of Physiology: A Human Perspective*, 2nd ed. Minneapolis, West: St. Paul, 1995.

[2] D.U. Silverthorn, *Human Physiology: An Integrated Approach*, 2nd ed. Upper Saddle River, New Jersey: Prentice Hall, 2001.

[3] S.C. Hsu and R.S. Molday, "Glucose metabolism in photoreceptor outer segments. Its role in phototransduction and in NADPH-requiring reactions," *J. Biol. Chem.*, vol. 269, pp. 17 954–9, 1994.

[4] E.E. Selkurt, *Basic Physiology for the Health Sciences*, 2nd ed. Little, Brown and Company, Inc., 1982.

[5] J.V. Forrester, A.D. Dick, P. McMenamin, and W.R. Lee, *The Eye Basic Sciences in Practice*, 2nd ed. WB Saunders, 2002.

[6] D.J. Spalton, R.A. Hitchings, and P.A. Hunter, *Atlas of Clinical Ophthalmology*. Gower Medical Publishing Ltd, 1984.

[7] M.W. Levine and J.M. Shefner, *Fundamentals of Sensation and Perception*, 2nd ed. Brooks, Cole Publishing Company, 1990.

[8] R.S. Snell and M.A. Lemp, *Clinical Anatomy of the Eye*, 2nd ed. Blackwell Science, 1998.

[9] I.R. Bicknell, R. Darrow, L. Barsalon, S.J. Fliesler, and D.T. Organisciak, "Alterations in retinal rod outer segment fatty acids and light-damage susceptibility in P23H rats," *Molecular Vision*, vol. 8, pp. 333–40, 2002.

[10] S.A. Bernstein, D.J. Breding, and S.K. Fisher, "The influence of light on cone disk shedding in the lizard, sceloporus occidentalis," *J. Cell Biol.*, vol. 99, pp. 379–89, 1984.

[11] A. Vander, J. Sherman, and D. Luciano, *Human Physiology: The Mechanisms of Body Function*, 7th ed. McGraw-Hill, 1998.

[12] E.R. Kandel, J.H. Schwartz, and T.M. Jessell, *Essentials of Neural Science and Behavior*. Stamford, Connecticut: Appleton & Lange, 1995.

[13] J.G. Nicholls, A.R. Martin, B.G. Wallace, and P.A. Fuchs, *From Neuron to Brain*, 4th ed. Sunderland, Massachusetts, USA: Sinauer Associates, Inc., 2001.

[14] C.U.M. Smith, *Elements of Molecular Neurobiology*, 3rd ed. John Wiley & Sons, LTD., 2002.

[15] I. Shaked, I. Ben-Dror, and L. Vardimon, "Glutamine synthetase enhances the clearance of extracellular glutamate by the neural retina," *J. Neurochem*, vol. 83, pp. 574–80, 2002.

[16] M. Tsacopoulos, "Metabolic signaling between neurons and glial cells: a short review," *J. Physio. Paris*, vol. 96, pp. 283–8, 2002.

[17] M.C. Papadopoulos, D.K. Binder, and A.S. Verkman, "Enhanced macromolecular diffusion in brain extracellular space in mouse models of vasogenic edema measured by cortical surface photobleaching," *The FASEB J.*, vol. 19, pp. 425–8, 2005.

[18] M. Erecinska and I.A. Silver, "Metabolism and role of glutamate in mammalian brain," *Prog. Neurobio.*, vol. 35, pp. 245–96, 1990.

[19] C.K. Vorwerk, S.A. Lipton, D. Zurakowski, B.T. Hyman, B.A. Sabel, and E.B. Dreyer, "Chronic low-dose glutamate is toxic to retinal ganglian cells," *Invest. Ophthalmol. Vis. Sci.*, vol. 37, pp. 1618–24, 1996.

[20] N.L. Barnett, D.V. Pow, and N.D. Bull, "Differential perturbation of neuronal and glial glutamate transport systems in retinal ischaemia," *Neurochem. Inter.*, vol. 39, pp. 291–9, 2001.

[21] J. Shen, K.F. Petersen, K.L. Behar, P. Brown, T.W. Nixon, G. O.A.C. Petroff, G.I. Shulman, R.G. Shulman, and D.L. Rothman, "Determination of the rate of the glutamate/glutamine cycle in the 13C NMR," *Proc. Natl. Acad. Sci.*, vol. 96, pp. 8235–40, 1999.

[22] Y. Daikhin and M. Yudkoff, "Compartmentation of brain glutamate metabolism in neurons and glia," *J. Nutr.*, vol. 130, pp. 1026S–31S, 2000.

[23] N.C. Danbolt, "Glutamate uptake," *Prog. Neurobio.*, vol. 65, pp. 1–105, 2001.

[24] R. Gruetter, E.R. Seaquist, and K. Ugurbil, "A mathematical model of compartmentalized neurotransmitter metabolism in the human brain," *Am. J. Physiol. Endocrinol Metab.*, vol. 281, pp. E100–E112, 2001.

[25] D.M. Cohen, "Inhibition of glutamine systhetase induces critical energy threshold for neuronal survival," *Ann. New York Acad. Sci.*, pp. 456–60.

[26] R.M. Solano, M.J. Casarejos, J. Menndez-Cuervo, J.A. Rodriguez-Navarro, and J. Garca de Ybenes, "Glial dysfunction in parkin null mice: Effects of aging," *J. Neurosci.*, vol. 28, pp. 598–611, 2008.

[27] A.J. Lotery, "Glutamate excitotoxicity in glaucoma: truth or fiction," *Eye*, vol. 19, pp. 369–70, 2005.

[28] C.M. Anderson and R.A. Swanson, "Astrocyte glutamate transport: Review of properties, regulation, and physiological functions," *GLIA*, vol. 32, pp. 1–14, 2000.

[29] E. Lieth, K.F. LaNoue, D.A. Berkich, B. Xu, M. Ratz, C. Taylor, and S.M. Hutson, "Nitrogen shuttling between neurons and glial cells during glutamate synthesis," *J. Neurochem*, vol. 76, pp. 1712–23, 2001.

[30] T.S. Rao, K.D. Lariosa-Willingham, and N. Yu, "Glutamate-dependent glutamine, aspartate and serine release from rat cortical glial cell cultures," *Brain Res.*, vol. 978, pp. 213–22, 2003.

[31] S. Poitry, C. Poitry-Yamate, J. Ueberfeld, P.R. MacLeish, and M. Tsacopoulos, "Mechanisms of glutamate metabolic signaling in retinal glial (Müller) cells," *J. Neurosci*, vol. 20, pp. 1809–21, 2000.

[32] B.S. Winkler, N. Kapousta-Bruneau, M.J. Arnold, and D.G. Green, "Effects of inhibiting glutamine synthetase and blocking glutamate uptake on *b*-wave generation in the isolated rat retina," *Visual Nerosci.*, vol. 16, pp. 345–53, 1999.

[33] J.L. Boulland, K.K. Osen, L.M. Levy, N.C. Danbolt, R.H. Edwards, J. Storm-Mathisen, and F.A. Chaudhry, "Cell-specific expression of the glutamine transporter SN1 suggest differences in dependence on the glutamine cycle," *Euro. J. Neurosci.*, vol. 15, pp. 1615–31, 2002.

[34] F.A. Chaudhry, D. Schmitz, R.J. Reimer, P. Larsson, A.T. Gray, R. Nicoll, M. Kavanaugh, and R.H. Edwards, "Glutamine uptake by neurons: interaction of proton with System A transporter," *J. Neuronsci.*, vol. 22, pp. 62–72, 2002.

[35] T.C. Welbourne, "Evidence for passive glutamine uptake coupled to glutaminase I," *Am. J. Physiol.*, vol. 226, pp. 549–54, 1974.

[36] G.J. Siegel, B.W. Agranoff, R.W. Albers, S.K. Fisher, and M.D. Uhler, *Basic Neurochemistry: Molecular, Cellular and Medical Aspects*, 6th ed. Lippincott Williams and Wilkins, 1999.

[37] D. Purves, G.J. Augustine, D. Fitzpatrick, W.C. Hall, A-S. LaMantia, J.O. McNamara, and L.E. White, *Neuroscience*, 4th ed. Sinaue Associates, Inc., 2008.

[38] E.R. Kandel, J.H. Schwartz, and T.M. Jessell, *Principles of Neural Science*, 4th ed. McGraw-Hill, 2000.

[39] P. Brodal, *The Central Nervous System: Structure and Function*, 2nd ed. Oxford University Press, 1998.

[40] M-A. Dronne, J-P. Boissel, and E. Grenier, "A mathematical model of ion movements in grey matter during a stroke," *J. Theo. Bio.*, vol. 240, pp. 599–615, 2006.

[41] D.R. Lucas and J.P. Newhouse, "The toxic effect of sodium L-Glutamate on the inner layers of the retina," *AMA. Arch. Ophth.*, vol. 58, pp. 193–201, 1957.

[42] S.E. Ostroy, S.M. Frede, E.F. Wagner, C.G. Gaitatzes, and E.M. Janle, "Decreased rhodopsin regeneration in diabetic mouse eyes," *Invest. Ophthalmol. Vis. Sci.*, vol. 35, pp. 3905–9, 1994.

[43] W. Fan, N. Lin, H.J. Sheedlo, and J.E. Turner, "Müller and RPE cell response to photoreceptor cell degeneration in aging fischer rats," *Exp. Eye Res.*, vol. 63, pp. 9–18, 1996.

[44] J.A. Phipps, P. Yee, E.L. Fletcher, and A.J. Vingrys, "Rod photoreceptor dysfunction in diabetes: Activation, deactivation, and dark adaptation," *Invest. Ophthalmol. Vis. Sci.*, vol. 47, pp. 3187–94, 2006.

[45] E.L. Fletcher, "Alterations in neurochemistry during retinal degeneration," *Microsc. Res. Tech.*, vol. 50, pp. 89–102, 2000.

[46] S. Bröer and N. Brookes, "Transfer of glutamine between astrocytes and neurons," *J. Neurochem*, vol. 77, pp. 705–19, 2001.

[47] R.N. Ranson, R.M. Santer, and A.H.D. Watson, "Ageing reduces the number of vesicular glutamate transporter 2 containing immunoreactive inputs to identified rat pelvic motoneurons," *Exp. Geron.*, vol. 42, pp. 506–16, 2007.

[48] C.M. Fraser, G.J. Sills, G. Forrest, G.G. Thompson, and M.J. Brodie, "Effects of anti-epileptic drugs on glutamine synthetase activity in mouse brain," *Br. J. Pharmacol.*, vol. 126, pp. 1634–8, 1999.

[49] C.D. Smith, J.M. Carney, P.E. Starke-Reed, C.N. Oliver, E.R. Stadtman, R.A. Floyd, and W.R. Markesbery, "Excess brain protein oxidation and enzyme dysfunction in normal aging and in Alzheimer disease," *Proc. Natl. Acad. Sci.*, vol. 88, pp. 10 541–3, 1991.

[50] G. Segovia, A. Del Arco, L. Prieto, and F. Mora, "Glutamate-glutamine cycle and aging in striatum of the awake rat: effects of a glutamate transporter blocker," *Neurochem. Res.*, vol. 26, pp. 37–41, 2001.

[51] I. Cauquil-Caubère, C. Oxhamre, J-M. Kamenka, and G. Barbanel, "Recurrent glutamate stimulations potentiate the hydroxyl radicals response to glutamate," *J. Neurosci. Res.*, vol. 56, pp. 160–5, 1999.

[52] D.W. Choi, "Glutamate neurotoxicity and diseases of the nervous system," *Neuron*, vol. 1, pp. 623–34, 1988.

[53] D. Andreucci, P. Bisegna, G. Caruso, H.E. Hamm, and E. DiBenedetto, "Mathematical model of the spatio-temporal dynamics of second messagers in visual transduction," *Biophysical J.*, vol. 85, pp. 1358–76, 2003.

[54] G. Caruso, H. Khanal, V. Alexiades, F. Rieke, H.E. Hamm, and E. DiBenedetto, "Mathematical and computational modelling of spatio-temporal signalling in rod phototransduction," *IEE Proc.-Syst.Biol.*, vol. 152, pp. 119–37, 2005.

[55] H. Khanal and V. Alexiades, "Models of phototransductions in rod photoreceptos," *Fifth International Conference on Dynamic Systems and Applications, editor M. Sambandham*, pp. 1–7, 2007.

[56] J. Kleinle, K. Vogt, H-R. Lüscher, L. Müller, W. Senn, K. Wyler, and J. Streit, "Transmitter concentration profiles in the synaptic cleft: an analytical model of release and diffusion," *Biophysical J.*, vol. 71, pp. 2413–26, 1996.

[57] K. Uffmann and R. Gruetter, "Mathematical modelling of ^{13}C label incorporation of the tca cycle: the concept of composite precursor function," *J. Neurosci. Res.*, vol. 85, pp. 3304–17, 2007.

[58] A. Goldbeter, G. Dupont, and M.J. Berridge, "Minimal model for single-induced Ca^{2+} oscillations and for their frequency encoding through protein phosphorylation," *Proc. Natl. Acad. Sci. USA*, vol. 87, pp. 1461–5, 1990.

[59] J. Sneyd, S. Girard, and D. Clapham, "Calcium wave propagation by calcium-induced calcium release: an unusual excitable system," *Bull. Math. Biol.*, vol. 55, pp. 315–44, 1993.

[60] B.J. Roth, S.V. Yagodin, L. Holtzclaw, and J.T. Russell, "A mathematical model of agonist-induced propagation of calcium waves in astrocytes," *Cell Calcium*, vol. 17, pp. 53–64, 1995.

[61] M. Marhl, T. Haberichter, M. Brumen, and R. Heinrich, "Complex calcium oscillations and the role of mitochondria and cytosolic proteins," *BioSystems*, vol. 57, pp. 75–86, 2000.

[62] M. Marhl, S. Schuster, and M. Brumen, "Mitochondria as an important factor in the maintenance of constant amplitudes of cytosolic calcium oscillations," *Biophys. Chem.*, vol. 71, pp. 125–32, 1998.

[63] V. Grubelnik, A.Z. Larsen, U. Kummer, L.F. Olsen, and M. Marhl, "Mitochondria regulate the amplitude of simple and complex calcium oscillations," *Biophys. Chem.*, vol. 94, pp. 59–74, 2001.

[64] M-A. Dronne, E. Grenier, T. Dumont, M. Hommel, and J.-P. Boissel, "Role of astrocytes in grey matter during stroke: a modelling approach," *Brain Res.*, vol. 1138, pp. 231–42, 2007.

[65] S. Tiveci, A. Akin, T. akir, H. Saybasili, and K. Ülgen, "Modelling of calcium dynamics in brain energy metabolism and alzheimer's disease," *Comp. Biol. Chem.*, vol. 29, pp. 151–62, 2005.

[66] E.E. Conn, P.K. Stumpf, G. Bruening, and R.H. Doi, *Outlines of Biochemistry*, 5th ed. John Wiley & Sons, Inc., 1990.

[67] E.L. Smith, R.L. Hill, I.R. Lehman, R.J. Lefkowitz, P. Handler, and A. White, *Principles of Biochemistry: General Aspects*, 7th ed. McGraw-Hill Book Company, 1983.

[68] S.C. Hsu and R.S. Molday, "Glycolytic enzymes and a GLUT-1 glucose transporter in the outer segments of rod and cone photoreceptor cells," *J. Biol. Chem.*, vol. 266, pp. 21 745–52, 1991.

[69] S. Duke-Elder and K.C. Wybar, *System of Ophthalmology volume II. The anatomy of visual system*, 1st ed. St. Louis: CV Mosby Co, 1961.

[70] J.R. Levick, *An introduction to cardiovascular physiology*, 3rd ed. London: Arnold, 2000.

[71] P.W. Atkins, *Physical Chemistry*, 4th ed. Oxford: Oxford University Press, 1990.

[72] J.D. Murray, *Mathematical Biology I: An Introduction*, 3rd ed. 2002: Springer, 1998.

[73] J. Keener and J. Sneyd, *Mathematical Physiology*. New York Inc.: Springer-Verlag, 1998.

[74] D. Attwell, "Brain uptake of glutamate: food for thought," *J. Nutr.*, vol. 130, pp. 1023S–5S, 2000.

[75] D.W. Choi and S.M. Rothman, "The role of glutamate neurotoxicity in hypoxic-ischemic neuronal death," *Annu. Rev. Neurosci*, vol. 13, pp. 171–82, 1990.

[76] J.T. Porter and K.D. Maccarthy, "Astrocytic neurotransmitter receptors in situ and in vivo," *Prog. Neurobio*, vol. 51, pp. 439–55, 1997.

[77] S.F. Traynelis and R. Dingledine, "Role of extracellular space in hyperosmotic suppression of potassium-induced electrographic seizures," *J. Neurophysiol.*, vol. 61, pp. 927–38, 1989.